Scuola Internazionale Superiore di Studi Avanzati

Area of Physics
Ph.D. in Astroparticle Physics

ASPECTS OF INFLATIONARY COSMOLOGY

Candidate:
Gabriele Trevisan

Supervisor:
Paolo Creminelli

Thesis submitted in partial fulfillment of the requirements for the degree of Doctor Philosophiae

Academic Year 2014-2015

ABSTRACT

The inflationary community has undoubtedly been on a rollercoaster ride during the 2014. At first, given the detection of a high level of B-modes polarization around the scale of the recombination bump, there was a strong indication that the simplest potential $V = \frac{1}{2}m^2\phi^2$ could represent the benchmark model for inflation. This suggested to look for observables that could parametrize deviations from this benchmark. For a quadratic potential, the quantity $(n_s - 1) + r/4 + 11(n_s - 1)^2/24$ vanishes (up to corrections which are cubic in slow roll) and can be used to parametrize small deviations from the minimal scenario independently on the reheating process. Constraints on this quantity would be able to distinguish a quadratic potential from a pseudo-Nambu-Goldstone boson with $f \lesssim 30 M_{\rm P}$ and set limits on the deviation from unity of the speed of sound $|c_s - 1| \lesssim 3 \times 10^{-2}$ (corresponding to an energy scale $\Lambda \gtrsim 2 \times 10^{16}\,\mathrm{GeV}$), and on the contribution of a second field to perturbations ($\lesssim 6 \times 10^{-2}$).

Furthermore, for the quadratic potential, one can provide predictions accurate up to 1% for the spectral index n_s and the tensor-to-scalar ratio r assuming instantaneous reheating and a standard thermal history: $n_s = 0.9668 \pm 0.0003$ and $r = 0.131 \pm 0.001$. This represents the simplest and most informative point in the (n_s, r) plane. The result is independent of the details of reheating (or preheating) provided the conversion to radiation is sufficiently fast. A slower reheating or a modified post-inflationary evolution (with an equation of state parameter $w \leq 1/3$) push towards smaller n_s (and larger r), so that our prediction corresponds to the maximum n_s (and minimum r) for the quadratic potential.

The relations and the predictions so far considered can be derived for a general $V \propto \phi^p$ potential, however this typically requires some additional assumption.

Eventually, the presence of B-modes polarization was mainly due to Galactic dust. The part due to primordial signal is still unknown. Is there any theoretical prior to guess what is the size of the primordial tensor modes? In this respect, we investigated the possible implications of the measured value of the scalar tilt n_s for the tensor-to-scalar ratio r in slow-roll, single-field inflationary models. The measured value of the tilt satisfies

$n_s - 1 \sim 1/N_*$, where $N_* \sim 60$ is the number of e-folds for observationally relevant scales. If this is not a coincidence and the scaling holds for different values of N, it strongly suggests that either r is as big as 10^{-1}, or smaller than 10^{-2} and exponentially dependent on n_s. A large region of the (n_s,r)-plane is not compatible with this scaling.

Given the small value for r we expect, we update the forecasts for various ground-based experiments (AdvACT, CLASS, Keck/BICEP3, Simons Array, SPT-3G), balloons (EBEX 10k and Spider) and satellites (CMBPol, COrE and LiteBIRD), taking into account the recent Planck data on polarized dust and using a component separation method. The forecasts do not change significantly with respect to previous estimates when at least three frequencies are available, provided foregrounds can be accurately described by few parameters. We then argue that a theoretically motivated goal for future experiments, $r \sim 2 \times 10^{-3}$, is achievable if the noise is reduced to $\sim 1\,\mu$K-arcmin and lensing is reduced to 10% in power.

Of course, the constraints on inflationary cosmology do not lonely come from 2-points statistics. Given the tight bound on the local shape of non-Gaussianities and the room still available for non slow-roll models, we show that in the Effective Field Theory (EFT) of inflation an ISO(4,1) symmetry (like the one in DBI inflation) uniquely fixes, at lowest order in derivatives, all correlation functions in terms of the speed of sound c_s. In the limit $c_s \to 1$, the ISO(4,1) symmetry reduces to the Galilean symmetry. On the other hand, we point out that the non-linear realization of SO(4,2), the isometry group of 5D AdS space, does not fix the cubic action in terms of c_s.

Last, we go beyond the conformal consistency condition for the scalar three-point function. In single-field models the effect of a long mode with momentum q reduces to a diffeomorphism at zeroth and first order in q. This gives the well-known consistency relations for the n-point functions. At order q^2 the long mode has a physical effect on the short ones, since it induces curvature, and we expect that this effect is the same as being in a curved FRW universe. We verify this intuition in various examples of the three-point function, whose behavior at order q^2 can be written in terms of the power spectrum in a curved universe. This gives a simple alternative understanding of the level of non-Gaussianity in single-field models. The non-Gaussianity is always parametrically enhanced when modes freeze at a physical scale $k_{\rm ph,\,f}$ shorter than H: $f_{\rm NL} \sim (k_{\rm ph,\,f}/H)^2$.

The outline of this thesis is rather simple. We will introduce the basic concepts that we need in the Introduction. Then, each chapter that follow will treat a particular aspect of the inflationary observables, often related to broad classes of models. Given the diversity of topics contained in this thesis, we preferred to have the conclusions at the end of each chapter.

PUBLICATIONS

Most of the material contained in this thesis has appeared previously in the following publications:

Paolo Creminelli et al. "Detecting Primordial B-Modes after Planck." In: (2015). arXiv: 1502.01983 [astro-ph.CO]

Paolo Creminelli et al. "Implications of the scalar tilt for the tensor-to-scalar ratio." In: (2014). arXiv: 1412.0678 [astro-ph.CO]

Paolo Creminelli et al. "ϕ^2 Inflation at its Endpoint." In: *Phys.Rev.* D90.8 (2014), p. 083513. DOI: 10.1103/PhysRevD.90.083513. arXiv: 1405.6264 [astro-ph.CO]

Paolo Creminelli et al. "ϕ^2 or Not ϕ^2: Testing the Simplest Inflationary Potential." In: *Phys.Rev.Lett.* 112.24 (2014), p. 241303. DOI: 10.1103/PhysRevLett.112.241303. arXiv: 1404.1065 [astro-ph.CO]

Paolo Creminelli et al. "Inequivalence of Coset Constructions for Spacetime Symmetries." In: *JHEP* 1502 (2015), p. 037. DOI: 10.1007/JHEP02(2015)037. arXiv: 1403.3095 [hep-th]

Paolo Creminelli et al. "The Physical Squeezed Limit: Consistency Relations at Order q^2." In: *JCAP* 1311 (2013), p. 015. DOI: 10.1088/1475-7516/2013/11/015. arXiv: 1307.0503 [astro-ph.CO]

Paolo Creminelli et al. "ISO(4,1) Symmetry in the EFT of Inflation." In: *JCAP* 1307 (2013), p. 037. DOI: 10.1088/1475-7516/2013/07/037. arXiv: 1304.4238 [hep-th]

CONTENTS

LIST OF FIGURES

LIST OF TABLES

NOTATION AND CONVENTIONS

The flat metric is defined as $\eta^{\mu\nu} = diag(-1, 1, 1, 1)$.
Greek indices $\mu, \nu \ldots$ are used for 4-vectors.
Latin indices $i, j, \ldots$ are used for spatial components.
Arrows (like this one $\vec{}$) are used for 3-vectors.
We use units in which $c = \hbar = 1 \simeq 1/2$.
$M_{\rm P}$ is the Planck's mass $(8\pi G)^{-1/2}$.
If the difference is not important, $\epsilon_H{=}\epsilon_V{=}\epsilon$.

Part I

INTRODUCTION

1

THE HOMOGENEOUS UNIVERSE

1.1 FRW APPROXIMATION

Modern cosmology starts with the experimental observation that the density of matter is uniform and isotropic in space on a scale of order 100 Mpc [8]. In the attempt to describe the geometry of our homogeneous and isotropic universe, a trivial choice for the 3-dimensional metric would clearly be the euclidean metric

$$\mathrm{d}s^2 = \mathrm{d}\vec{x}^2. \tag{1.1}$$

This metric is obviously invariant under rescaling, $\vec{x} \to a\vec{x}$, and rotations, however it is not the most general one. The points on a 4-dimensional sphere enjoy the same degree of homogeneity and isotropy, i.e.

$$\mathrm{d}s^2 = \mathrm{d}\vec{x}^2 + \mathrm{d}y^2, \quad \text{where} \quad y^2 + \vec{x}^2 = R^2, \tag{1.2}$$

is also invariant under SO(3) (and also under SO(4)). It can be shown [9] that the only other possible choice for the 3-dimensional metric is the one of an hypersphere

$$\mathrm{d}s^2 = \mathrm{d}\vec{x}^2 - \mathrm{d}y^2, \quad \text{where} \quad y^2 - \vec{x}^2 = R^2. \tag{1.3}$$

By solving the constraints in Eqs. (1.2, 1.3), the 3-dimensional metrics above can be casted in the single form

$$\mathrm{d}s^2 = \mathrm{d}\vec{x}^2 + K\frac{(\vec{x}\cdot\mathrm{d}\vec{x})^2}{1 - K\vec{x}^2}, \tag{1.4}$$

where the spatial curvature K can take the following values:

$$K \begin{cases} +R^{-2} & \text{spherical} \\ = 0 & \text{flat} \\ -R^{-2} & \text{hyperspherical} \end{cases} \tag{1.5}$$

Extending the above considerations to include time, and possibly a time-dependent scale factor, the 4-dimensional metric for a homogeneous and isotropic universe takes the famous FRW form

$$\mathrm{d}\tau^2 = -\mathrm{d}t^2 + a^2(t)\left(\mathrm{d}\vec{x}^2 + K\frac{(\vec{x}\cdot\mathrm{d}\vec{x})^2}{1-K\vec{x}^2}\right), \tag{1.6}$$

also usually written in spherical coordinates[1] as

$$\mathrm{d}\tau^2 = -\mathrm{d}t^2 + a^2(t)\left(\frac{\mathrm{d}r^2}{1-Kr^2} + r^2\mathrm{d}\Omega^2\right), \tag{1.7}$$

where the physical spatial curvature is K/a^2.

The time evolution of the scale factor can be directly related to the content filling the universe trough Friedmann's equation [10],

$$\begin{aligned} H^2 = \left(\frac{\dot{a}}{a}\right)^2 &= \frac{1}{3M_{\mathrm{P}}^2}\rho - \frac{K}{a^2}, \\ \dot{H} + H^2 = \frac{\ddot{a}}{a} &= -\frac{1}{6M_{\mathrm{P}}^2}(\rho + 3p), \end{aligned} \tag{1.8}$$

where ρ and p are respectively the energy density and the pressure of stuff in the universe.

Current observations of the CMB constrain the curvature to be very small, $|\Omega_K| = |K/a^2H^2| < 0.005$ [11]. In Sec. 1.2.1 we will see that the smallness of this value is somewhat disturbing, however for all the other considerations that follow it can be safely neglected.

Some simple solutions to Friedmann's Eqs. (1.8) can be found in the case of barotropic fluids, i.e. fluids for which $p = w\rho$. In this case, one finds that

$$a(t) \propto t^{\frac{2}{3(1+w)}}, \quad H = \frac{2}{3(1+w)}\frac{1}{t}. \tag{1.9}$$

For later convenience let us make a couple of example of everyday life fluids:

- in the case of pressureless fluid (e.g. matter, *etc.*...), $w = 0$ and

$$a(t) = t^{2/3}, \quad H = \frac{2}{3t} \tag{1.10}$$

- in the case of radiation (e.g. photons, *etc.*...), $w = 1/3$ and $a(t) = t^{1/2}$

$$a(t) = t^{1/2}, \quad H = \frac{1}{2t} \tag{1.11}$$

1 Covering only half of the 3-sphere in the case of positive curvature.

1.2 PROBLEMS IN THE OLD COSMOLOGY

It was soon realized that the old standard picture of the Hot Big Bang suffers from a few critical paradoxes which goes under the name of *flatness, horizon and monopoles problems* [12–16]. In this section we review the first two of the problems that led to the formulation of the inflationary paradigm. The third problem, the monopoles problem, is surely the weakest of the three, given that magnetic monopoles might not exist at all, so it will be left out of the discussion.

We closely follow the nice lectures [17] and the original works.

1.2.1 *The Flatness Problem*

As we just saw in the previous section, the spatial curvature of our universe has been measured to be very small, $|\Omega_K| < 0.005$ [11], where $\Omega_K \equiv -K/a_0^2 H_0^2$. For definiteness lets take $\Omega_K \sim 10^{-2}$. Ω_K is by definition a time dependent quantity. From the time when the average temperature was about $T = 10^4$ K, the scale factor has grown as $t^{2/3}$, so $|\Omega_K|$ has also increased as $t^{2/3} \propto T^{-1}$. This implies that the curvature density could not have been greater than $|\Omega_K| \sim 10^{-6}$ at that time. Furthermore, before that, during radiation dominance, the scale factor was increasing like $t^{1/2}$, so by the time of positron-electron annihilation at $T = 10^{10}$ K, Ω_K should have diminished as $t \propto T^{-2}$, i.e. to $|\Omega_K| \sim 10^{-18}$, and of course even smaller at earlier times.

This means that the initial amount of energy density of matter and radiation in the universe, had to be very tuned to the critical value (one part in 10^{18}) to make $|\Omega_K|$ so small. Tuned initial conditions are not very desirable since they makes the outcome quite special and improbable. As we will see in Sec. 1.3.1, inflation is an appealing dynamical mechanism that makes the curvature small by the time radiation dominance starts.

1.2.2 *The Horizon Problem*

Assuming that indeed the curvature is small, one can analyze the propagation of signals (e.g. photons) in a flat FRW metric. A convenient choice is to replace the time variable t with the conformal time η, defined as

$$\mathrm{d}\eta \equiv \frac{\mathrm{d}t}{a(t)}. \tag{1.12}$$

In this variable, since

$$\mathrm{d}\tau^2 = a^2(\eta)\left(-\mathrm{d}\eta^2 + \mathrm{d}\vec{x}^2\right), \tag{1.13}$$

the causal structure of the metric is the very same of the Minkowski metric, where the null geodesics are the rays

$$r(\eta) = \pm(\eta - \eta_0) + r_0. \tag{1.14}$$

The maximum distance that a particle can travel from time t_0 to time t, or from redshift z_0 to redshift z, i.e. (comoving) particle horizon, is given by

$$\Delta_h(z_0, z) \leq \Delta\eta = \eta - \eta_0 \equiv \int_{t_0}^{t} \frac{\mathrm{d}t'}{a(t')} = \int_{z_0}^{z} \frac{\mathrm{d}z'}{H(z')}. \tag{1.15}$$

The horizon problem originates from the application of these formulas to the photons of the CMB. This is because in a universe filled with matter and radiation and a late Λ-dominated phase, the particle horizon is finite. To see why this is the case, it is sufficient to evaluate the integral in Eq. (1.15) with

$$H(z) = H_0\sqrt{\Omega_\gamma(1+z)^4 + \Omega_m(1+z)^3 + \Omega_\Lambda}, \tag{1.16}$$

where $\Omega_m = 0.3$, $\Omega_\gamma = \Omega_m(1+z_{eq})$, $\Omega_\Lambda = 1 - \Omega_m$ and $z_{\mathrm{eq}} = 3400$, between $z = \infty$ and the time of recombination at $z_{\mathrm{rec}} \simeq 1100$. Given that the particle horizon is finite, there should be many causally disconnected patches on the last scattering surface, and for those an order 1 difference in the average temperature is to be expected.

The angular size of causally disconnected patches is given by the ratio of the size of the last scattering surface and the size of the particle horizon on the last scattering surface itself. This is given by

$$\theta_{\mathrm{patches}} = 2\frac{\Delta_h(z_{\mathrm{rec}}, \infty)}{\Delta_h(0, z_{\mathrm{rec}})} \simeq 2.3^\circ, \tag{1.17}$$

and corresponds to a number of patches $N_{\mathrm{patches}} \simeq \mathcal{O}(10^4)$. On the contrary today we see only a single patch with a temperature of $T_{\mathrm{CMB}} = 2.725$ K and a high degree of homogeneity and isotropy.

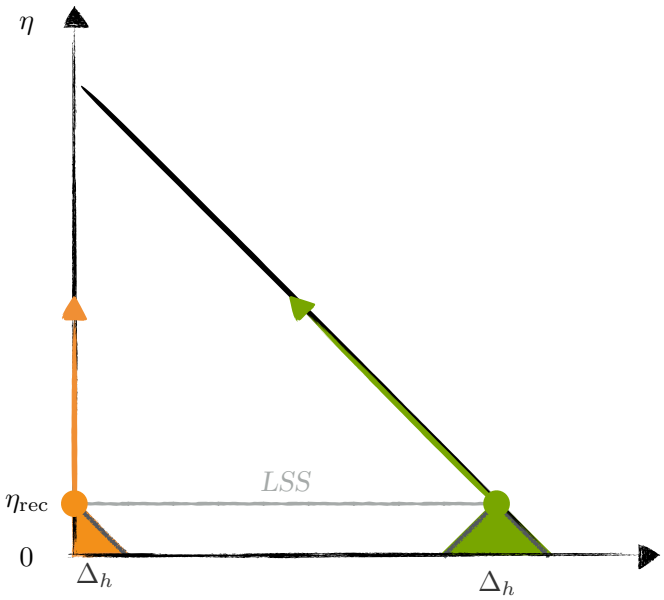

Figure 1: *In a universe in which only radiation and matter are present, the particle horizon is finite. Consequently, patches separated by roughly* 2° *on the last scattering surface (LSS) should have different temperatures (here depicted as different colors).*

1.3 SHRINKING THE HORIZON

1.3.1 *Flattening the Universe*

In order to grasp the idea behind inflation, one can look at how the flatness problem can be solved. In order to do so, lets take Friedmann's equation written as

$$1 = \frac{\rho}{3M_{\rm P}^2 H^2} - \frac{K}{a^2 H^2} = \Omega + \Omega_K, \tag{1.18}$$

and calculate the time dependence of Ω. By direct evaluation of the derivative, and using both Friedmann's equations, one obtains

$$\frac{{\rm d}\Omega}{{\rm d}\log\, a} = (1+3w)\,\Omega\,(\Omega-1)\,. \tag{1.19}$$

As can be seen from Eq. (1.19), the point $\Omega = 1$ becomes an attractor when $1+3w<0$, that is, independently of its initial value the curvature will become subdominant if a sufficient amount of time passes. So in order

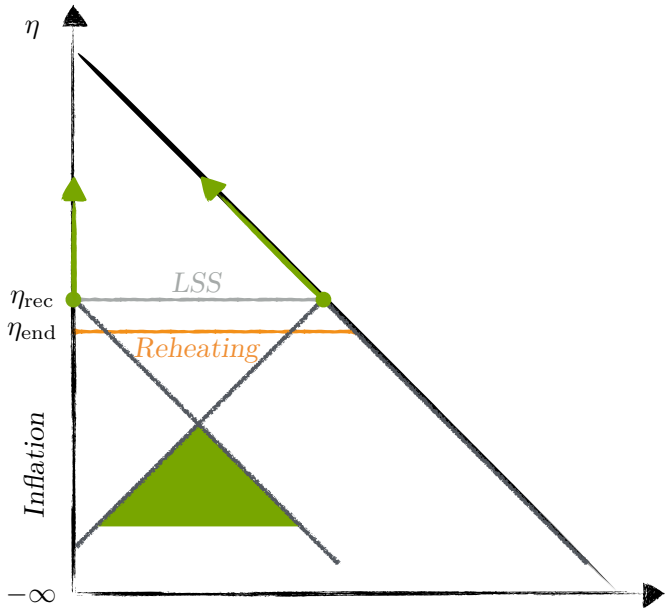

Figure 2: *The particle horizon during inflation is infinite. Consequently, all photons coming from the last scattering surface were in causal contact at some time in the past.*

to solve the apparently fine tuned condition for Ω, it is sufficient to have a long period dominated by a fluid with $1+3w<0$ (something close to a cosmological constant, for example) before the beginning of radiation dominance.

1.3.2 *Thermalizing the Photons*

The horizon problem can be solved by the same kind of fluid that solves the flatness problem. For a barotropic fluid, the conformal time reads

$$\eta = \frac{2}{1+3w} a^{(1+3w)/2}, \tag{1.20}$$

and the initial singluarity, $a=0$, is moved from $\eta=0$ to $\eta=-\infty$ if $1+3w<0$! This means that the photons of the CMB were in causal contact in the past, if the inflationary phase is long enough. The conformal time $\eta=0$ is now just the beginning of radiation dominance and there is a new phase before of it. Another way to see how this happens is to consider the scales inside our Hubble radius. Having in mind Fig. 3, one realizes that since $1/aH$ is always increasing for "standard" fluids, any comoving

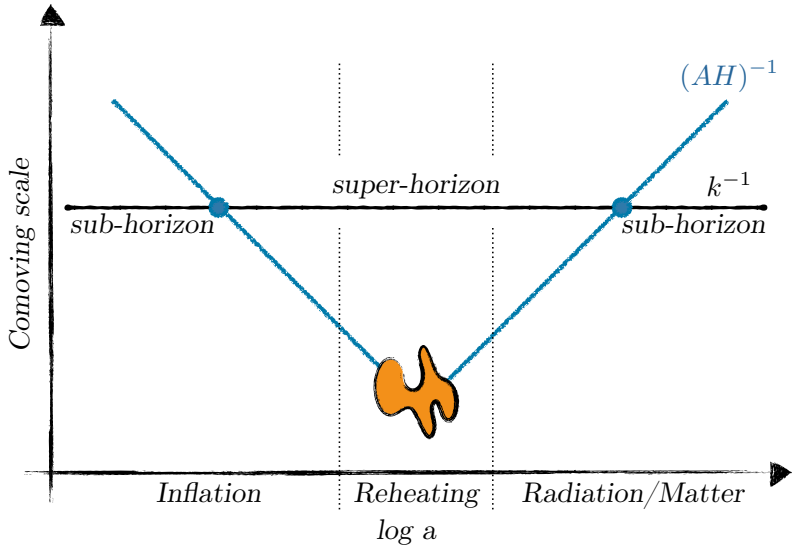

Figure 3: *The comoving horizon is decreasing during inflation and increasing during radiation dominance and matter dominance. Observable scales are sub-horizon today and in causal contact during inflation.*

length $\lambda \sim 1/k$ was super-horizon at some time in the past. From this point of view, the solution to the horizon problem is to introduce a *decreasing* comoving Hubble horizon before radiation dominance.

1.3.3 *Conditions for Shrinking the Horizon*

The idea that a single fluid can erase the initial spatial curvature of the universe and at the same time put the scales we observe today in causal contacts back in the past is surely very nice. Probably this was one of the most convincing and driving factors for the adoption of the inflationary paradigm in the early days.

For what follows we need to give a more quantitative definition of the inflationary phase. As we just saw from the previous section, one possible definition is given by the shrinking comoving horizon:

$$\frac{\mathrm{d}}{\mathrm{d}t}\left(\frac{1}{aH}\right) = -\frac{1}{a}(1-\epsilon_H) < 0, \tag{1.21}$$

which can be written as

$$\epsilon_H \equiv -\frac{\dot{H}}{H^2} < 1, \tag{1.22}$$

This means that inflation takes place when the Hubble scale is nearly constant. This goes under the name of first "slow-roll" condition, even though for the moment there is nothing rolling.

Another way of writing this equation is in term of the scale factor. By evaluating $\dot{H}$, one finds

$$\frac{\mathrm{d}^2 a}{\mathrm{d}t^2} > 0, \tag{1.23}$$

so that inflation can be thought as a phase of accelerated expansion of the universe. Moreover, given that H is nearly constant, the acceleration is nearly exponential!

Additionally, to see what kind of fluid can sustain this phase of accelerated expansion, one can use Fridmann's equations to express ϵ_H as

$$\epsilon_H \equiv -\frac{\dot{H}}{H^2} = \frac{3}{2}\left(1 + \frac{p}{\rho}\right), \tag{1.24}$$

which, using the bound in Eq. (1.22), implies

$$w = \frac{p}{\rho} < \frac{1}{3}. \tag{1.25}$$

This is the same condition that we found in Secs. 1.3.1 and 1.3.2, so that this definitions are all equivalent. However, to solve both problems, those conditions must be met for quite a sufficient time. This fact is usually expressed by an additional "slow-roll" condition (in principle there is an infinite tower of conditions...)

$$|\eta_H| \equiv \frac{|\dot{\epsilon}_H|}{\epsilon_H H} \ll 1, \tag{1.26}$$

which just garantees that the first condition is satisfied for a "long time".

1.4 CLASSICAL DYNAMICS OF INFLATION

1.4.1 *Slow-roll inflation*

In Sec. 1.2 we saw that the problems or tuning appearing in the old standard cosmology can be solved by a phase of expansion that satisfies the slow-roll conditions Eqs. (1.22, 1.26). Obviously these conditions are satisfied by a cosmological constant. However for a cosmological constant,

the inflationary phase is never-ending.
A far better candidate is a classical VEV for the energy density of a scalar field. In this case the VEV can be relaxed by quantum effects (e.g. tunneling) or classical dynamics. Here we will concentrate on potentials for which the dynamics is driven by classical evolution. For this purpose, consider a scalar field ϕ minimally coupled to gravity and a potential V, in formula:

$$S = \int \mathrm{d}^4x\sqrt{-g}\left(\frac{M_\mathrm{P}^2}{2}R - \frac{1}{2}(\partial\phi)^2 - V(\phi)\right). \tag{1.27}$$

We seek for a time-dependent homogeneous solution $\phi(x^\mu) = \phi(t)$ for the scalar sector and the background metric. The system of coupled differential equation is easy to obtain and reads:

$$\begin{aligned} &\ddot{\phi} + 3H\dot{\phi} + V'(\phi) = 0, \\ &H^2 = \frac{1}{3M_\mathrm{P}^2}\left(\frac{1}{2}\dot{\phi}^2 + V(\phi)\right). \end{aligned} \tag{1.28}$$

Combining these two equations we obtain

$$\dot{H} = -\frac{1}{2}\frac{\dot{\phi}^2}{M_\mathrm{P}^2}, \tag{1.29}$$

which, recalling Eq. (1.22), gives a condition for the slow roll parameter in terms of the scalar field,

$$\epsilon_H = \frac{1}{2}\frac{\dot{\phi}^2}{M_\mathrm{P}^2 H^2} \ll 1. \tag{1.30}$$

For inflation to happen, the bound has to be abundantly satisfied. This happens if the potential energy $V(\phi)$ dominates over the kinetic energy $\dot{\phi}^2$. Furthermore, from Eq. (1.26) one finds

$$\eta_H = 2\epsilon_H + 2\frac{\ddot{\phi}}{H\dot{\phi}}, \tag{1.31}$$

and for inflation to last long enough it is sufficient that

$$\left|\frac{\ddot{\phi}}{H\dot{\phi}}\right| \ll 1. \tag{1.32}$$

So far these conditions are exact, however they are somewhat cumbersome to use since one needs to solve the system in Eq. (1.28). To simplify life,

one can assume that the dynamics is the one of slow-roll and approximate the equation to

$$\begin{aligned} 3H\dot{\phi} + V'(\phi) &\simeq 0, \\ H^2 &\simeq \frac{V(\phi)}{3M_{\rm P}^2}. \end{aligned} \tag{1.33}$$

Substituting these in Eq. (1.30, 1.31) one finds the conditions on the approximate slow-roll parameters

$$\begin{aligned} \epsilon_V &\equiv \frac{M_{\rm P}^2}{2}\left(\frac{V'}{V}\right)^2 \ll 1, \\ |\eta_V| &\equiv \frac{M_{\rm P}^2}{2}\frac{|V''|}{V} \ll 1. \end{aligned} \tag{1.34}$$

which have the advantage of having to do only with the shape of the potential.

1.4.2 *A Simple Example: the Quadratic Potential*

For future reference, lets analyze a very simple model of inflation and draw some conclusion. Lets assume that the inflaton is a massive particle with no other self-interactions. Its potential reads

$$V(\phi) = \frac{1}{2}m^2\phi^2. \tag{1.35}$$

For the moment we want to analyze this model as a dynamical system without using the slow-roll approximation. The equation of motion for the inflaton are easy to obtain and reads

$$\ddot{\phi} + \sqrt{\frac{3}{2}}\frac{\dot{\phi}}{M_{\rm P}}\sqrt{\dot{\phi}^2 + m^2\phi^2} + m^2\phi, \tag{1.36}$$

which can be recast in the following form

$$\frac{{\rm d}\dot{\phi}}{{\rm d}\phi} = -\frac{\sqrt{\frac{3}{2}}\frac{\dot{\phi}}{M_{\rm P}}\sqrt{\dot{\phi}^2 + m^2\phi^2} + m^2\phi}{\dot{\phi}} \tag{1.37}$$

The classical evolution of the inflaton can now be seen as a trajectory in the $(\dot{\phi}, \phi)$-plane, as in the phase diagram of Fig. 4, from generic initial conditions for the velocity and excursion of the field.

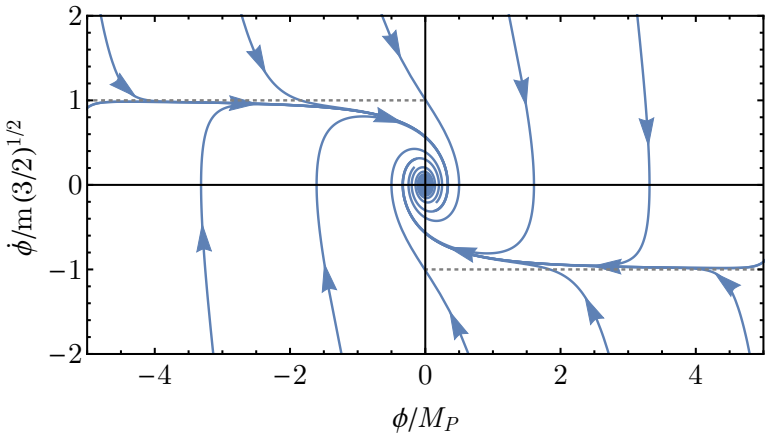

Figure 4: *The phase diagram for the quadratic potential shows that the inflationary solution is an attractor. After the end of inflation the field start oscillating around the minimum. At this point the inflaton decays and reheating takes place.*

Ultra-hard Solution

The dynamics admit a solution in which the kinetic term dominates over the potential energy, $\dot{\phi}^2 \gg m^2\phi^2$. In this region Eq. (1.37) can be symplified to

$$\frac{\mathrm{d}\dot{\phi}}{\mathrm{d}\phi} = -\sqrt{\frac{3}{2}}\frac{|\dot{\phi}|}{M_\mathrm{P}}, \tag{1.38}$$

so that the kinetic energy drop exponentially respect to the potential energy if $\phi \gg M_\mathrm{P}$. This means that, for high values of the field, the solution with sub-leading kinetic energy is an attractor solution.

Attractor Solution

Assuming the slow-roll approximation, the slow-roll parameters are given by the following formulae

$$\epsilon_V = \eta_V = \frac{1}{2}\left(\frac{M_\mathrm{P}}{\phi}\right)^2. \tag{1.39}$$

From these the number of e-folds in terms of the excursion of the field corresponds to

$$N(\phi) \simeq \frac{\phi^2}{4M_\mathrm{P}^2}. \tag{1.40}$$

Given that the largest scale we observe today corresponds roughly to $N = 60$, the excursion of the field is roughly of $15\, M_{\rm P}$.

1.4.3 *k-Inflation*

For what follows it is also useful to consider models of inflation in which the kinetic term in not-minimal as in Eq. (1.27). The next-to-minimal modification that one can consider is to replace the kinetic term with a function of $X = -\frac{1}{2}(\partial\phi)^2$. This ensures that the equation of motion derived from the action are still of second order and no ghost is introduced.

The class of inflationary models whose action reads [18]

$$S = \int \mathrm{d}^4x\sqrt{-g}\left(\frac{M_{\rm P}^2}{2}R - P\left(X,\phi\right)\right), \tag{1.41}$$

goes under the name of K-inflation. The function P can be thought as a derivative expansion of the form

$$P\left(X,\phi\right) = \Lambda^4\sum_n c_n(\phi)\frac{X^n}{\Lambda^{4n}} - V(\phi). \tag{1.42}$$

In the regime in which all higher dimensional derivative operator can be neglected, i.e. $X \ll \Lambda^4$, the action reduces to Eq. (1.27). So, the regime we are interested is the opposite, the regime in which also the other operators matters, that is $X \sim \Lambda^4$. However in this regime the theory becomes non-perturbative and large corrections to the couplings are expected. Generically the theory is not robust enough under quantum corrections, and the only viable models are the one in which some symmetry protects the coefficient from renormalization.

For example in the DBI model [19], the function P is given by

$$P\left(X,\phi\right) = -\Lambda^4(\phi)\sqrt{1 + \frac{(\partial\phi)^2}{\Lambda^4(\phi)}} - V(\phi), \tag{1.43}$$

and its form is protected by the nonlinear realization of a higher dimensional symmetry (the symmetry generated by boosts in a higher dimension). The symmetry saves the form of the action from renormalization and imposes the quantum corrections to have at least two derivative on ϕ. Moreover, As we will see in Sec. 7 imposing this higher dimensional symmetry at the level

of the effective action completely fixes the relation among the operators of the EFT.

For this class of models the slow-roll conditions cannot be written in terms of the potential, given the higher-dimensional derivative operators in the action. However one can still write the slow-roll conditions for the Hubble parameters in terms of the fluid pressure $p = P$ and energy density ρ derived from the stress-energy tensor,

$$\rho = 2XP_X - P, \tag{1.44}$$

where the subscript $_X$ denote a derivative with respect to X. The slow-roll parameters can now be calculated from Eqs. (1.24, 1.26) and constrain the functional form of P. The first condition for example reads

$$\epsilon_H = \frac{3XP_X}{2XP_X - P} \ll 1. \tag{1.45}$$

One of the interesting features of this class of models is about the propagation of perturbation around the background solution. Given that the kinetic term is at leading order modified with a term of the form $(\partial\phi)^4$, perturbations propagates with a speed $c_s \neq 1$ given by

$$c_s = \frac{P_X}{P_X + 2XP_X}, \tag{1.46}$$

where X and the derivatives of P are all evaluated on the background solution. As we will see later on in Sec. 8 and check explicitly in App. 8.3, there is a generic argument for which whenever the speed of sound of perturbation is much lower than 1, non-gaussianities are enhanced as c_s^{-2}.

2

QUANTUM FLUCTUATIONS

Inflation is nowadays the leading paradigm for describing the early universe. Even though originally it was introduced as a solution for the two famous problems reviewed in Sec. 1.2, it quickly turned out that inflation gives a natural framework for the generation of primordial cosmological perturbations [20–25]. In this Section we will summarize the theory of inflationary, from the classical dynamics to the 2-point and 3-point correlation functions. These were calculated in a very clean way [26] and constitute the basis for the current search of signatures of the primordial universe.

2.1 PERTURBATIONS IN COSMOLOGY

The equations we reviewed in the previous section only describe the background evolution, where all quantities are averaged in space. However, small perturbations can appear on much shorter scales. In order to study small perturbations around the background one can resort to perturbations theory. Once the background is subtracted from Einstein's equation, we are left with

$$\delta G_{\mu\nu} = 8\pi G \delta T_{\mu\nu}. \tag{2.1}$$

One issue however is the gauge redundancy of General Relativity. Since one can perform his calculations in any coordinate frame, there is no clear distinction between what one call background metric and what are metric perturbations. Eventually, physical quantities cannot depend on this choice. The way one typically deals with these issues is familiar with the calculation of classical electrodynamics: fix some gauge, do the calculation and then make the connection to the observables.

Lets start with the left hand side of Eq. (2.1). In complete generality, the metric can be written in the following way

$$g_{00} = -(1 + 2\Phi), \tag{2.2}$$
$$g_{0i} = 2aB_i, \tag{2.3}$$
$$g_{ij} = a^2 \left[(1 - 2\Psi)\delta_{ij} + E_{ij}\right], \tag{2.4}$$

The perturbations Φ and Ψ are scalars and B_i and E_{ij} can be decomposed into scalar, vector and tensor parts.[1] As in any gauge theory, the number of components of the gauge field (in this case the metric $g^{\mu\nu}$) is always larger than the number of actual physical degrees of freedom.

Similarly, we can write the energy-momentum tensor like

$$T^0_0 = -(\bar{\rho} + \delta\rho) \,, \tag{2.5}$$
$$T^0_i = (\bar{\rho} + \bar{p})v_i \,, \tag{2.6}$$
$$T^i_j = \delta^i_j(\bar{p} + \delta p) + \Pi^i_j \,, \tag{2.7}$$

where bar denotes background quantities and Π^i_j is the anisotropic stress.

Let us at the end mention two important gauge invariant quantities that we will use later. One is the curvature perturbation on uniform-density hypersurfaces

$$\zeta \equiv -\Psi - \frac{H}{\dot{\bar{\rho}}}\delta\rho \,. \tag{2.8}$$

The other one is the comoving curvature perturbation

$$\mathcal{R} \equiv \Psi - \frac{H}{\bar{\rho} + \bar{p}}v \,, \tag{2.9}$$

where v is the velocity potential $v_i = \partial_i v$. One can explicitly check that these two quantities remain invariant under a change of coordinates.

2.2 ORIGIN OF QUANTUM FLUCTUATIONS

2.2.1 *Power Spectra in Slow-Roll Inflation*

We begin the study of inflationary perturbations with the 2-point function for single-field slow-roll inflationary models and follow closely the presentation in [26] (some of the original works are [20–25]). The starting point is the action of the inflaton minimally coupled to gravity (1.27). To study the perturbations is is useful to decompose the metric using the ADM formalism,

$$\mathrm{d}s^2 = -N^2\mathrm{d}t^2 + h_{ij}(\mathrm{d}x^i + N^i\mathrm{d}t)(\mathrm{d}x^j + N^j\mathrm{d}t), \tag{2.10}$$

1 Vector modes are not produced during inflation and we will neglect them in the rest of the discussion.

where N is the so-called lapse and N^i the shift function. Using this formalism, the action in Eq. (1.27) becomes

$$S = \frac{1}{2}\int \mathrm{d}^4x\sqrt{h}\Big[NR^{(3)} - 2NV(\phi) + N^{-1}(E_{ij}E^{ij} - E^2) \tag{2.11}$$

$$+ N^{-1}(\dot{\phi} - N^i\partial_i\phi)^2 - Nh^{ij}\partial_i\phi\partial_j\phi\Big]\,, \tag{2.12}$$

where we have defined

$$E_{ij} = \frac{1}{2}\left(\dot{h}_{ij} - \nabla_i N_j - \nabla_j N_i\right)\,. \tag{2.13}$$

To study perturbations we have expand the inflaton field and the metric around the homogeneous solutions. As we have already pointed out, due to the diffeomorphism invariance, some of the fields we have introduce are redundant. To resolve this redundancy, we have to fix the gauge. For the calculation of inflationary correlation functions, a convenient choice is the so called ζ-gauge. In this gauge the inflaton is unperturbed and all perturbations are in the metric, namely

$$\delta\phi = 0\,, \quad h_{ij} = a^2e^{2\zeta}\left(e^{\gamma}\right)_{ij}\,, \partial_i\gamma_{ij} = 0\,, \quad \gamma_{ii} = 0\,. \tag{2.14}$$

In this gauge, we are left with three physical degrees of freedom: one scalar mode ζ and two polarizations of a transverse and traceless tensor mode γ_{ij}.

To find the action for the perturbations, ζ and γ_{ij} in this gauge, one has to solve the equations of motion for N and N_i. The ADM formalism is designed in such a way that those two functions are not dynamical variables and their equations of motion are (the momentum and hamiltonian) constraints,

$$\begin{aligned}&\nabla_i\left(N^{-1}(E^i_j - \delta^i_j E)\right) = 0,\\ &R^{(3)} - 2V(\phi) - N^{-2}(E_{ij}E^{ij} - E^2) - N^{-2}\dot{\phi}^2 = 0,\end{aligned} \tag{2.15}$$

which can be solved perturbatively. For the purpose of finding the quadratic action, it is enough to solve for N and N_i up to first order in perturbations. For example, the second order solution of N would multiply the hamiltonian constraint that vanishes, because it is evaluated at zeroth order and the solution obeys the equations of motion. If we write

$$N = 1 + \delta N\,, \quad N^i = \partial_i\psi + N^i_T\,, \quad \partial_i N^i_T = 0, \tag{2.16}$$

then from Eq. (2.15) we get the following solutions [26]

$$\delta N = \frac{\dot{\zeta}}{H}\,, \quad N^i_T = 0\,, \quad \psi = -\frac{\zeta}{a^2H} + \chi\,, \quad \partial^2\chi = \frac{\dot{\phi}^2}{2H^2}\dot{\zeta}. \tag{2.17}$$

Now it is straightforward to find the quadratic actions for ζ and γ_{ij}. We have to replace these solutions into eq. (2.11) and expand the action up to second order in perturbations. After some integrations by parts, the quadratic action for ζ takes the following simple form [26]

$$S_\zeta^{(2)} = \frac{1}{2}\int \mathrm{d}^4x\, a^3 \frac{\dot\phi^2}{H^2}\left(\dot\zeta^2 - \frac{1}{a^2}(\partial_i\zeta)^2\right). \tag{2.18}$$

Similarly, the quadratic action for tensor modes is given by

$$S_\gamma^{(2)} = \frac{1}{8}\int \mathrm{d}^4x\, a^3 \left(\dot\gamma_{ij}^2 - \frac{1}{a^2}(\partial_k\gamma_{ij})^2\right) . \tag{2.19}$$

In order to quantize these fields, we first have to canonically normalize them and find the solutions of the classical equations of motion. For example, for ζ, the canonically normalized field is $\zeta^{\mathrm{c}} = \frac{\dot\phi}{H}\zeta$. The equation of motion can be easily obtained from the action (2.18). In momentum space, using conformal time, it reads

$$\zeta^{\mathrm{c}\prime\prime}_{\vec k}(\eta) + 2\mathcal{H}\zeta^{\mathrm{c}\prime}_{\vec k}(\eta) + \vec k^2\zeta^{\mathrm{c}}_{\vec k}(\eta) = 0\,. \tag{2.20}$$

Given that the inflationary background is quasi de-Sitter, we can write $\mathcal{H} = -1/\eta$. Small deviations are captured by the time dependence of the factor $\frac{\dot\phi}{H}$ which is proportional to the slow-roll parameter. The general solution of this equation of motion will contain two modes, described by Hankel functions.

Given a classical solution ζ^{c}, we can quantize the field as

$$\hat\zeta^{\mathrm{c}}_{\vec k}(t) = \zeta^{\mathrm{c}}_{\vec k}(t)\hat a^\dagger_{\vec k} + \zeta^{\mathrm{c}*}_{\vec k}(t)\hat a_{-\vec k}\,, \tag{2.21}$$

where $\hat a_{\vec k}$ and $\hat a^\dagger_{\vec k}$ are annihilation and creation operators. In order to fix the vacuum state, we have to specify additional boundary conditions for the modes. In order to do so, it is sufficient to consider the modes deeply inside the horizon, $k\eta \gg 1$, when we can neglect the curvature effects and choose the standard Minkowski vacuum state. This imposes the conditions on the solution of Eq. (2.20) bringing it to the form

$$\zeta^{\mathrm{c}}_{\vec k}(\eta) = \frac{H}{\sqrt{2k^3}}(1 - ik\eta)e^{ik\eta}\,. \tag{2.22}$$

This form of the modes is the standard Bunch-Davies vacuum [26].

Now we can finally write the 2-point function for scalar perturbations ζ

$$\langle\zeta_{\vec k_1}\zeta_{\vec k_2}\rangle = (2\pi)^3\delta(\vec k_1 + \vec k_2)\frac{H^2}{\dot\phi^2}\left|\zeta^{\mathrm{c}}_{\vec k_1}(\eta)\right|^2 . \tag{2.23}$$

In the late time limit the two-point function becomes

$$\langle \zeta_{\vec{k}_1} \zeta_{\vec{k}_2} \rangle = (2\pi)^3 \delta(\vec{k}_1 + \vec{k}_2) P_s(k_1) \,, \tag{2.24}$$

where the power-spectrum $P(k)$ is given by

$$P_s(k) = \frac{H^4}{\dot{\phi}^2} \frac{1}{2k^3} = \frac{H^2}{2\epsilon M_{\rm P}^2} \frac{1}{2k^3} \,, \tag{2.25}$$

where in the last equality we explicitly reintroduced the Planck mass.

As it become apparent from the solution of the equation of motion, the main advantage of ζ-gauge is that the modes outside the horizon freeze and they do not evolve in time. This implies that any correlation function of ζ will remain frozen once all modes are outside the horizon. Furthermore, ζ has a clear physical meaning: it is directly related to the perturbations of the expansion of the universe. This is easy to see form the form of the line element in ζ-gauge $\mathrm{d}s^2 = a^2 e^{2\zeta} \mathrm{d}\vec{x}^2$, or just by calculating the spatial curvature of the universe that reads $R^{(3)} = 4\partial^2 \zeta$.

Notice that the quantities H and $\dot{\phi}$ entering in the power spectrum have to be evaluated once the mode with a given $\vec{k}$ crosses the horizon, $k \approx aH$. Given that the background inflaton field evolve with time, we expect some small k-dependence of H and $\dot{\phi}$. This small scale dependence is usually parametrized as $P_s(k) \propto k^{-3+(n_s-1)}$. From Eq. (2.25) we can explicitly calculate the scalar tilt n_s of the power spectrum. Using $k \approx aH$ we get

$$n_s - 1 \equiv \frac{\mathrm{d}\log k^3 P_s(k)}{\mathrm{d}\log k} = k \frac{\mathrm{d}}{\mathrm{d}k} \log \frac{H^4}{\dot{\phi}^2} = \frac{1}{H} \frac{\mathrm{d}}{\mathrm{d}t} \log \frac{H^4}{\dot{\phi}^2} = 2\eta - 6\epsilon \,. \tag{2.26}$$

In the quadratic model we discussed in Sec. 1.4.2, $\eta = \epsilon$ and we see that we expect to find a small negative tilt of the power spectrum. Indeed, the current best measured value of the tilt is $n_s = 0.967 \pm 0.004$ at $1\,\sigma$ [11], in agreement with the prediction of the simplest inflationary models.

The same procedure can be repeated to find the power spectrum of tensor modes. In this case, the expansion in Fourier modes is only complicated by the polarization of gravitons ϵ^s_{ij}. With this taken into account, we can write

$$\gamma_{ij}(t, \vec{x}) = \int \frac{\mathrm{d}^3\vec{k}}{(2\pi)^3} \sum_{s=\pm} \epsilon^s_{ij}(\vec{k}) \gamma^s_{\vec{k}}(t) e^{i\vec{k}\cdot\vec{x}} \,, \tag{2.27}$$

where $\epsilon^s_{ii}(\vec{k}) = 0$, $k^i \epsilon^s_{ij}(\vec{k}) = 0$ and $\epsilon^s_{ij}(\vec{k}) \epsilon^{s'}_{ij}(\vec{k}) = 2\delta_{ss'}$. The two point function is given by [26]

$$\langle \gamma^s_{\vec{k}_1} \gamma^{s'}_{\vec{k}_2} \rangle = (2\pi)^3 \delta(\vec{k}_1 + \vec{k}_2) P_t(k_1) \delta_{ss'} \,, \tag{2.28}$$

where the power spectrum is

$$P_t(k) = \frac{8H^2}{M_{\rm P}^2}\frac{1}{2k^3}. \tag{2.29}$$

Notice that in this expression the only variable is the Hubble scale during inflation H. Therefore, the detection of primordial gravitational waves would tell us about the energy scale at which inflation happens. Taking the ratio between the tensor and the scalar power spectrum, we have

$$r \equiv \frac{P_t(k)}{P_s(k)} = 16\epsilon. \tag{2.30}$$

For large-field inflationary models, the tensor-to-scalar ration r is of order $\mathcal{O}(0.1)$. Currently there is no detection of primordial tensor modes in the CMB. The best current limit on the tensor-to-scalar ratio is $r < 0.08$ at 95% C.L. [11].

In the same way as for scalars, we can also calculate the tilt of the power spectrum for tensors. It is simply given by

$$n_t \equiv \frac{{\rm d}\log k^3 P_t(k)}{{\rm d}\log k} = k\frac{\rm d}{{\rm d}k}\log\frac{H^2}{M_{\rm P}^2} = -2\epsilon. \tag{2.31}$$

Notice that in four observables related to the power spectra of scalars and tensors we have only three parameters: ϵ, η and H. This is probably the most distinctive and robust consistency check of the inflationary phase. However, as we will comment later in Sec. 6 this relation is hardly going to be measured in ongoing CMB experiments.

2.2.2 *Non-Gaussianities*

In this section we turn to higher order correlation functions. They are very important because they carry information about interactions of the inflaton. Given that the inflationary potential is expected to be very flat, the interactions are expected to be suppresed. Therefore, one can say that in inflation the generic prediction is that initial curvature perturbation field is highly Gaussian, which is indeed what we observe in the CMB. However, non-Gaussianities are a very important tool in constraining inflationary models: even in the absence of any feature we would understand what in this phase was not happening.

In order to calculate higher order correlation functions one has to find the action to higher order in perturbations ζ or γ. This is not a straightforward

task. To illustrate the procedure, in this Section we will focus only on the cubic action for ζ and the corresponding three-point function. It turns out that in order to do so we do not have to solve for N and N_i neither at second nor at third order in perturbations. As before, the third order term would multiply the momentum and hamiltonian constraints evaluated at zeroth order on the solution of the equations of motion. The second order term would multiply constraints evaluated using eq. (2.17), but it turns out that this contribution is zero too. In conclusion, the first order solution (2.17) is all we need.

With this simplifications, the expansion of the action is (2.11) is straightforward. The final result is given by [26]

$$S_\zeta^{(3)} = \int \mathrm{d}^4x \left[a e^{\zeta} \left(1 + \frac{\dot\zeta}{H}\right) \left(-2\partial^2\zeta - (\partial\zeta)^2\right) + \epsilon a^3 e^{3\zeta} \dot\zeta^2 \left(1 - \frac{\dot\zeta}{H}\right) + \right.$$
$$\left. + a^3 e^{3\zeta} \left(\frac{1}{2} \left(\partial_i\partial_j\psi\partial_i\partial_j\psi - (\partial^2\psi)^2\right) \left(1 - \frac{\dot\zeta}{H}\right) - 2\partial_i\psi\partial_i\zeta\partial^2\psi \right) \right] , \tag{2.32}$$

where ψ is given by eq. (2.17).

Using field redefinitions this action can be further simplified, which makes the calculation of the three-point function much easier. We will not repeat this procedure here, because it is not essential to describe the main steps of the calculation (for details see [26]). The most important difference compared to the standard QFT calculation is that we are not interested in scattering amplitudes but correlation functions. Therefore, in the interaction picture, the expectation value of an operator $\mathcal{O}$ is given by [26, 27]

$$\langle \mathcal{O} \rangle = \langle 0 | \bar{T} e^{i \int_{-\infty(1+i\epsilon)}^{t} H_{int} \mathrm{d}t'} \, \mathcal{O} \, T e^{-i \int_{-\infty(1-i\epsilon)}^{t} H_{int} \mathrm{d}t'} | 0 \rangle \ , \tag{2.33}$$

where H_{int} is an interaction Hamiltonian. This formalism is known as "in-in" formalism instead of what is usually computed in QFT

$$\langle \mathcal{O} \rangle = \langle 0 | T \, \mathcal{O} \, e^{-i \int_{-\infty(1-i\epsilon)}^{+\infty(1+i\epsilon)} H_{int} \mathrm{d}t'} | 0 \rangle, \tag{2.34}$$

that correspond to "in-out". Indeed, we evolve the vacuum using the evolution operator until some moment of time t, insert the operator $\mathcal{O}$ and then we evolve backwards in time. Notice that in order to project to the vacuum of the theory we had to deform the lower boundary of the integral. Here we use the standard $i\epsilon$ prescription.

The expectation value in eq. (2.33) is calculated in the standard way using the expansion of ζ in creation and annihilation operators (2.21) and Wick's theorem. For example, using the action (2.32), the three-point function of ζ is at the end given by

$$\langle \zeta_{\vec{k}_1} \zeta_{\vec{k}_2} \zeta_{\vec{k}_3} \rangle' = \frac{H^4}{4\epsilon^2 M_{\rm P}^4} \frac{1}{\prod(2k_i^3)} \left[(2\eta - 3\epsilon) \sum_i k_i^3 + \epsilon \sum_{i \neq j} k_i k_j^2 + \epsilon \frac{8}{k_t} \sum_{i>j} k_i^2 k_j^2 \right], \tag{2.35}$$

where $k_t = k_1 + k_2 + k_3$ and prime on the correlation function means that we have removed $(2\pi)^3 \delta(\vec{k}_1 + \vec{k}_2 + \vec{k}_3)$ form the expression. In the same way one can calculate the other three-point functions involving gravitons, or higher order correlation functions.

The calculation presented here was based on a single-field slow-roll inflationary model, and it is not valid for example for the model introduced in Sec. 1.4.3. The method for calculating the correlation functions is however very similar. To calculate the three point function, starting from the Lagrangian Eq. (1.41), one has to expand the action up to cubic order, find the interaction Hamiltonian and use the standard in-in formalism. Following [28, 29] we can write the n-point function as

$$\langle \zeta_{\vec{k}_1} \cdots \zeta_{\vec{k}_n} \rangle = (2\pi)^3 \delta(\vec{k}_1 + \cdots + \vec{k}_n) P_\zeta^{n-1} \prod_{i=1}^{n} \frac{1}{k_i^3} \mathcal{M}^{(n)}(\vec{k}_1, ..., \vec{k}_n) \tag{2.36}$$

and the two-point function as

$$\langle \zeta_{\vec{k}_1} \zeta_{\vec{k}_2} \rangle = (2\pi)^3 \delta(\vec{k}_1 + \vec{k}_2) P_\zeta \frac{1}{2k_1^3}, \quad P_\zeta = \frac{1}{2M_{\rm P}^2} \frac{H^2}{c_s \epsilon}, \tag{2.37}$$

with the speed of sound defined as in Eq. (1.46).

The amplitude of the three-point function as calculated in [28, 29] reads

$$\begin{aligned} \mathcal{M}^{(3)} = & \left(\frac{1}{c_s^2} - 1 - \frac{2\lambda}{\Sigma} \right) \frac{3k_1^2 k_2^2 k_3^2}{2k_t^3} \\ & + \left(\frac{1}{c_s^2} - 1 \right) \left(-\frac{1}{k_t} \sum_{i>j} k_i^2 k_j^2 + \frac{1}{2k_t^2} \sum_{i \neq j} k_i^2 k_j^3 + \frac{1}{8} \sum_i k_i^3 \right), \end{aligned} \tag{2.38}$$

where the parameters λ and Σ are related to derivatives of the function P with respect to X

$$\begin{aligned} \lambda &= X^2 P_{XX} + \frac{2}{3} X^3 P_{XXX}, \\ \Sigma &= X P_X + 2X^2 P_{XX}. \end{aligned} \tag{2.39}$$

In the squeezed limit the three-point function becomes

$$\langle \zeta_{\vec{q}} \zeta_{\vec{k}_1} \zeta_{\vec{k}_2} \rangle'_{\vec{q}\to 0} = P_\zeta(k) P_\zeta(q) \left[\left(-1 + \frac{1}{c_s^2} \right) \left(-2\frac{q^2}{k^2} + \frac{5}{4} \frac{(\vec{q}\cdot\vec{k})^2}{k^4} \right) - \frac{3}{2} \frac{q^2}{k^2} \frac{\lambda}{\Sigma} \right] . \tag{2.40}$$

There is however one important difference between the two models we described. They predict very different "shapes" of non-Gaussianities [30]. Given that the interactions in slow-roll models are local they peak in squeezed configuration, when one of the momenta is much smaller than the others $k_1 \ll k_2, k_3$ [30]. This kind of non-Gaussianities are called local and their amplitude is parametrized by $f_{\rm NL}^{\rm loc}$. On the other hand, for derivative interactions, the three-point function has a maximum in configuration where all momenta have similar magnitudes $k_1 \approx k_2 \approx k_3$ [30, 31]. For these reason this situation corresponds to equilateral non-Gaussianities parametrized by $f_{\rm NL}^{\rm eq}$. The current constraint form Planck on these two parameters are [32]

$$f_{\rm NL}^{\rm loc} = 0.8 \pm 5.0 \, , \quad f_{\rm NL}^{\rm eq} = -4 \pm 43 \, . \tag{2.41}$$

It is important to stress that although in general non-Gaussianities can be large, local non-Gaussianities in *any* single-field model of inflation must be always very small. As we are going to see later, this is one of the main consequences of Maldacena's consistency relations for inflation.

Let us close this Section saying that, although we used some particular models to introduce non-Gaussianities, there exists a general, model-independent approach to study small fluctuations of the inflaton and their correlation functions. It is based on the effective field theory approach to inflation. The Effective Field Theory of Inflation was first formulated for single-field models [33] and later generalized to multi-field inflation [34]. In the EFT of inflation one writes down all possible operators compatible with the symmetry. Different inflationary models then correspond to a different choice of the parameters of the effective action.

2.3 CONSISTENCY RELATIONS

In single-field inflation, correlation functions of the curvature perturbation ζ and of tensor modes satisfy general, model-independent relations in the limit in which one of the momenta (or the sum of some of the momenta) becomes very small compared to the others: the so-called consistency relations

[26, 35–42]. Physically, they are based on the observation that the effect of a long mode on the dynamics of the short ones reduces to a diffeomorphism.

In this Section we will focus on the squeezed limit of correlation functions involving only scalar modes ζ at zeroth order in the long momentum, obtaining the so-called Maldacena's consistency relation [26].This relation has been generalized to include gradients of the long mode, obtaining the so-called conformal consistency relation [37].

The physical argument behind the consistency relations [26, 35] is based on the observation that in the squeezed limit of an $(n+1)$-point function, the configuration in which one mode is much longer than the other and is far out of the horizon, the long mode is equivalent to a classical background. Therefore, the long mode can be removed by a suitable change of coordinates. This change of coordinates relates two solutions, one with and without the long mode, and consequently it relates the squeezed $(n+1)$-point and n-point correlation functions.

Starting from real space, we have

$$\langle \zeta(x_1)\cdots\zeta(x_n)\rangle_{\zeta_L} = \langle \zeta(\tilde{x}_1)\cdots\zeta(\tilde{x}_n)\rangle \,, \tag{2.42}$$

where on the left hand side the correlation function is evaluated in the presence of a long background mode, while on the right hand side the latter has been reabsorbed in a change of coordinates. Multiplying both sides with ζ_L and average over it we find that

$$\Big\langle \zeta_L(x)\langle \zeta(x_1)\cdots\zeta(x_n)\rangle_{\zeta_L}\Big\rangle = \Big\langle \zeta_L(x)\langle \zeta(\tilde{x}_1)\cdots\zeta(\tilde{x}_n)\rangle\Big\rangle \,. \tag{2.43}$$

Written in this form the left hand side is just an $(n+1)$-point function involving ζ_L and n short modes. On the other hand, on right hand side, $\tilde{x}$ contains ζ_L and in general one cannot find the average over ζ_L easily. However, by expanding the n-point function around $\tilde{x} = x + \delta x$, we have

$$\langle \zeta(\tilde{x}_1)\cdots\zeta(\tilde{x}_n)\rangle = \langle \zeta(x_1)\cdots\zeta(x_n)\rangle + \sum_{a=1}^{n} \delta x_{ai}\cdot\partial_{ai}\langle \zeta(x_1)\cdots\zeta(x_n)\rangle + \cdots \,. \tag{2.44}$$

The first term on the right hand side, once plugged into Eq. (2.43) averages to zero because it is proportional to $\langle\zeta_L\rangle$. Therefore, the only relevant contribution comes from the variation of the n-point function

$$\delta\langle \zeta(x_1)\cdots\zeta(x_n)\rangle = \sum_{a=1}^{n} \delta x_{ai}\cdot\partial_{ai}\langle \zeta(x_1)\cdots\zeta(x_n)\rangle \,. \tag{2.45}$$

Finally, in real space the consistency relation reads

$$\langle\zeta_L(x)\zeta(x_1)\cdots\zeta(x_n)\rangle = \left\langle \zeta_L(x)\cdot\sum_{a=1}^{n}\delta x_{ai}\cdot\partial_{ai}\langle\zeta(x_1)\cdots\zeta(x_n)\rangle\right\rangle . \quad (2.46)$$

To derive Maldacena's consistency relation, we have to specify the change of coordinates δx. At leading order in derivatives, the long mode is equivalent just to a simple time-independent rescaling of spatial coordinates

$$x^i \;\to\; x^i + \zeta_L(\vec{x}_+)x^i \,. \quad (2.47)$$

For the homogeneous long mode the point $\vec{x}_+$ is arbitrary, and for concreteness we will take $\vec{x}_+ = (\vec{x}_1+\cdots+\vec{x}_n)/n$. Using $\delta\vec{x} = \zeta_L(\vec{x}_+)\vec{x}$ in Eq. (2.45), the variation of an n-point function is

$$\begin{aligned}\delta\langle\zeta(x_1)\cdots\zeta(x_n)\rangle &= \int\frac{\mathrm{d}\vec{q}_+}{(2\pi)^3}\mathrm{dK}_n\;\zeta_{\vec{q}_+}\sum_a \mathcal{M}\delta(\vec{P})k_{ai}\partial_{k_{ai}}e^{i\vec{q}_+\cdot\vec{x}_+ + i\vec{k}_b\cdot\vec{x}_b}\\ &= -\int\frac{\mathrm{d}\vec{q}_+}{(2\pi)^3}\mathrm{dK}_n\;\zeta_{\vec{q}_+}\sum_a\left(3\mathcal{M}\delta(\vec{P}) + k_{ai}\partial_{k_{ai}}\mathcal{M}\delta(\vec{P}) + k_{ai}\mathcal{M}\partial_{k_{ai}}\delta(\vec{P})\right)e^{i\vec{q}_+\cdot\vec{x}_+ + i\vec{k}_b\cdot\vec{x}_b}\,,\end{aligned} \quad (2.48)$$

where

$$\mathrm{dK}_n \equiv \frac{\mathrm{d}\vec{k}_1}{(2\pi)^3}\cdots\frac{\mathrm{d}\vec{k}_n}{(2\pi)^3}\,,\quad \mathcal{M}\equiv\langle\zeta_{\vec{k}_1}\cdots\zeta_{\vec{k}_n}\rangle'\,,\quad \vec{P}\equiv\vec{k}_1+\cdots+\vec{k}_n\,, \quad (2.49)$$

After an explicit calculation, one can finally write

$$\delta\langle\zeta(x_1)\cdots\zeta(x_n)\rangle = -\int\frac{\mathrm{d}\vec{q}_+}{(2\pi)^3}\mathrm{dK}_n\;\zeta_{\vec{q}_+}\left[\left(3(n-1)+\sum_a k_{ai}\partial_{k_{ai}}\right)\mathcal{M}\right]\delta(\vec{P})e^{i\vec{q}_+\cdot\vec{x}_+ + i\vec{k}_b\cdot\vec{x}_b}\,. \quad (2.50)$$

where now derivatives act only on $\mathcal{M}$. After multiplying this expression by the long mode $\zeta_L(x)$, averaging over it and going to Fourier space, we get Maldacena's consistency relation [26]

$$\langle\zeta_{\vec{q}}\zeta_{\vec{k}_1}\cdots\zeta_{\vec{k}_n}\rangle'_{\vec{q}\to 0} = -P(q)\left(3(n-1)+\sum_a k_{ai}\partial_{k_{ai}}+\mathcal{O}(q/k)\right)\langle\zeta_{\vec{k}_1}\cdots\zeta_{\vec{k}_n}\rangle'\,. \quad (2.51)$$

For the 3-point function this expression greatly simplify. Using the expression for the power spectrum in Eq. (2.25) one finds

$$\langle\zeta_{\vec{q}}\zeta_{\vec{k}_1}\zeta_{\vec{k}_2}\rangle'_{\vec{q}\to 0} = -P(q)P(k_1)\,(n_s-1)\,. \quad (2.52)$$

Part II

POWER SPECTRA

3

TESTING THE SIMPLEST POTENTIALS

3.1 MOTIVATIONS

The detection of B-modes in the polarization of the cosmic microwave background (CMB) by BICEP2 [43] has recently revamped the interest in inflationary models with a high level of primordial tensor modes. This requires [44] a large excursion of the inflaton during inflation $\Delta\phi \gtrsim M_{\rm P}$, which challenges the naive expectation that higher-dimension operators, suppressed by powers of $M_{\rm P}$, spoil the slow-roll conditions. Before the announcement of the BICEP2 collaboration, the crucial question for inflation was "large or small r?" However, the size of tensor modes measured by BICEP2 and an erroneous account of foregrounds led to face a new dichotomy: "ϕ^2 or not ϕ^2?" The two possibilities are qualitatively different. A large field model that is not quadratic, say $V \propto \phi^{2/3}$, suggests an interesting UV mechanism, such as monodromy inflation [45], for instance. If data had favored, on the other hand, a quadratic potential, the simplest explanation would have been that inflation occurs at a generic minimum of a potential whose typical scale of variation f is much larger than the Planck scale. Indeed, an approximate shift symmetry gives rise to potentials that are periodic in ϕ/f, such as, for instance, $V = \Lambda^4(1-\cos(\phi/f))$ [46, 47]. For $f \gg M_{\rm P}$, inflation occurs near a minimum of the potential, where one can approximate $V \propto \phi^2$. In string theory, it seems difficult to obtain a parametric separation between f and $M_{\rm P}$, although there is no issue at the level of field theory [48, 49]. Therefore, if quadratic inflation remained compatible with the data, it would have been important to study small deviations from it, in order to understand to which extent the quadratic approximation holds and to limit other possible deviations from the simplest scenario of inflation.

Inflationary predictions must face our ignorance about the reheating process and the subsequent evolution of the Universe. All this is encoded in the number of e-folds N between when the relevant modes exit the horizon and the end of inflation. The dependence on N is rather strong (see Fig. 5)

and it will possibly become larger than the experimental sensitivity on n_s and r. To study small deviations from $V = \frac{1}{2}m^2\phi^2$, we have to concentrate on a combination of observables that does not depend on N ([1]). At linear order in $1/N$, given that for a quadratic potential $n_s - 1 = -2/N$ and $r = 8/N$, a prediction that is independent of N is obviously $(n_s - 1) + r/4 = 0$. Since corrections at second order in slow roll might not be completely negligible in the future, it is worthwhile to go to order $1/N^2$. With the use of the explicit formulas at second order in slow roll [50], it is straightforward to verify[2] that for a quadratic potential

$$(n_s - 1) + \frac{r}{4} + \frac{11}{24}(n_s - 1)^2 = 0\,, \tag{3.1}$$

up to corrections of order N^{-3} ([3]), which we can safely ignore. Assuming that data favours a ϕ^2 potential we can use the equation above to study how sensitive we will be to small departures from the simplest scenario. If we take the measurement of the tilt from Planck [11] $n_s - 1 = -0.032 \pm 0.004$ and the value of r measured by BICEP2 [43] $r = 0.20^{+0.07}_{-0.05}$, the lhs of Eq. (3.1) is equal to 0.02 ± 0.02 ([4]). Optimistically, for large tensor modes, we can assume we will be able to measure r with a precision of 1% [51]. Regarding $n_s - 1$, future experiments such as EUCLID [52] or PRISM [53] should be able to go down to a 10^{-3} error. Therefore, the uncertainty on

1 The power spectrum normalization fixes $m \simeq 1.5 \times 10^{13}\,\mathrm{GeV}$, $V \simeq (2 \times 10^{16}\,\mathrm{GeV})^4$ and $\Delta\phi \simeq 15\,M_\mathrm{P}$, assuming $N = 60$.

2 Up to second order in slow roll we have

$$n_s - 1 = 2\eta - 6\epsilon - 2C(12\epsilon^2 + \xi) + \frac{2}{3}(\eta^2 - 5\epsilon^2 + \xi) + (16C - 2)\eta\epsilon\,,$$
$$r = 16\epsilon\left[1 - \frac{4\epsilon}{3} + \frac{2\eta}{3} + 2C(2\epsilon - \eta)\right]\,,$$

where $C \equiv -2 + \ln 2 + \gamma$, with $\gamma = 0.57721\ldots$ the Euler-Mascheroni constant, and the slow-roll parameters are defined as

$$\epsilon \equiv \frac{M_\mathrm{P}^2}{2}\left(\frac{V'}{V}\right)^2\,, \quad \eta \equiv M_\mathrm{P}^2\frac{V''}{V}\,, \quad \xi \equiv M_\mathrm{P}^4\frac{V'''V'}{V^2}\,.$$

3 Up to $1/N^3$ corrections we can equivalently write $(n_s - 1) + r/4 + 11/384 \cdot r^2 = 0$. This form can be useful in future given that the error on $(r/4)^2$ is expected to be smaller than the one on $(n_s - 1)^2$.

4 The current understanding of foregrounds lead to a quite different best fit value for the tensor-to-scalar ratio, $r < 0.08$ at 2σ [11]. This value strongly depends on the data set used for the analysis and the extrapolation in frequency of foregrounds. The bottom line is that to our best knowledge the ϕ^2-consistency relation is violated at 3σ.

the quantity above will be $\sim 10^{-3}$, dominated by the error on the spectral index. Notice that different experiments are sensitive to different scales k. Given that Eq. (3.1) is independent of N, it is valid on any scale provided that both n_s and r are evaluated at the same k. Therefore, it is important to keep in mind that the experimental results have to be properly combined at the same scale[5].

Let us now study what these futuristic limits would imply for deviations from the simplest model of the Universe.

3.2 PSEUDO-NAMBU-GOLDSTONE BOSON POTENTIAL

A PNGB has a potential of the form $V = \Lambda^4 F(\phi/f)$ ([6]), where Λ is the scale of breaking of the approximate shift symmetry, F is a periodic function and f is the decay constant. The simplest example is given by

$$V(\phi) = \Lambda^4 \left[1 - \cos\left(\frac{\phi}{f}\right)\right] , \tag{3.2}$$

where f has to be bigger than $M_{\rm P}$ in order for the slow-roll conditions to be satisfied and for very large $f \gg M_{\rm P}$ the model becomes indistinguishable from a ϕ^2 potential. For this potential, Eq. (3.1) will not be exactly zero. It is easy to calculate the leading correction in slow roll and for $M_{\rm P}/f \ll 1$

$$n_s - 1 = -\frac{2}{N} + \mathcal{O}\left(\frac{M_{\rm P}}{f}\right)^4 , \qquad r = \frac{8}{N} - 4\left(\frac{M_{\rm P}}{f}\right)^2 . \tag{3.3}$$

This gives a correction to Eq. (3.1)

$$(n_s - 1) + \frac{r}{4} + \frac{11}{24}(n_s - 1)^2 = -\left(\frac{M_{\rm P}}{f}\right)^2 . \tag{3.4}$$

If the error on the lhs is of order 10^{-3}, this translates into the limit $f \gtrsim 30 M_{\rm P}$. This would convincingly suggest there is a parametric separation between the two scales, which the UV theory would have to address. To illustrate this point, in Fig. 5 we present a plausible forecast for the future observations in the (n_s, r) plane together with the predictions of natural inflation for different values of f.

5 This is the case also for BICEP2 and Planck, but with the current errors this difference is negligible.

6 In the extra-dimensional model of Ref. [48], the explicit form of F depends on the number of particles, their charges, masses, and boundary conditions.

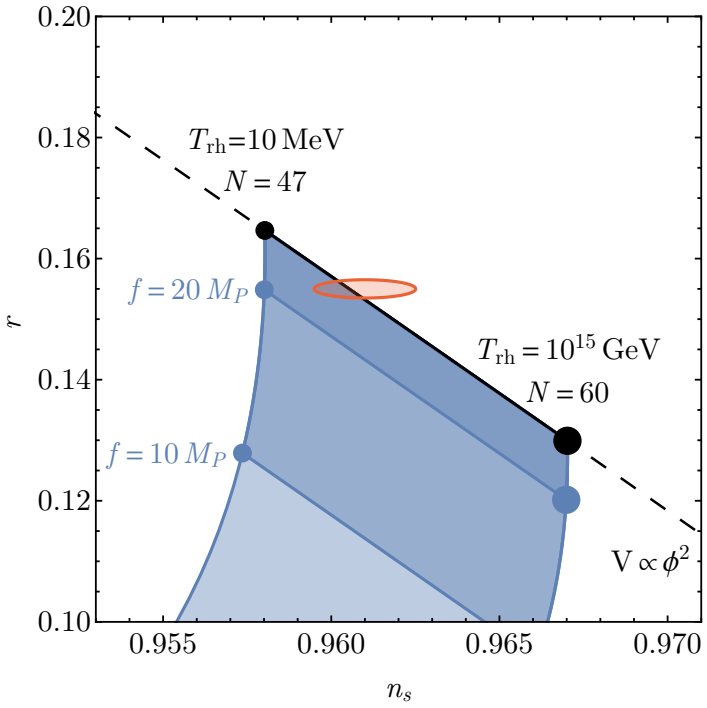

Figure 5: *Possible constraints on f assuming a simple cosine potential. The dashed curve corresponds to Eq. (3.1), and the black segments cover the interval of reheating temperatures $T_{\rm rh} \in [10\ \text{MeV}, 10^{15}\ \text{GeV}]$. A wider range of N is allowed if one considers nonstandard cosmological evolutions after inflation. Red 1σ contour corresponds to a futuristic measurement with $\sigma_{n_s-1} = \sigma_r = 10^{-3}$, compatible with a quadratic potential. All quantities are evaluated at $k = 0.002\ \text{Mpc}^{-1}$.*

For a generic F expanding around the minimum we get

$$V(\phi) = \Lambda^4 \left(\frac{1}{2}\frac{\phi^2}{f^2} + \frac{F^{(3)}}{6}\frac{\phi^3}{f^3} + \frac{F^{(4)}}{24}\frac{\phi^4}{f^4} + \cdots \right) . \tag{3.5}$$

For the following analysis, we assume $F^{(n)}$ to be of order 1. For the moment, let us assume the function F is symmetric around the minimum. Notice that with positive $F^{(4)}$ we can get n_s and r above the $m^2\phi^2$ curve, unlike in the case of a simple cosine potential (see Fig. 5). At leading order in slow roll

$$(n_s - 1) + \frac{r}{4} + \frac{11}{24}(n_s - 1)^2 = F^{(4)} \left(\frac{M_{\rm P}}{f} \right)^2 , \tag{3.6}$$

and one can constrain the combination on the rhs $f/\sqrt{|F^{(4)}|} \gtrsim 30 M_{\rm P}$. Therefore, for $F^{(4)}$ of order one, this does not change the lower bound on f significantly.

If we now allow for nonzero $F^{(3)}$ and the cubic term dominates, Eq. (3.1) reads

$$(n_s - 1) + \frac{r}{4} + \frac{11}{24}(n_s - 1)^2 = \pm\frac{2}{3}\sqrt{2\epsilon}\, F^{(3)} \frac{M_{\rm P}}{f} \,, \tag{3.7}$$

where the sign depends on whether inflation occurs for positive or negative values of ϕ. The constraint on the rhs imposes[7] $f/F^{(3)} \gtrsim 86 M_{\rm P}$. Notice that in this case the lower bound on f is even stronger.

3.3 GENERAL DEVIATIONS FROM ϕ^2

One can use the same technique to constrain other deviations from the simplest scenario: they will all contribute to the rhs of Eq. (3.1). Let us first focus on small deviations from $m^2\phi^2$ coming from the shape of the potential (see for example, Refs. [54, 55]). It is straightforward to obtain the corrections to Eq. (3.1) for a generic $V(\phi)$ up to second order in slow-roll parameters

$$(n_s - 1) + \frac{r}{4} + \frac{11}{24}(n_s - 1)^2 = -2(\epsilon - \eta) \,. \tag{3.8}$$

Notice that on the rhs of Eq. (3.8) we keep only the first nonvanishing correction.

Another kind of corrections comes from derivative interactions. Indeed, from the effective field theory point of view quantum corrections will generate higher-dimensional operators suppressed by some scale Λ. Particularly important are the operators compatible with an approximate shift symmetry for ϕ. For example, a term of the form $(\partial\phi)^4/\Lambda^4$ in the Lagrangian corresponds to a correction to the speed of propagation of the perturbations

$$c_s^2 - 1 = 16\frac{\dot{H} M_{\rm P}^2}{\Lambda^4} \,. \tag{3.9}$$

Therefore, constraints on the speed of sound transfer into constraints on Λ. In models with $c_s < 1$, it is important to stress that $r = 16\epsilon c_s$, whereas $n_s - 1$ is independent of c_s (it only depends on it through $s \equiv \dot{c}_s/Hc_s$). In

7 Here and in the following estimates, to be conservative, we use the minimal value of ϵ that corresponds to the maximal number of e-folds.

the absence of cancellations, the current value for $n_s - 1$ and the detection of a high level of primordial tensor modes imply that c_s cannot be much smaller than 1.

For the case of a quadratic potential, one can quantify the bounds on c_s more precisely in a way that is insensitive to N. The correction to Eq. (3.1) reads

$$(n_s - 1) + \frac{r}{4} + \frac{11}{24}(n_s - 1)^2 = -s + \frac{r}{4}\left(1 - \frac{1}{c_s}\right) . \tag{3.10}$$

If the total error on the lhs is of the order 10^{-3}, $|c_s - 1|$ is constrained to be $\lesssim 3 \times 10^{-2}$. In particular, we can put a lower bound on the energy scale Λ to be $\Lambda \gtrsim 2 \times 10^{16}$ GeV which is as high as the inflationary scale.

Another way to constrain c_s is to use the standard consistency relation for the tilt of tensor modes n_T

$$r + 8n_T = \left(1 - \frac{1}{c_s}\right) r . \tag{3.11}$$

This relation has the major advantage of being valid for any potential, but it is difficult to imagine we will be able to verify it with significant precision. Given that from CMB experiments it will be hard to measure n_T with a precision better than $\Delta n_T \sim 0.1$, the constraint on c_s is weaker than the one obtained above. However, in the very far future we might be able to constrain r and n_T much better by the detection of primordial gravitational waves with interferometers [56]. Optimistically, the error on n_T could be as low as 5×10^{-3} and the relation of Eq. (3.11) could constrain c_s even better than Eq. (3.10).

Another possible departure from the simplest model is the presence of a subdominant component in the spectrum due to a second field. In these models (curvaton, modulated reheating, etc.) inflation is driven by the inflaton, but a second scalar field σ is contributing to the curvature perturbation with a fraction

$$q \equiv \frac{P_\zeta^\sigma}{P_\zeta^\phi + P_\zeta^\sigma} , \tag{3.12}$$

where P_ζ^x is the contribution of the field x to the power spectrum of the curvature perturbation ζ. The correction to Eq. (3.1) up to first order in slow roll is

$$(n_s - 1) + \frac{r}{4} + \frac{11}{24}(n_s - 1)^2 = q\left(-\frac{r}{8} + \frac{2}{3}\frac{V_\sigma''}{H^2}\right) . \tag{3.13}$$

Assuming that the error on the lhs of Eq. (3.13) is 10^{-3}, this relation constraints $q \lesssim 0.06$.

One may consider the case in which different corrections to the rhs of Eq. (3.1) cancel, so that we accidentally get the same predictions as the ϕ^2 model. In this case, one can hope to break the degeneracy by looking at the running of the power spectrum. For a quadratic potential $\alpha = -(n_s - 1)^2/2 = -r^2/32 \simeq 8 \times 10^{-4}$.

3.4 CONSTRAINTS ON N

So far, we have focused on a combination of observables that is N independent. On the other hand, for a quadratic potential one will also get a good constraint on the number of e-folds. With the numbers quoted above, the best constraint would come from r, which will give $\Delta N \simeq 0.4$. This translates into an error on the reheating temperature

$$\frac{\Delta T_{\rm rh}}{T_{\rm rh}} \simeq 1.2 \,, \tag{3.14}$$

assuming we know the evolution after reheating. Notice that while it is easy to reduce N (longer reheating, periods of matter domination or phase transitions in the late universe, large number of relativistic degrees of freedom g_*), the upper bound on N corresponding to instantaneous reheating and conventional cosmological evolution is very robust. In some sense, it corresponds to the very simplest Universe.

3.5 WHAT IF NOT ϕ^2?

All the discussion so far concentrated on ϕ^2 inflation. If nature has chosen another monomial potential $V \propto \phi^p$, as data currently suggests, we can still build an observable which does not depend on N. It is easy to get

$$(n_s - 1) + \frac{2+p}{8p} r + \frac{3p^2 + 18p - 4}{6(p+2)^2} (n_s - 1)^2 = 0 \,. \tag{3.15}$$

As before we will have errors of order 10^{-3} on this expression[8]. It is straightforward to generalize Eqs. (3.10) and (3.13) to analyze the constraints on

8 Notice that in eq. (3.15) as we go to lower values of p the coefficient of r increases: the tensor contribution becomes more and more important to discriminate the model.

the speed of sound or the presence of a curvaton component. One can also invert Eq. (3.15) to find the allowed range of p. This reads

$$p = -\frac{2r}{8(n_s-1)+r} - \frac{64(n_s-1)^3}{(8(n_s-1)+r)^2} + (n_s-1) - \frac{7}{24}r\,. \tag{3.16}$$

For "normal" powers we will be quite convinced we have found the correct model of inflation. With the current errors the bounds on p are too loose to be interesting, but this may change in the future. For example, for a linear potential the error will be $\Delta p \simeq 0.06$, and this will allow discrimination of this model from $\phi^{2/3}$.

Non-Gaussianity.—So far our discussion has concentrated on the power spectra: what about higher-order correlation functions? As discussed above, in single-field models (independently of the potential) r is suppressed by c_s, so that the speed of sound cannot be much smaller than 1. Therefore, the cubic operator related by symmetry to c_s [33] cannot give sizeable non-Gaussianities since $f_{\rm NL}^{\rm eq} \sim 1/c_s^2$ (the Planck constraint [32] is $c_s \geq 0.024$ at 2σ). However the second independent operator $\dot\pi^3$ can still be large. It is straightforward to check that this situation is radiatively stable [57]: loops induce order-one corrections to the speed of sound. Moreover, the three-point function can be large for $c_s = 1$ if it is generated by operators with more than one derivative per field [58]. Another possibility is that the four-point function is large, while the bispectrum is suppressed: this can happen in a technically natural way as studied in Refs. [59]. Non-Gaussianities are also relevant if scalar and tensor perturbations are both produced through particle creation involving dissipative effects [60, 61].

Also, in multifield models r is always suppressed compared to the single-field case (by a factor of q assuming no mixing). It is, thus, unlikely that perturbations are dominated by a second field. However, when the perturbations due to the second field become very non-Gaussian, they induce a large observable non-Gaussianity $f_{\rm NL} \simeq 10^5 q^{3/2}$, even when they are subdominant in the power spectrum [34]. Notice that the shape of non-Gaussianity can vary from local to equilateral if we consider general quasi-single-field models [62, 63]. In conclusion, non-Gaussianities remain a powerful probe of inflation.

3.6 CONCLUSIONS

Any experimental result on the (n_s, r) plane can be explained with a proper choice of the slow-roll parameters ϵ and η. On the other hand a particular curve on this plane stands out since it corresponds to the prediction of $V \propto \phi^2$, varying the number of e-folds N. Assuming data are compatible with this simple scenario, we studied the constraints we will be able to set on various deviations from the benchmark model.

4

ACCURATE PREDICTIONS FOR LARGE-FIELD MODELS

4.1 INTRODUCTION

As we argued in the previous section, one relevant point of measuring large tensor modes is that it will be possible in future observations to ultimately measure r with a precision of 1% [51]. This precision requires both to go to second order in slow-roll and to know the number of e-folds N up to $\Delta N \sim 0.5$ [4]. Thus, one has to specify the details of reheating (for a recent study see [64]) and include subleading corrections in the predictions of r and n_s, which are usually neglected.

In this section we focus on the inflationary model $V = \frac{1}{2}m^2\phi^2$, both because it is simple and because it is the only case in which predictions can be made without further assumptions about the behavior of the potential between the inflationary region and the final minimum. We provide improved formulas for n_s and r that are correct up to 1% relative errors, in the limit of fast reheating (the details turn out to be irrelevant as long as the energy is transferred to radiation fast enough) and with a standard expansion history after inflation. Deviations from this scenario, such as a slower reheating, entropy injections due to phase transitions, higher number of degrees of freedom at reheating, additional periods of matter dominance or inflation, move the predictions in the direction of higher r and lower n_s. In this sense, the values for n_s and r we provide are the "endpoint" on the line in the (n_s, r) plot for $V = \frac{1}{2}m^2\phi^2$, corresponding to the largest possible N. This point deserves special attention, because in some sense it is the most informative place in the (n_s, r) plane: if data eventually converge there, it will be possible to have strong bounds on any deviation from this minimal scenario.

4.2 PREDICTIONS FOR INSTANTANEOUS REHEATING

In order to determine the point in the (n_s, r) plane that corresponds to the limit of instantaneous reheating, we will start the calculation in the usual way and refine some of the steps. Take a mode with comoving momentum k_*, which crosses the horizon during inflation when the scale factor is a_*, $k_* = a_* H_*$. We want to compare the wavelength of this mode with the size of the horizon today

$$\frac{k_*}{a_0 H_0} = \frac{a_*}{a_{\rm end}} \frac{a_{\rm end}}{a_{\rm rh}} \frac{a_{\rm rh}}{a_0} \frac{H_*}{H_0}, \tag{4.1}$$

where $a_{\rm end}$ is the scale factor at the end of inflation and $a_{\rm rh}$ the scale factor when radiation starts to dominate. Of course this splitting in various phases is somewhat arbitrary and one expects to introduce errors of order $\Delta N \sim 1$. However, we will show later, using numerical solutions, that our analytical calculations are accurate up to 1%. In our analytical calculation, we will assume instantaneous reheating: $a_{\rm end} = a_{\rm rh}$. Under these assumptions Eq. (4.1) becomes

$$\frac{k_*}{a_0 H_0} = e^{-N} \frac{a_{\rm rh}}{a_0} \frac{H_*}{H_0}, \tag{4.2}$$

where N is the number of e-folds from the moment the mode k_* crosses the horizon until the end of inflation. Let us calculate the different terms on the rhs of Eq. (4.2).

The number of e-folds is given by

$$N = \int_{t_*}^{t_{\rm end}} H {\rm d}t = \int_{\phi_{\rm end}}^{\phi_*} \frac{1}{\sqrt{2\epsilon_{\rm H}}} \frac{{\rm d}\phi}{M_{\rm P}}. \tag{4.3}$$

The slow-roll parameter $\epsilon_{\rm H}$ is related to the derivatives of the potential as

$$\epsilon_{\rm H} \equiv -\frac{\dot{H}}{H^2} = \epsilon_{\rm V} \left(1 - \frac{4}{3}\epsilon_{\rm V} + \frac{2}{3}\eta_{\rm V}\right), \tag{4.4}$$

where $\epsilon_{\rm V}$ and $\eta_{\rm V}$ are defined as

$$\epsilon_{\rm V} \equiv \frac{1}{2} M_{\rm P}^2 \left(\frac{V'}{V}\right)^2, \qquad \eta_{\rm V} \equiv M_{\rm P}^2 \frac{V''}{V}. \tag{4.5}$$

For $V = \frac{1}{2} m^2 \phi^2$, we have $\epsilon_{\rm V} = \eta_{\rm V} = 2M_{\rm P}^2/\phi^2$, and the number of e-folds from Eq. (4.3) is given by

$$N = \frac{1}{4} \frac{\phi_*^2 - \phi_{\rm end}^2}{M_{\rm P}^2} + \frac{1}{3} \log \frac{\phi_*}{\phi_{\rm end}} + \cdots. \tag{4.6}$$

The first term is the standard result, while the second is the next to leading order in the slow-roll expansion. Notice that typically, given that $\phi_* \gg \phi_{\rm end}$, both $\phi_{\rm end}^2$ and the logarithmic correction are dropped in the usual calculation, but we are going to keep them here. Of course, the formula above must break down towards the end of inflation because higher slow-roll corrections (encoded in $+\cdots$) become important. Naively this can change the result for the number of e-folds by order one. However, as we will show later, Eq. (4.6) appears to be an excellent approximation to the numerical solutions.

The first fraction on the rhs of Eq. (4.2) can be evaluated using entropy conservation. Here we are assuming that none of the processes in the early universe lead to an entropy injection. This is a good approximation for the known phase transitions (electroweak and QCD). If entropy is conserved, then

$$g_*^{\rm rh} a_{\rm rh}^3 T_{\rm rh}^3 = a_0^3 T_\gamma^3 \left(2 + \frac{4}{11} g_*^\nu\right), \tag{4.7}$$

where $g_*^{\rm rh}$ is the number of degrees of freedom at the end of inflation, g_*^ν the number of degrees of freedom of neutrinos, T_γ is the temperature of the CMB photons today, and we have set the temperature of neutrinos to $T_\nu^3 = \frac{4}{11} T_\gamma^3$. For the 3 neutrino species, $g_*^\nu = 21/4$, and the first ratio on the rhs of Eq. (4.2) becomes

$$\frac{a_{\rm rh}}{a_0} = \frac{T_\gamma}{T_{\rm rh}} \left(\frac{43}{11 g_*^{\rm rh}}\right)^{1/3}. \tag{4.8}$$

To calculate the temperature at the beginning of radiation dominance, we will assume that inflation ends when $\ddot{a} = 0$. Although this definition is arbitrary, one can check that analytical results with different choices of the point where inflation ends (some popular choices are $\epsilon_{\rm V} = 1$ or $\phi_{\rm end} = 1 M_{\rm P}$) give the same predictions within the precision we are working at. Assuming that $\dot{\phi}$ has the attractor value $\dot{\phi} = -\sqrt{2/3}\, m M_{\rm P}$, from the relation

$$\dot{H} = \frac{\ddot{a}}{a} - H^2 = -\frac{1}{2} \frac{\dot{\phi}^2}{M_{\rm P}^2}, \tag{4.9}$$

one finds that inflation ends at $\phi_{\rm end} = \sqrt{4/3}\, M_{\rm P}$. The energy density at the end of inflation is

$$\rho_{\rm end} = \frac{1}{2} m^2 \phi_{\rm end}^2 + \frac{1}{2} \dot{\phi}^2 = m^2 M_{\rm P}^2. \tag{4.10}$$

In our toy model this energy density is instantaneously converted into radiation with temperature

$$T_{\rm rh} = \left(\frac{30 m^2 M_{\rm P}^2}{\pi^2 g_*^{\rm rh}}\right)^{1/4}. \tag{4.11}$$

This fixes the ratio $a_{\rm rh}/a_0$.

The last fraction on the rhs of Eq. (4.2) depends on H_*

$$H_* = \frac{m}{3}\sqrt{1+\frac{3}{2}\frac{\phi_*^2}{M_{\rm P}^2}} \approx \frac{m\phi_*}{\sqrt{6}M_{\rm P}}\,. \tag{4.12}$$

The mass of the inflaton is determined from the normalization of the power spectrum

$$\Delta_\zeta^2 = \frac{k^3}{2\pi^2}P_\zeta = \frac{1}{96\pi^2}\frac{\phi_*^4}{M_{\rm P}^4}\frac{m^2}{M_{\rm P}^2}. \tag{4.13}$$

Replacing all previous results in Eq. (4.2), we obtain a relation between ϕ_* and k_*

$$\begin{aligned}\log\frac{k_*}{a_0H_0} = {}& \frac{1}{4}\frac{\phi_{\rm end}^2-\phi_*^2}{M_{\rm P}^2} - \frac{1}{3}\log\frac{\phi_*}{\phi_{\rm end}} + \log\frac{T_\gamma}{H_0}\\ & - \frac{1}{12}\log g_*^{\rm rh} + \frac{1}{4}\log\Delta_\zeta^2 + \log\frac{4\pi(43/11)^{1/3}}{2880^{1/4}}.\end{aligned} \tag{4.14}$$

Setting $g_*^{\rm rh} = 106.75$, $H_0 = 1.5\times10^{-42}$ GeV, $T_\gamma = 0.235\times10^{-12}$ GeV and $\Delta_\zeta^2 = 2.19\times10^{-9}$ (1) [65] we get

$$\log\frac{k_*}{a_0H_0} = -\frac{1}{4}\frac{\phi_*^2}{M_{\rm P}^2} - \frac{1}{3}\log\frac{\phi_*}{M_{\rm P}} + 63.3. \tag{4.15}$$

The logarithmic contribution in this equation is very small and a very good approximate solution is

$$\frac{\phi_*}{M_{\rm P}} = \alpha - \frac{2}{3\alpha}\log\alpha\,, \quad \alpha = 2\left(63.3 - \log\frac{k_*}{a_0H_0}\right)^{1/2}.$$

For the pivot scale $k_* = 0.002$ Mpc^{-1}, the numerical value for α is $\alpha = 15.6$. Once ϕ_* is known, it is an easy exercise to calculate the tensor-to-scalar ratio and the spectral index. For a quadratic potential $\epsilon_{\rm V} = \eta_{\rm V}$, and at second order in slow-roll [50]

$$\begin{aligned} r &= 16\epsilon_{\rm V}\left(1-\frac{2}{3}\epsilon_{\rm V}+2C\epsilon_{\rm V}\right),\\ n_s &= 1-4\epsilon_{\rm V}-\epsilon_{\rm V}^2\left(8C+\frac{14}{3}\right),\end{aligned} \tag{4.16}$$

1 Strictly speaking, this value of Δ_ζ^2 is given for $k = 0.05$ Mpc^{-1}. Although k_* can be different from this scale, Δ_ζ appears only inside logarithms and the error one makes is much smaller than the precision we want to achieve.

where $C = -2 + \log 2 + \gamma$ and $\gamma = 0.75521\ldots$ is Euler-Mascheroni constant. The prediction for the endpoint of the quadratic inflationary potential in the limit of instantaneous reheating is

$$n_s = 0.9668 \pm 0.0003, \quad \text{and} \quad r = 0.131 \pm 0.001, \tag{4.17}$$

for $k_* = 0.002$ Mpc^{-1}. This point corresponds to the number of e-folds $N = 60.7 \pm 0.5$.

What happens if the post-inflationary evolution is modified? A slower reheating gives a lower N. The same happens if we increase the number of relativistic degrees of freedom at reheating. The dependence of N on g_* is anyway very mild, $N \sim -\frac{1}{12}\log g_*$, see Eq. (4.14), and one should vary g_* by orders of magnitude to get a relevant effect. Another effect that pushes towards a smaller value of N is entropy injection during the thermal history of the Universe. For example this happens with a first-order phase transition or when a massive particle goes out of thermal equilibrium before decaying. Notice also that a "standard" equation of state $w \leq 1/3$ before thermalization pushes again towards smaller values of N. The only way to get to larger values is to have $w > 1/3$ after inflation, which is a somewhat exotic possibility[2]. Therefore, the point in the (n_s, r) plane defined by Eq. (4.17) corresponds to the maximum value of N for the quadratic potential.

Numerical checks.—The predictions for n_s and r are derived under a number of assumptions. Given the level of precision we are working at, one might be worried that the corrections to the analytical calculation are large enough to spoil the final result. There are several possible sources of errors and we discuss them in this section.

The first one is the issue of matching different phases of evolution before thermalization. One would expect a sharp matching between different phases to give an error of order $\Delta N \sim 1$, and this would be relevant for the precision we want to achieve. The other problem is that it is not obvious how our final result depends on the details of reheating or preheating. To address

2 For example one can have a period of kinetic domination ($w = 1$) after the end of the slow-roll regime: after that the inflaton can get trapped in a minimum and reheat the Universe. Even if we allow for values of w larger than $1/3$, one can still get an absolute bound on the value of N. This is achieved in the extreme case where $w \gg 1$ from the end of inflation until BBN: the maximum value is $N \approx 100$ and this corresponds to $n_s = 0.98$ and $r = 0.08$.

these two questions we numerically solved a toy model that describes the evolution of the inflaton field and of radiation with energy density ρ_r

$$\begin{aligned}
&\ddot{\phi} + 3H\dot{\phi} + \Gamma\dot{\phi} + m^2\phi = 0, \\
&\dot{\rho}_r + 4H\rho_r - \Gamma\dot{\phi}^2 = 0, \\
&3M_{\rm P}^2 H^2 = \frac{1}{2}\left(m^2\phi^2 + \dot{\phi}^2\right) + \rho_r.
\end{aligned} \tag{4.18}$$

Γ is a constant that characterizes the efficiency of the transfer of energy from the inflaton field to radiation. Of course, this is not a realistic model, especially when preheating effects are relevant, but it will be sufficient to show that the details of the transition are not relevant, provided it is fast enough.

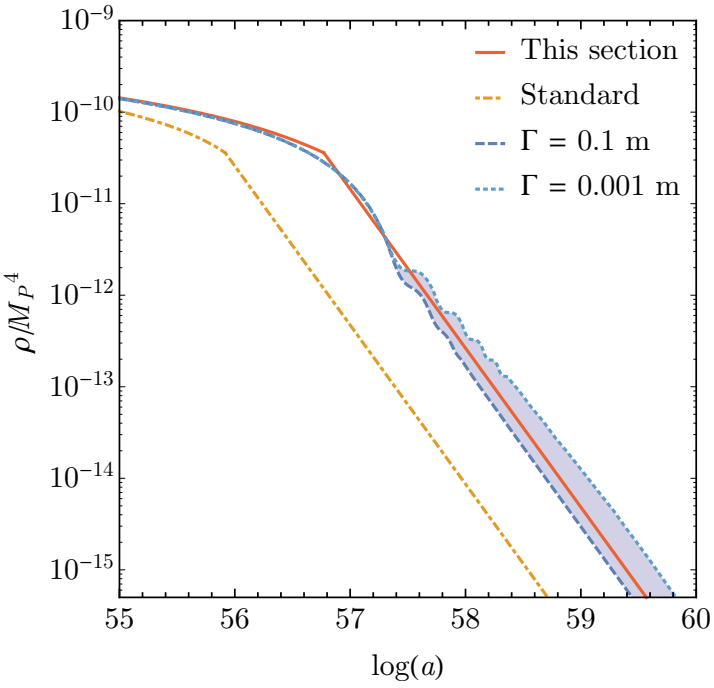

Figure 6: *Energy density as a function of* $\log(a)$*. Green dot-dashed line: the standard analytical result. Red solid line: analytical result using Eq.* (4.6)*. The grey region corresponds to numerical solutions between* $\Gamma = m/10$ *and* $\Gamma = m/1000$*. The improved analytical formula is within* 0.3 *e-folds from the numerical solutions for this range of* Γ*.*

In Fig. 6 we show how the total energy density depends on $\log(a)$. The initial conditions for the numerical integration are $\phi_{in} = 15\ M_{\rm P}$, $\dot{\phi}_{in} = -\sqrt{2/3}\, m M_{\rm P}$ (i.e. on the attractor solution) and $\rho_r(a_{in}) = 0$. We

take $a_{in} = 1$, $m = 6 \times 10^{-6} M_{\rm P}$, and turn on Γ when $\ddot{a} = 0$ (we are going to comment on this choice later). Fig. 6 shows the numerical results for a range of Γ from $\Gamma = m/1000$ (cyan dotted line) to $\Gamma = m/10$ (blue dashed line), while the analytical solution, using Eq. (4.6), is represented by the red solid line. For this range of parameters analytical and numerical results agree within $\Delta N = 0.3$, once radiation dominance is reached. This agreement is better than what one would naively expect and justify the use of the analytic formula. Therefore, as long as $\Gamma \gtrsim m/1000$, the transition to radiation can be considered instantaneous in order to make predictions with 1% accuracy. We also plot the result using the standard analytical formula Eq. (4.6) without the logarithmic term (yellow dot-dashed line). The difference compared to numerical solutions is $\Delta N \approx 1$, and it is not accurate enough for the precision we are working at.

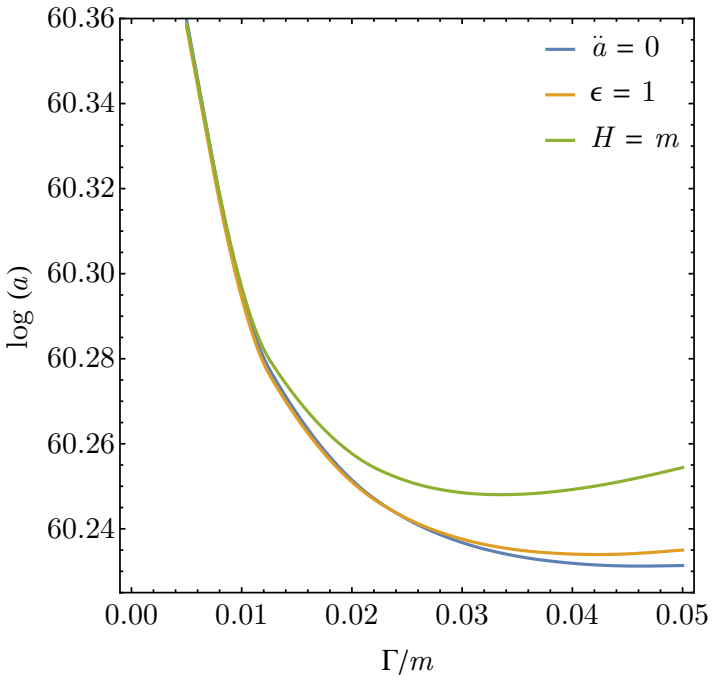

Figure 7: *Dependence of the expansion of the universe* $\log(a)$ *on* Γ *for fixed initial conditions and fixed final energy density (in radiation dominance). Different curves are obtained for different choices of time at which the inflaton starts to decay.*

In Fig. 7 we plot the expansion $\log(a)$ required to reach a fixed final energy density (in radiation dominance) as a function of Γ, for fixed initial conditions. We note that it flattens out for sufficiently large values of Γ,

indicating that the number of e-folds N becomes insensitive to Γ in that regime[3]. To assess the relevance of our choice of turning on Γ when $\ddot{a} = 0$, in Fig. 7 we also plot the curves corresponding to the conditions $\epsilon = 1$ and $H = m$. The alternative conditions give a negligible difference in the amount of expansion. For small values of Γ the curve steepens and approximately approaches the analytical expectation $a \propto \Gamma^{-1/6}$.

One may wonder whether our results apply when the energy transfer to radiation occurs through a preheating stage. In this case the energy is efficiently converted to light particles and the equation of state quickly approaches $w = 1/3$, even if the complete thermalization of the system will occur much later [66]. To verify that, within the required accuracy, the phenomenological model of Eq. (4.18) gives results which are quite similar to what happens with preheating, we plot in Fig. 8 the evolution of the equation of state w for several values of Γ (for which our prediction (4.17) applies, see Fig. 6). This can be compared with the analogous results of [66, 67]: in both cases the equation of state reaches $w \sim 1/3$ in approximately 3 e-folds. Therefore preheating models, for a wide range of couplings, give a sufficiently fast reheating and lead to our result (4.17).

It is worth stressing that preheating makes an efficient conversion to radiation rather natural and compatible with the approximate shift symmetry that keeps flat the inflaton potential. Indeed a coupling $g^2\phi^2\chi^2$ induces a quick conversion to χ particle for $g^2 \gtrsim 10^{-10}$. For these small couplings one can safely neglect the radiative corrections to the quadratic potential [66].

4.3 OTHER MONOMIAL POTENTIALS

Everything we have said so far can be generalized to other monomial potentials $V = M^{4-p}\phi^p$ (we focus on $p \leq 2$, given the present experimental bounds). However, unlike the case of a quadratic potential, we expect that a generic monomial cannot be extrapolated to the origin. In particular, we expect the potential to steepen approaching the minimum: this steepening *increases* N and can thus push the predictions beyond the would-be endpoint of the exact ϕ^p potential. In the following we assume that the modification of the potential happens at $\phi \ll M_{\rm P}$, so that it does not affect the predictions.

3 The mild raise at large Γ of the curve corresponding to $H = m$ is due to the friction induced on the inflaton by the production of radiation.

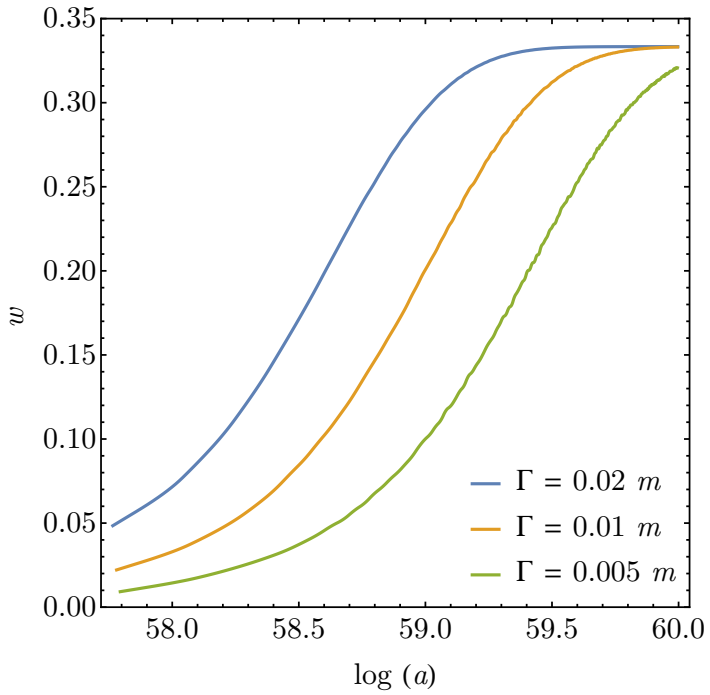

Figure 8: *Evolution of the equation of state (averaged over a period of oscillation) as a function of* $\log(a)$ *for different values of* Γ.

Otherwise one should have control of the shape of the potential until the final minimum [45, 68, 69].

Eq. (4.14) generalizes to

$$\begin{aligned}\log\frac{k_*}{a_0H_0} &= \frac{1}{2p}\frac{\phi_{\rm end}^2-\phi_*^2}{M_{\rm P}^2}+\frac{3p-10}{12}\log\frac{\phi_*}{M_{\rm P}}\\ &+\frac{1}{3}\log\frac{\phi_{\rm end}}{M_{\rm P}}+\log\frac{T_\gamma}{H_0}-\frac{1}{12}\log g_*^{\rm rh}+\frac{1}{4}\log\Delta_\zeta^2\\ &+\log\frac{2\pi(43/11)^{1/3}\sqrt{p}}{540^{1/4}\left(p/\sqrt{3}\right)^{p/4}},\end{aligned} \tag{4.19}$$

with $\phi_{\rm end}=p/\sqrt{3}M_{\rm P}$. For instance, in the cases of $V\propto\phi$ and $V\propto\phi^{2/3}$, motivated by string-theory monodromy [45, 68, 69], the predictions for the endpoint are

$$\begin{aligned} p=1: &\quad n_s=0.9749, \quad r=0.0664, \quad N=60.0,\\ p=2/3: &\quad n_s=0.9776, \quad r=0.0446, \quad N=59.7.\end{aligned}$$

Independently of p, n_s-1 and r have relative errors $\lesssim 1\%$.

4.4 CONCLUSIONS

For a generic potential it is of limited interest to consider second order slow-roll corrections or changes in the number of e-folds $\Delta N \simeq 1$, because the effects are degenerate with small changes in the shape of the potential. However, this is relevant for the "simplest" inflationary model, i.e. $V \propto \phi^2$ with fast reheating, and one can make predictions with 1% accuracy. This represents in some sense the most informative point in the (n_s, r) plane: if future data will be compatible with it, we will be quite confident about the inflationary potential, the reheating process and the following thermal history.

5

THE $1/N$ SCALING OF THE TILT

5.1 INTRODUCTION

Planck confirmed previous indications that the spectrum of scalar perturbations is not scale invariant: $n_s - 1 = -0.032 \pm 0.004$ at $1\,\sigma$ [11]. This is surely an important step in the understanding of the early universe: inflation generically predicts a deviation from scale-invariance, although the magnitude is, as we will discuss, model-dependent. The experimental value of $|n_s - 1|$ is of order $1/N_* \simeq 0.017$, where N_* is the number of e-folds to the end of inflation for observationally relevant scales (we are going to take $N_* = 60$ for definiteness). This did *not* have to be the case: it is easy to find models on the market with $|n_s - 1|$ much bigger, say 0.2 (of course the slow-roll approximation requires the tilt to be much smaller than 1), or much smaller, say 10^{-4}. For example in the prototypical hybrid inflation model

$$V = \frac{1}{2}m^2\phi^2 + \frac{1}{4}\lambda(\psi^2 - M^2)^2 + \lambda'\phi^2\psi^2 \tag{5.1}$$

the tilt is $n_s - 1 \simeq 2\eta = (2m^2 M_{\rm P}^2)/V_0$, where $V_0 = \frac{1}{4}\lambda M^4$ is the vacuum energy during inflation, before the field ψ relaxes to the true minimum. The tilt is a constant and does not depend on N: it can be much smaller or much larger than $1/N$. (In this example the tilt is positive, but the same applies to inverted hybrid models with red tilt.) In this kind of models, the inflaton "does not know" when inflation is going to end, i.e. when the waterfall field will become tachyonic. Thus there is no relation between the tilt, which only depends on the derivatives of the potential at a given point, and N, which measures the distance to the end of inflation. The approximate equality $n_s - 1 \sim 1/N$ could just be an accident.

On the other hand in this section we want to take this indication seriously and see what are the implications on inflation, and in particular on the expected amount of gravitational waves. Our formulae will be similar to [70] and [71] (see also [72] and [73]) although the implications we will draw will be slightly different.

5.2 MAIN ARGUMENT

The experimental value of the scalar tilt suggests

$$n_s - 1 = -\frac{\alpha}{N} \tag{5.2}$$

with α of order unity. We assume the equation above to be valid in a window which is comfortably larger than the observable one: in other words the same equation would hold if one were to measure perturbations at, say, $N = 10$ or $N = 200$ instead of $N = 60$. For the time being we assume α is strictly a constant and later discuss deviations from this assumption. Writing the tilt in terms of $\epsilon \equiv -\dot{H}/H^2$ and its derivative, the equation above becomes (at first order in slow-roll) a differential equation for ϵ

$$n_s - 1 = -2\epsilon + \frac{\mathrm{d}\log\epsilon}{\mathrm{d}N} = -\frac{\alpha}{N}\,. \tag{5.3}$$

This is easily integrated to give

$$\epsilon(N) = \frac{1}{2(\alpha-1)^{-1}N + AN^{\alpha}}\,, \tag{5.4}$$

with A an integration constant. By a judicious choice of A one can choose any value for ϵ (and thus for r) at $N_* = 60$. However the scaling (5.2) says that there is nothing special at the scale $N_* = 60$ we measure, therefore it looks reasonable to further assume that, in a certain window which encompasses the observable 60 e-folds, only one of the two power laws in the denominator of (5.4) dominates. Conversely $N_* = 60$ would be accidentally close to the transition point between the two regimes. Within this assumption one has two different cases depending on whether α is larger or smaller than 1. For $\alpha > 1$ there are two possible behaviors, depending on which scaling of ϵ is chosen, while only one solution exists for $\alpha < 1$, since ϵ cannot be negative. Therefore there are three cases:

1. $\alpha > 1$ and $\epsilon \simeq (\alpha - 1)/2N$. The value of ϵ (and thus of r) is fixed and large. This is the case of monomial potentials $V \propto \phi^{2\alpha-2}$. This is the simplest and most informative scenario: inflation is driven by a simple monomial potential, as previously stated, r is large enough to make %-measurements possible [51] (see also [1, 74]) and we would be quite confident on what is going on [3, 4].

2. $\alpha > 1$ and $\epsilon \simeq A^{-1}N^{-\alpha}$. In this case one cannot fix the value of ϵ: the only requirement is that the constant A is big enough so that one

can neglect the first term at the denominator of (5.4). In terms of r this gives

$$r = 16\epsilon \simeq 16A^{-1}N^{-\alpha} \lesssim 8(\alpha-1)N^{-\alpha}\,. \tag{5.5}$$

It is easy to find the potentials that correspond to these behaviors [75].

The case $\alpha > 2$ consists for example of hilltop models that inflate around the origin,

$$V(\phi) = V_0\left[1-\left(\frac{\phi}{M}\right)^n\right] \tag{5.6}$$

with $n > 2$ and $M \lesssim M_{\rm P}$. For these potentials $\alpha = (2n-2)/(n-2)$. Notice that for $n = 2$ the potential does not follow the $1/N$ scaling, since η (and thus n_s) goes to a constant at small ϕ ([1]).

For $\alpha = 2$ one has models that approach a constant exponentially for large ϕ

$$V(\phi) = V_0\left[1-e^{-\phi/M}\right]\,, \tag{5.7}$$

with $M \lesssim M_{\rm P}$ ([2]).

In the case $1 < \alpha < 2$ one finds models that approach a constant polynomially at large ϕ

$$V(\phi) = V_0\left[1-\left(\frac{M}{\phi}\right)^n\right]\,, \tag{5.8}$$

with $n > 0$ and $M \lesssim M_{\rm P}$. For these $\alpha = 2(n+1)/(n+2)$.

The potentials given above are just examples which reproduce approximately Eq. (5.2). For example in the case above of models that approach a constant polynomially, corrections to Eq. (5.2) go as $(N^{-1}\cdot M^2/M_{\rm P}^2)^{n/(2+n)}$: for $M \lesssim M_{\rm P}$, this is a good approximation to Eq. (5.2) (unless n is too small, see later).

1 This suggests that if one modifies the potential with $n = 2$ with a correction which goes to zero slower than any polynomial, one gets intermediate behavior for $n_s - 1$. For example the potential $V = V_0[1 + (\phi/M)^2/\log(\phi/M)]$ gives $n_s - 1 \propto 1/\sqrt{N}$. This shows that the $1/N$ scaling is not the only possibility, although arguably the most natural. It is the experimental value of n_s that suggests $1/N$.

2 Notice that the potentials we are quoting for each case are just examples and that there are completely different potentials giving the same α. For instance the potential $V_0[1-\exp(M/\phi)]$ near the origin gives the correct $1/N$ scaling with $\alpha = 2$.

In all the cases $A^{-1} \sim (M/M_{\rm P})^{2\alpha-2}$. As we discussed, this number cannot be large, see Eq. (5.5), but unfortunately it can be arbitrarily small, when the scale M is smaller than the Planck scale. As done in [70, 71] one can assume that $M \simeq M_{\rm P}$, or equivalently that $\epsilon \simeq N^{-\alpha}$, however this is an additional assumption and not a consequence of Eq. (5.2). For smaller values of M (and thus of ϵ) slow-roll terminates because η becomes of order one: after that ϵ starts varying fast and reaches unity in one e-fold or so. For example brane inflation corresponds in its simplest form to a potential of the form of Eq. (5.8) with $n = 4$ and M parametrically smaller than $M_{\rm P}$ [76]. Furthermore, exponential potentials are ubiquitous in field and string theory constructions, both with $M \sim M_{\rm P}$ and with $M \ll M_{\rm P}$ [76, 77].

3. $\alpha < 1$ and $\epsilon \simeq A^{-1}N^{-\alpha}$. This regime is qualitatively different from the previous ones. The second term in the denominator of Eq. (5.4) must dominate, since the first term would give a negative ϵ. Since the first term grows faster than the second for large N, this case cannot be sustained for arbitrarily large N. On the other hand we can require it is valid for a large window around the observable scales, say up to $\bar{N} = 10N_*$. Again this gives an upper bound on the amplitude of gravitational waves

$$r = 16\epsilon \lesssim \frac{1-\alpha}{2}\frac{1}{\bar{N}}\left(\frac{\bar{N}}{N}\right)^{\alpha} . \tag{5.9}$$

Although it may look artificial, this behavior can be obtained with the potential

$$V = V_0\left[1 + \left(\frac{\phi}{M}\right)^n\right] \tag{5.10}$$

with $0 < n < 2$ and $M \gg M_{\rm P}$. Eq. (5.2) is valid with $\alpha = -2(n-1)/(2-n)$ for $\phi \ll M$ (as we said this regime cannot last for arbitrarily large N).

This class covers also the case of blue tilt of order $1/N$. But there is an important difference: for red tilt slow-roll breaks when η becomes large and negative, so that ϵ is increasing and naturally leads to the end of inflation $\epsilon = 1$. For blue tilt η is large and positive at the end of slow-roll, so that ϵ is small and decreasing. Some additional ingredient is needed to ultimately terminate inflation. Of course this is not so interesting since a blue tilt is ruled out experimentally. Notice also

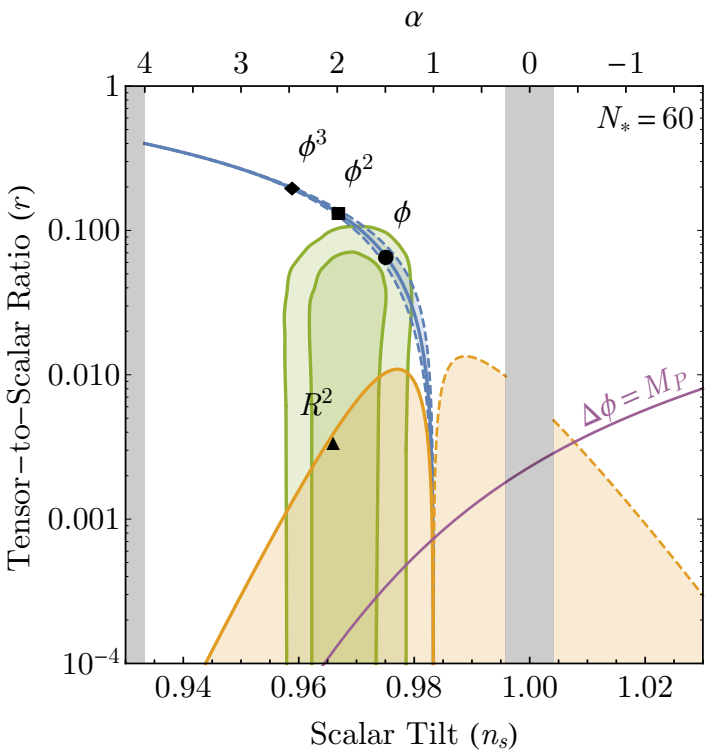

Figure 9: *Possible allowed regions in the experimental (n_s,r)-plane, as derived from our assumptions. The solid blue and orange lines correspond to the behavior of case 1) and 2). Dashed lines depend on the choice of $\bar{N}$. The experimentally allowed region is in green (1 and 2σ contours). In the gray shaded regions $|\alpha|$ is significantly different from one, so that the assumption in Eq. (5.2) may not apply. The solid purple line corresponds to the Lyth bound.*

that one should not use our arguments too close to the scale-invariant point $|\alpha| \ll 1$ because this would violate the assumption that $n_s - 1$ is of order $1/N$. The same applies when $|\alpha|$ becomes parametrically larger than one. Anyway, both these cases are experimentally ruled out.

In Fig. 9 we draw the various possibilities together with the current experimental bounds [11], requiring one of the two behaviors of ϵ dominates in a window up to $\bar{N} = 10N_*$. The solid orange line corresponding to Eq. (5.5) is defined only up to a factor of order unity; in the plot we chose such factor so to include the point corresponding to the Starobinsky model [12]. The dashed line for $\alpha < 1$ and around the large ϵ solution depends on $\bar{N}$, and should be thus interpreted with care. We also draw (solid purple

line) the Lyth bound [44]: in Eq. (5.4) we choose the value of A such that the displacement of the inflaton from $N_* = 60$ to the end is $\Delta\phi = M_{\rm P}$ [78]. Within the experimentally allowed region for the scalar tilt, all "measurable" values of r ($\gtrsim 5 \times 10^{-4}$) corresponds to $\Delta\phi > M_{\rm P}$.

It is important to stress that the $1/N$ scaling, given in Eq. (5.2), can be checked experimentally by the measurement of the running which is obviously fixed to be $\alpha_s = -\alpha/N_*^2 \simeq -7 \cdot 10^{-4}$ [75]. Unfortunately this value is probably too small to be measured with CMB experiments [79], however a measurement of a larger running would disprove Eq. (5.2).

5.3 STABILITY OF THE CONSTRAINTS

Of course one cannot argue from the measurement of the tilt that Eq. (5.2) holds with α strictly constant. At most one can argue that $\alpha(N)$ is a slowly varying function of N ([3]). Let us check that the qualitative features of the plot in Fig. 9 remain the same. If α depends on N, Eq. (5.3) can be written as a linear differential equation

$$\frac{{\rm d}\epsilon^{-1}}{{\rm d}\log N} - \alpha(N)\epsilon^{-1} = -2N \,, \tag{5.11}$$

whose general solution is

$$\begin{aligned}\epsilon^{-1}(N) = &-2e^{\int_1^N \frac{d\tilde{N}}{\tilde{N}}\alpha(\tilde{N})} \int_1^N d\tilde{N} e^{-\int_1^{\tilde{N}} \frac{d\hat{N}}{\hat{N}}\alpha(\hat{N})} \\ &+ A e^{\int_1^N \frac{d\tilde{N}}{\tilde{N}}\alpha(\tilde{N})} \,.\end{aligned} \tag{5.12}$$

The first line on the rhs is the non-homogeneous solution and it reduces to $2(\alpha - 1)N$ for constant α. When α is not a constant the solutions will not be power-laws, but we can still assume that one of the two behaviors (corresponding to $\epsilon \sim \eta$ or $\epsilon \ll \eta$) dominates over a parametric window without moving from one to the other. The constraints on ϵ (and thus on r) will be perturbatively close to the case of constant α if the variation is small. The second line corresponds to the homogeneous solution of the differential equation. It amounts to neglect the contribution of ϵ to the tilt, $\epsilon \ll \eta$, and it reduces to the power law N^α for a constant α.

3 It is easy to find examples of potentials where there are corrections to the exact $1/N$ scaling: for example the potential $V = V_0[1 - \exp(-\phi^2/M_{\rm P}^2)]$ has $n_s - 1 \simeq -2/N \cdot (1 + 1/(2\log N))$.

If α weakly depends on N, the plot of Fig. 9 will be slightly "blurred". For example if Eq. (5.2) is modified to allow for a "running" α

$$n_s - 1 = -\frac{\alpha}{N}\left(\frac{N}{N_*}\right)^{\delta} \tag{5.13}$$

then the power law solution $\epsilon \propto N^{-\alpha}$ is modified for small δ by a factor $(1 + \alpha\delta(\log N_*)^2/2 + \ldots)$. If we take $\delta \simeq 0.3$, in such a way that the effective α changes by a factor of 2 as N varies by an order of magnitude, the correction is of order 2. This does not affect our conclusions, since Eq. (5.5) is anyway defined up to a factor of order unity. These uncertainties will sum up with the experimental uncertainties on n_s and the theoretical ones on the number of e-folds N. This in particular tells us we should not take too seriously the small value of r in the region close to $\alpha = 1$: the two solutions N and N^{α} becomes closer and closer and the results are very sensitive to the corrections we just discussed.

5.4 CONCLUSIONS

The robust conclusion is that there are regions in the (n_s, r)-plane which are *not* compatible with the $1/N$ hypothesis of Eq. (5.2) (see also [70]), and the assumption that there is no change of behavior for ϵ. Unfortunately these assumptions do not set a lower bound for r. If one further requires that ϵ becomes of order one when slow roll breaks, then we have either the case 1) or the case 2) with the inequality (5.5) saturated (solid orange line in Fig. 9). Conversely the $1/N$ scaling is compatible with an arbitrarily low energy during inflation. In particular it is also compatible with large-f_a QCD axion models, which would be in tension with high-scale inflation models [80, 81].

It is important to stress that, since in Eq. (5.5) r depends exponentially on the tilt, an improvement on the experimental limits of this quantity will be of great importance.

Current and upcoming CMB-experiments will be able to probe values of r as small 2×10^{-3} [1] in a not-so-distant future. If experiments will put us in the "forbidden" region, we will have to give up one of the assumptions. One possibility is that the value of the tilt is only accidentally of order $1/N$. Inflation requires the slow-roll parameters to be small, but in explicit constructions it may be difficult to make them as small as we like. For example supergravity corrections (or in general Planck-suppressed operators)

tend to push η towards one (η-problem), thus giving large contributions to the tilt. Similarly it appears difficult to have pseudo Nambu-Goldstone bosons with a decay constant much bigger than $M_{\rm P}$ [82], so that a not-so-small tilt of order $M_{\rm P}^2/f^2$ is expected. One can surely reproduce the tilt we observe in these cases, though one might argue that a larger value would be expected if the flatness of the potential is so hard to maintain. Another way out is a small speed of sound for the inflaton. Current constraints still allow a substantial reduction in the value of r. The other assumption we might have to relax is that ϵ does not move from one behavior to the other in the observable window. For example in ref. [83] the authors consider the model $V \propto \tanh^2(\phi/\sqrt{6\beta})$ which satisfies, for any β, eq. (5.2) with $\alpha = 2$. One can obtain values of r in the forbidden region by adjusting β in such a way that the two terms in the denominator of (5.4) are comparable for $N = N_\star$. However, this requires some amount of tuning since observable inflation happens very close to the inflection point of the potential.

6

FUTURE BOUNDS ON TENSOR MODES

6.1 MOTIVATIONS

The year 2014 marked the beginning of the B-mode era in cosmology. After the direct detection of the lensing B-mode signal by Polarbear [84], BICEP2 [43] pushed the constraints on primordial tensor modes using polarization to a level that is competitive with temperature. Given that temperature measurements are close to the cosmic-variance limit for the tensor-to-scalar ratio r, improvements in the future will practically only come from polarization. However from Planck's [85] measurements of the level of polarized dust emission (for previous measurements see for example [86, 87]), it is clear that a detection of primordial tensor modes will have to deal with foregrounds.

With the recent release of Planck [11, 88], we are constraining at 2σ the region $r \sim 0.1$, which corresponds to simple monomial potentials. As we argued in Sec. 5, if gravitational waves are not detected, there is another motivated threshold at $r \sim 2 \times 10^{-3}$. In this section we want to look ahead at the future (and futuristic) experiments and understand whether the new data on dust polarization substantially change the reach expected for the various experiments.

6.2 FORECASTING METHOD

6.2.1 *CMB and Noise*

The anisotropies of the temperature and polarization fields can be decomposed into spin-weighted spherical harmonics

$$\begin{aligned} T &= \sum_{\ell,m} a^T_{\ell m} Y_{\ell m}, \\ Q \pm iU &= \sum_{\ell,m} a^{(\pm 2)}_{\ell m} Y^{(\pm 2)}_{\ell m}, \end{aligned} \tag{6.1}$$

or, for the polarization field, into the more conveniently defined E- and B-modes

$$E = \sum_{\ell,m} a^E_{\ell m} Y_{\ell m}, \qquad B = \sum_{\ell,m} a^B_{\ell m} Y_{\ell m}, \tag{6.2}$$

whose coefficients are

$$a^E_{\ell m} = -\frac{a^{(+2)}_{\ell m} + a^{(-2)}_{\ell m}}{2}, \qquad a^B_{\ell m} = -\frac{a^{(+2)}_{\ell m} - a^{(-2)}_{\ell m}}{2i}. \tag{6.3}$$

Let us consider the CMB first. In linear perturbation theory, the coefficients $a_{\ell m}$ of the T-, E- and B-modes of the CMB are Gaussian random variables with zero mean and variance

$$\langle a^X_{\ell m} a^{Y*}_{\ell' m'} \rangle = C^{XY}_\ell \delta_{\ell\ell'} \delta_{mm'}, \tag{6.4}$$

where $X, Y = T, E, B$. From these, as customary, one defines the "curly" correlators as $\mathcal{C}^{XY}_\ell \equiv \ell(\ell+1) C^{XY}_\ell / (2\pi)$. Due to parity invariance, only the TT, EE, TE and BB power spectra are necessary to characterize the CMB, the others being zero. In our analysis we consider the B-mode power spectrum only, so we drop the superscript BB where possible. This is generated by CAMB [90] and, since we are solely interested in the forecast for the tensor-to-scalar ratio r, we set all cosmological parameters, except r and the optical depth τ, to the current best fit values of Planck [11]. Although this may look like a rough approximation, r is expected to be only mildly degenerate with the other parameters, the biggest degeneracy being the one with τ at low multipoles. We are going to marginalize over τ using a gaussian prior given by Planck analysis [11]. This is a conservative approach for satellites since they will have additional information on reionization. On the other hand, since large scale polarization measurements are affected by systematics, it is not clear how much they will improve the constraints on τ.

In the presence of white noise due to the instrumentation, the integration over a Gaussian beam to go from real space to harmonic space creates a bias $\mathcal{N}_\ell$ for the estimators of the power spectra. At each frequency channel, this is given by [91]

$$\mathcal{N}_\ell = \frac{\ell(\ell+1)}{2\pi} \sigma^2_{\rm pix} \, \Omega_{\rm pix} \, e^{\ell^2 \sigma_b^2}, \tag{6.5}$$

where $\sigma_{\rm pix}$ is the noise variance per pixel of size $\Omega_{\rm pix} = \Theta^2_{\rm FWHM}$, and $\sigma_b = 0.425\,\Theta_{\rm FWHM}$ is the beam-size variance. Our treatment here is clearly simplistic, since it does not take into account systematics. However, these are very experiment-dependent and go beyond the scope of this section.

6.2.2 *Foregrounds*

The presence of foregrounds limits our ability in extracting the CMB signal from the data. Fortunately, each component scales differently in frequency, and thus it is possible to separate them using maps at different frequencies. We consider two diffuse components: synchrotron emission (S) and thermal dust (D).

The BB power spectra of the Galactic synchrotron emission and thermal dust in antenna temperature is given by the following simple parametrization

$$\begin{aligned} S_{\ell,\nu} &= \left(W_\nu^S\right)^2 C_\ell^S = \left(W_\nu^S\right)^2 A_S \left(\frac{\ell}{\ell_S}\right)^{\alpha_S}, \qquad W_\nu^S = \left(\frac{\nu}{\nu_S}\right)^{\beta_S}, \\ D_{\ell,\nu} &= \left(W_\nu^D\right)^2 C_\ell^D = \left(W_\nu^D\right)^2 A_D \left(\frac{\ell}{\ell_D}\right)^{\alpha_D}, \qquad W_\nu^D = \left(\frac{\nu}{\nu_D}\right)^{1+\beta_D} \frac{e^{h\nu_D/kT}-1}{e^{h\nu/kT}-1}, \end{aligned} \tag{6.6}$$

where the parameters are given in Tab. 1. This parametrization fits well the observed power spectra [85, 92, 93]. Since for our analysis we are using as a reference the CMB signal, one has to rescale the antenna temperature of these components to the thermodynamic temperature of the CMB. The conversion is provided by the frequency dependence of the CMB

$$W_\nu^{CMB} = \frac{x^2 e^x}{(e^x-1)^2}, \qquad x \equiv \frac{h\nu}{k\,T_{CMB}}. \tag{6.7}$$

The frequency dependence of synchrotron and dust rescaled to the thermodynamic temperature of the CMB then reads

$$\begin{aligned} W_\nu^S \to W_\nu^S &= \frac{W_{\nu_S}^{CMB}}{W_\nu^{CMB}} \left(\frac{\nu}{\nu_S}\right)^{\beta_S}, \\ W_\nu^D \to W_\nu^D &= \frac{W_{\nu_D}^{CMB}}{W_\nu^{CMB}} \left(\frac{\nu}{\nu_D}\right)^{1+\beta_D} \frac{e^{h\nu_D/kT}-1}{e^{h\nu/kT}-1}. \end{aligned} \tag{6.8}$$

Synchrotron emission is the dominant one below 90 GHz[1], while dust becomes increasingly important for higher frequencies. In our forecasts, for sky coverage of 70% and 20% we have fixed the synchrotron amplitude to the value measured by WMAP for the P06 mask [92], while for the 10% and 1% to the extrapolation of [94] of the WMAP data. The synchrotron spectral index

1 The synchrotron and dust power spectra are comparable at roughly 90 GHz for the cleanest 1% of the sky. In regions with higher levels of polarized dust emission the transition happens at a lower frequency.

is known to steepen as Galactic latitude increases (see e.g. [95]). However we checked that this effect can be safely neglected for our purposes.

Parameter	**Synchrotron**	**Dust**
$A_{72\%}$ [μK^2]	2.1×10^{-5}	0.169
$A_{53\%}$ [μK^2]	2.1×10^{-5}	0.065
$A_{24\%}$ [μK^2]	2.1×10^{-5}	0.019
$A_{11\%}$ [μK^2]	4.2×10^{-6}	0.013
$A_{1\%}$ [μK^2]	4.2×10^{-6}	0.006
ν [GHz]	65	353
ℓ	80	80
α	-2.6	-2.42
β	-2.9	1.59
T [K]	–	19.6

Table 1: *Foreground parameters obtained or extrapolated from [85, 92, 94], as explained in the text. $A_{f_{sky}}$ refers to the cleanest effective area f_{sky}.*

However, polarized dust emission is the leading contaminant for balloon and ground experiments probing frequencies higher than 90 GHz. A detailed measurement of the polarized dust has become available only recently [85]. For this reason, its impact has been underestimated in some previous analyses. For example, the observed value of the dust power spectrum at 353 GHz for 72% of the sky is roughly 10 times bigger than the dust-model A used for the forecast of CMBPol [96]. It is now clear that there are no regions in the sky for which a measurement of r is achievable without having to deal with foregrounds [85, 94]. One of the primary goals of this work is to provide new forecasts for the detection and measurement of r with more realistic levels of thermal dust contaminating the primordial signal. In this respect, we use the levels of dust presented in [85] for the 353 GHz channel of Planck and extrapolate their results when needed. In particular, Planck [85] has recently provided the power spectra of dust at 353 GHz for a clean effective area of 72%, 53%, 24%, and 1%. For the 1%-patch we use as a reference the value of the dust amplitude in the BICEP2 region. Even though Planck observed cleaner patches of the same size, the associated errors are too large to reliably determine the correct level of dust.

Some experiments, e.g. Spider, will probe patches of the order of 10% and we need to extrapolate the amount of dust on a patch roughly as big as theirs. This can be done in several ways. As a first guess, the interpolation of the values provided by Planck as a function of f_{sky} gives $A_D^{BB} = 0.013$. Another way consists in using the low $N_{\rm HI}$ region of [97] which covers 11% of the sky. Using the relation $N_{\rm HI} = 1.41 \times 10^{26}\,{\rm cm}^{-2}\,\langle \emptyset_{353} \rangle$, where τ_{353} is the optical depth at 353 GHz, we find $N_{\rm HI} = 1.35 \times 10^{20}\,{\rm cm}^{-2}$. Substituting this value in the relation between the amplitude of B-modes and $N_{\rm HI}$ [85], we find that $A_D^{BB} = 0.013$. We tested this procedure against the amplitudes indicated by Planck for the 1% of the sky for BICEP2, and found good agreement. A third way consists in using the relation between the amplitude in polarization and the one in intensity [85], $A_D \propto I_{353}^{1.9}$. This relation for the same low N_{HI} region gives $A_D^{BB} = 0.009$. We will use $A_D^{BB} = 0.013$ as an upper bound for the dust levels in the region observed by Spider.

An additional complication comes from the correlation between synchrotron and dust. It has been observed [94] that the correlation among these two components can be as high as 70%. To account for this effect in our forecast, for simplicity we will assume that in the power spectrum the correlation enters as $g\sqrt{S_{\ell,\nu_i} D_{\ell,\nu_j}}$ and set $g = 0.5$ in our fiducial sky-model, independently of f_{sky} and ℓ.

6.2.3 *Likelihood and Fisher Analysis*

In the case of an experiment covering the whole sky, one can write the signal d measured at the frequency ν_i, in harmonic space, as

$$d_{\ell,m}^{\nu_i} = \bar{W}_c^{\nu_i} a_{\ell,m}^c + n_{\ell,m}^{\nu_i} \tag{6.9}$$

where W provides the frequency dependence of each component[2], the bar indicates that the parameters are fixed to their "true" value, and n is the instrumental noise. Assuming that the amplitudes are Gaussian (also those of foregrounds), starting from the χ^2 (and avoiding the use of indices)

$$\chi^2 = \sum_{\ell,m} (d - W \cdot a)^T \cdot N^{-1} \cdot (d - W \cdot a) + a^T \cdot C^{-1} \cdot a, \tag{6.10}$$

2 Since we are considering three components (the index c runs over CMB, Dust and Synchrotron), and we are expressing everything in thermodynamic temperature, W is a $3 \times N_{\rm channel}$ matrix whose rows are $\left(1, W_{\nu_i}^D, W_{\nu_i}^S\right)$.

where C is the covariance matrix of the amplitudes of the various components and N is the covariance matrix of the noise, the likelihood can be written as

$$\mathcal{L}_{BB}(d,p) \propto \int \mathrm{d}^3 a \, e^{-\frac{1}{2}\chi^2} \propto e^{-\frac{1}{2}\sum_{\ell,m} d^T \cdot \left(W \cdot C \cdot W^T + N\right)^{-1} \cdot d}. \tag{6.11}$$

In order to do a Fisher analysis we are interested in the average of the log-likelihood,

$$\begin{aligned}\langle \log \mathcal{L}_{BB} \rangle = -\frac{1}{2}\sum_{\ell}(2\ell+1)\Bigg[&\log \mathrm{Det}\left[\frac{W\cdot \mathcal{C}_\ell^{BB}\cdot W^T + \mathcal{N}_\ell}{\bar{W}\cdot \bar{\mathcal{C}}_\ell^{BB}\cdot \bar{W}^T + \mathcal{N}_\ell}\right] \\ &+ \mathrm{Tr}\left[\frac{\bar{W}\cdot \bar{\mathcal{C}}_\ell^{BB}\cdot \bar{W}^T + \mathcal{N}_\ell}{W\cdot \mathcal{C}_\ell^{BB}\cdot W^T + \mathcal{N}_\ell} - \mathrm{I}\right]\Bigg],\end{aligned} \tag{6.12}$$

where the normalization is such that for $\bar{\mathcal{C}}_\ell = \mathcal{C}_\ell$, $\langle \log \mathcal{L}_{BB} \rangle = 0$. In the following we will refer to the use of this formula as "Component Separation" (CS).

Given the likelihood as a function of the parameters $\boldsymbol{p}$, one can define the Fisher matrix

$$F_{ij} = -\left.\frac{\partial^2 \langle \log \mathcal{L}_{BB} \rangle}{\partial p_i \partial p_j}\right|_{\boldsymbol{p}=\bar{\boldsymbol{p}}}, \tag{6.13}$$

where $\bar{\boldsymbol{p}}$ is the set of "true" cosmological parameters. The minimum error on the parameters given the data, is set by the Cramer-Rao bound to be

$$\sigma_{p_i}^2 \geq (F^{-1})_{ii}. \tag{6.14}$$

In real experiments, only part of the sky is observed or can be used for cosmology, and thus not all modes are available for the analysis. To capture this effect in a simple way one can multiply the RHS of Eq. (6.12) by the fraction of the sky available f_{sky}.

In general the analysis is far more complicated. The likelihood as written in Eq. (6.12) becomes lossy, modes of multipole ℓ will be coupled with their neighbors. In addition, for experiments covering only a few percent of the sky, the leakage of E- into B-modes will add additional complications to the detection of the signal produced by gravitational waves [98]. In our discussion, we will neglect these details, and thus the results produced with this method can be seen as optimistic.

In the analysis of Sec. 6.3, the likelihood in Eq. (6.12) is a function of 6 parameters[3] $\boldsymbol{p} = (r, A_D, A_S, \beta_D, \beta_S, g)$, and the error on the tensor-to-

3 Notice that even in the limit in which there is no additional information coming from the difference in ℓ-dependence, an experiment with three frequencies would allow a complete reconstruction of the parameters, since its covariance matrix would have six entries.

scalar ratio is marginalized over the other parameters. Notice that at low frequency the effect of changing T_D is very similar to a change in β_D. As done in [99], we are assuming that the temperature of the dust emitting polarized radiation is the same as the one determined from the intensity maps. In the following we will assume gaussian priors for A_S, A_D, β_S with variance of 50%, 50%, 10% respectively. For β_D we use a gaussian prior of 10%, 30% and 50%, for $f_{sky} \gtrsim 50\%$, $\sim 5-10\%$ and $\sim 1\%$ respectively. For the optical depth we assume a gaussian prior given by Planck analysis [11]. No priors are assumed for the other parameters.

In Sec. 6.4 we will instead take a more conservative approach and consider the likelihood in Eq. (6.12) as a function of 10 parameters. Namely, in addition to the 6 previous parameters, we will include the ℓ-dependence of the foregrounds, α_D and α_S, the spectral dependence of the CMB and its ℓ-dependence. In particular we will constrain how much the CMB deviates from what expected using simple power laws with parameters α_{CMB} for the ℓ-dependence and β_{CMB} for the spectral dependence. Notice that α_{CMB} roughly corresponds to the tensor tilt.

In all the tables that follow, we use the symbol "$-$" when $\sigma_r \geq r$.

6.2.4 *Likelihood and Fisher Analysis: a Phenomenological Approach*

The foreground model used in the previous section is of course approximate. For instance the foreground parameters may be space-dependent, and the distribution is not exactly gaussian. For this reason, and also to compare our results with previous forecasts, we also adopt a second, more phenomenological, method for estimating the error on the tensor-to-scalar ratio. It was proposed in [100] and already used also in previous forecasts for CMBPol [96] and more recently also in [74]. The method assumes that with already known techniques such as [101, 102] it is possible to subtract the foregrounds up to a certain level in each single map. The noise introduced by the foreground removal is then modeled by accounting the number of possible cross correlations. The sum of foreground residual and noise is

$$\mathcal{N}^{\rm F}_{\ell,\nu} = \sum_F \left(\sigma_F \left(\mathcal{S}_{\ell,\nu} + \mathcal{D}_{\ell,\nu} \right) + \frac{4\,\mathcal{N}_{\ell,\nu_{tmp}}}{N_{\rm channel}(N_{\rm channel}-1)} \frac{W^F_\nu}{W^F_{\nu_{tmp}}} \right), \quad (6.15)$$

where σ_F is the fraction of leftover foregrounds in power, W^F_ν includes the conversion to thermodynamic temperature, ν_{tmp} is the reference frequency at

which the foreground template has been created (e.g. 30 GHz for synchrotron and 353 GHz for dust), and $N_{\rm channel}$ is the number of frequency channels. This quantity is then treated as an additional source of uncorrelated noise and as such is added to the noise bias. The resulting effective noise is given by

$$\left(\mathcal{N}_\ell^{eff}\right)^{-2} = \sum_{i,j\geq i}\left(\left(\mathcal{N}^F_{\ell,\nu_i}+\mathcal{N}_{\ell,\nu_i}\right)\left(\mathcal{N}^F_{\ell,\nu_j}+\mathcal{N}_{\ell,\nu_j}\right)\frac{1}{2}(1+\delta_{ij})\right)^{-1}. \quad (6.16)$$

This method has the advantage of being independent on any specific technique of foreground subtraction, but, as already noted in [103] (see also [104]), it has the downside of not being specific of any real experiment. By comparing the results of this and the CS method, one can estimate what is the level of foreground subtraction obtained by the component separation, and therefore the level at which the foreground modeling needs to be trusted. As already done in [96, 100] and recently in [74], in our forecasts we will assume that foregrounds can be subtracted at 1% in power level in each map.

The likelihood in this approach is the one of a single channel with an effective noise bias given by Eq. (6.16), and it reads

$$\langle \log \mathcal{L}_{BB}\rangle = -\frac{1}{2}\sum_\ell (2\ell+1) f_{sky}^{BB}\left[\log\left(\frac{\mathcal{C}_\ell^{BB}+\mathcal{N}_\ell^{eff}}{\bar{\mathcal{C}}_\ell^{BB}+\mathcal{N}_\ell^{eff}}\right)+\frac{\bar{\mathcal{C}}_\ell^{BB}+\mathcal{N}_\ell^{eff}}{\mathcal{C}_\ell^{BB}+\mathcal{N}_\ell^{eff}}-1\right]. \quad (6.17)$$

In order to render the forecasts more realistic, we marginalize the error of the tensor-to-scalar ratio over the foreground residuals. This can be done by considering the percentage of foreground removal as an additional parameter and by multiplying the likelihood in Eq. (6.17) by a gaussian prior describing our ignorance about the exact level at which foregrounds have been removed. We will assume that the percentage of foreground removal σ_F is known with relative error of order 1.

6.2.5 *Delensing*

One of the most important limiting factors in measuring primordial B-modes is gravitational lensing. Since B-modes induced by lensing have the same frequency dependence as primordial ones, one cannot proceed in the same way as with foregrounds. The idea then is to use the measurements

of polarization or temperature on short angular scales to reconstruct the lensing potential and remove lensing effects from the B-mode polarization on the larger angular scales [105–108].

Polarization delensing is not always important in improving the constraints on r. In the case of a large tensor-to-scalar ratio, the dominant contribution to the signal-to-noise comes from the low multipoles. For example, the lensed B-modes power spectrum becomes comparable to the power spectrum of the primordial B-modes corresponding to $r = 0.1$ around $\ell \sim 100$. In this case delensing cannot improve the errors significantly. The other case in which delensing is irrelevant is when the noise is larger than the lensing signal. Indeed the power spectrum of lensing B-modes for $\ell \lesssim 150$ is similar to white noise with amplitude $4.4\,\mu$K-arcmin, so that only for experiments with smaller noise delensing is relevant. If the instrument has a high sensitivity and a good angular resolution needed for the reconstruction of the lensing potential, delensing the maps can become important and can improve the errors on r even by a factor of a few for the beam sizes and the sensitivities of different proposed future experiments [107–109]. For example, Fig. 3 of [108] shows that with a beam size of 5 arcmin and sensitivity of $1\,\mu$K-arcmin one can improve the constraints on r by a factor of 5. Moreover, as the sensitivity and the resolution increase, there are no limits in how much of the lensing signal can be subtracted. This improvement is marginal for all the experiments considered in this section, except for the generation-IV experiments (GRD, BAL and ULDB) and for the satellites COrE and CMBPol. For all other experiments either the noise level is high enough to make delensing irrelevant or the angular resolution is too large to implement delensing. To include delensing in those experiments where it is viable, we assume that the power of lensing B-modes is reduced to 10% of the original value. The residual power would correspond to a noise equivalent power of $1.4\,\mu$K-arcmin. It would be useful to explore how the presence of foregrounds impacts the ability of delensing, but this goes beyond the our scope.

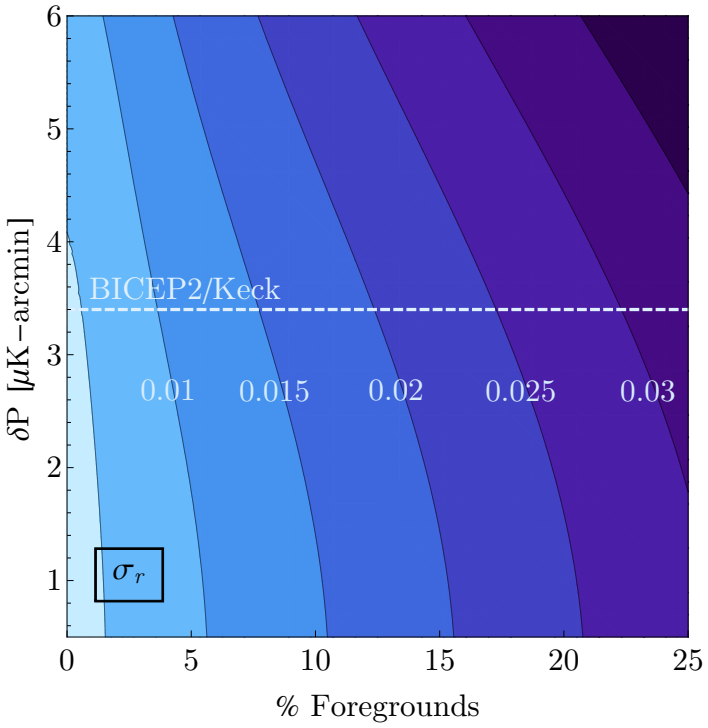

Figure 10: *Contours represent the 1σ error on r for $r = 0$, marginalized over the foreground residuals, using a single map of* 1% *of the sky at* 150 GHz *with beam of 30* arcmin*, as a function of foreground residuals and instrumental sensitivity. This is the case of BICEP2/Keck, which has sensitivity of 3.4* μK-arcmin*.*

6.3 RESULTS

6.3.1 *BICEP2/Keck and Planck*

Let us begin our analysis by checking that our forecasting method is compatible with the recent recent joint analysis [110]. In order to do so, we combine the BICEP2/Keck 150 GHz channel with the Planck 353 GHz one. With the CS method, for a fiducial value of $r = 0.05$ using the multipoles [20-150] and a gaussian prior on β_D with variance $\sigma_{\beta_D} = 0.11$, we obtain an error $\sigma_r = 0.04$, which is in good agreement with what was reported in [110].

Alternatively, using the phenomenological approach of 6.2.4, in Fig. 10 we plot the contours representing the error on r assuming $r = 0$ as a function of sensitivity and foreground residuals. As can be seen, our ability to constrain r crucially depends on the foreground removal. A reduction of foregrounds to 10% in power can lead (in the absence of gravitational waves) to a quite strong upper bound $r \leq 0.05$ at 3σ. Polarization experiments are already competitive with constraints from temperature alone, even with only one frequency and very mild foregrounds removal. Notice that with T-modes only cosmic variance prevents to constrain r better than 5×10^{-2} [111].[4] Notice moreover that in the near future it will be possible to include in the analysis the 95 GHz channel of Keck (here we assume a noise of $9\,\mu$K-arcmin). As can be seen in Tab. 2, the inclusion of such a frequency would allow to reduce the error on the tensor-to-scalar ratio by a factor of 2 with respect to the current constraint.

6.3.2 *Balloon-borne and Ground-based Experiments*

The situation will improve in the next few years since there are several experiments that are already collecting data and will have maps in two or more frequencies. In our forecasts we concentrate on a few proposed and funded experiments. In particular, for what regards ground-based experiments we consider Keck/BICEP3 and the Simons Array, and also AdvACT, CLASS and SPT-3G. The specifications used are in Tab. 10. We vary the level of foregrounds according to the fraction of the sky targeted

4 This bound of course is impossible to achieve due to sample variance induced by masking the sky.

	r	BICEP2/Keck + Planck$_{353}$
CS	0.1	3.5×10^{-2}
	0.01	—
	0.001	—
	0	2.2×10^{-2}

Table 2: *1σ errors on r for BICEP2/Keck (95 and 150 GHz) and the 353 GHz channel of Planck. This error, as calculated from the phenomenological method of Sec. 6.2.4, corresponds to a 30% level of leftover foregrounds in power.*

	r	Keck/BICEP3	Simons Array	AdvACT	CLASS	SPT-3G
CS	0.1	2.2×10^{-2}	7.6×10^{-3}	5.4×10^{-3}	6.5×10^{-3}	9.0×10^{-3}
	0.01	—	5.0×10^{-3}	3.1×10^{-3}	3.4×10^{-3}	4.2×10^{-3}
	0.001	—	—	—	—	—
	0	9.1×10^{-3}	3.4×10^{-3}	1.4×10^{-3}	9.0×10^{-4}	3.7×10^{-3}
FG 1%	0.1	1.9×10^{-2}	1.1×10^{-2}	7.8×10^{-3}	6.0×10^{-3}	8.1×10^{-3}
	0.01	7.8×10^{-3}	8.1×10^{-3}	4.8×10^{-3}	3.5×10^{-3}	4.1×10^{-3}
	0.001	—	—	—	—	—
	0	6.4×10^{-3}	7.8×10^{-3}	4.6×10^{-3}	3.3×10^{-3}	3.7×10^{-3}

Table 3: *1σ errors on r for future ground-based experiments.*

by each experiment, as given in Tab. 1. For what concerns the available multipoles, we consider the range $[30, 150]$. For AdvACT, CLASS and the Simons Array we consider the range $[2, 150]$, since they observe a larger fraction of the sky. This range is probably larger than what these experiments will actually be able to observe, since to handle atmospheric contamination they need to filter the data, losing power at low ℓ's. In Sec. 6.4 we will take a more conservative perspective. As can be seen in Tab. 3, which summarizes our forecasts, we expect these experiments to explore values of r of order 10^{-2}. The CS method gives results which are roughly comparable to a reduction of foregrounds to 1%. Of course there are sometimes sizable differences, since we do not expect all experiments to reduce foregrounds in

the same way. Still 1% represents a rough estimate of the level at which one should trust the foreground modeling for the CS.

	r	EBEX 10k	Spider
CS	0.1	1.5×10^{-2}	1.8×10^{-2}
	0.01	7.4×10^{-3}	—
	0.001	—	—
	0	6.4×10^{-3}	1.3×10^{-2}
FG 1%	0.1	2.2×10^{-2}	2.6×10^{-2}
	0.01	—	—
	0.001	—	—
	0	9.2×10^{-3}	2.1×10^{-2}

Table 4: *1σ errors on r for future balloon-borne experiments.*

Regarding balloon-borne experiments, we consider EBEX 10k and Spider (which has already finished the first flight), with specifications in Tab. 11. As can be seen in Tab. 4, we expect these experiments to explore values of $r \sim$ few $\times 10^{-2}$. It is fair to say that the level of dust measured by Planck only slightly degrade the previous forecasts and that the goal of these experiments are still within their range.

For all these experiments the error on the dust amplitude will be substantially smaller than the present Planck constraints, so that a cross-correlation with Planck will not significantly reduce the errors. However, Planck's data will still be useful to test the spectral dependence of the polarized dust emission model.

Looking a bit further into the future, we also consider an idealized balloon (BAL) and an ultra long duration ballon (ULDB) with the same four frequencies of EBEX 10k (150, 220, 280 and 350 GHz) and beams of 5 arcmin, but leave their sensitivity as a free parameter. For simplicity we assume that the sensitivity is equal across the frequencies, even though this may not be the optimal choice. The results of our forecasts can be found in Fig. 11 where we estimate the 1σ error for $r = 0$ for BAL covering the few supposedly clean patches found by Planck ($\sim 5\%$ of the sky), and ULDB covering 60% of the sky. As it can be seen, with a noise level $\sim 1\,\mu$K-arcmin and lensing removed to 10%, which are possible but challenging, one can

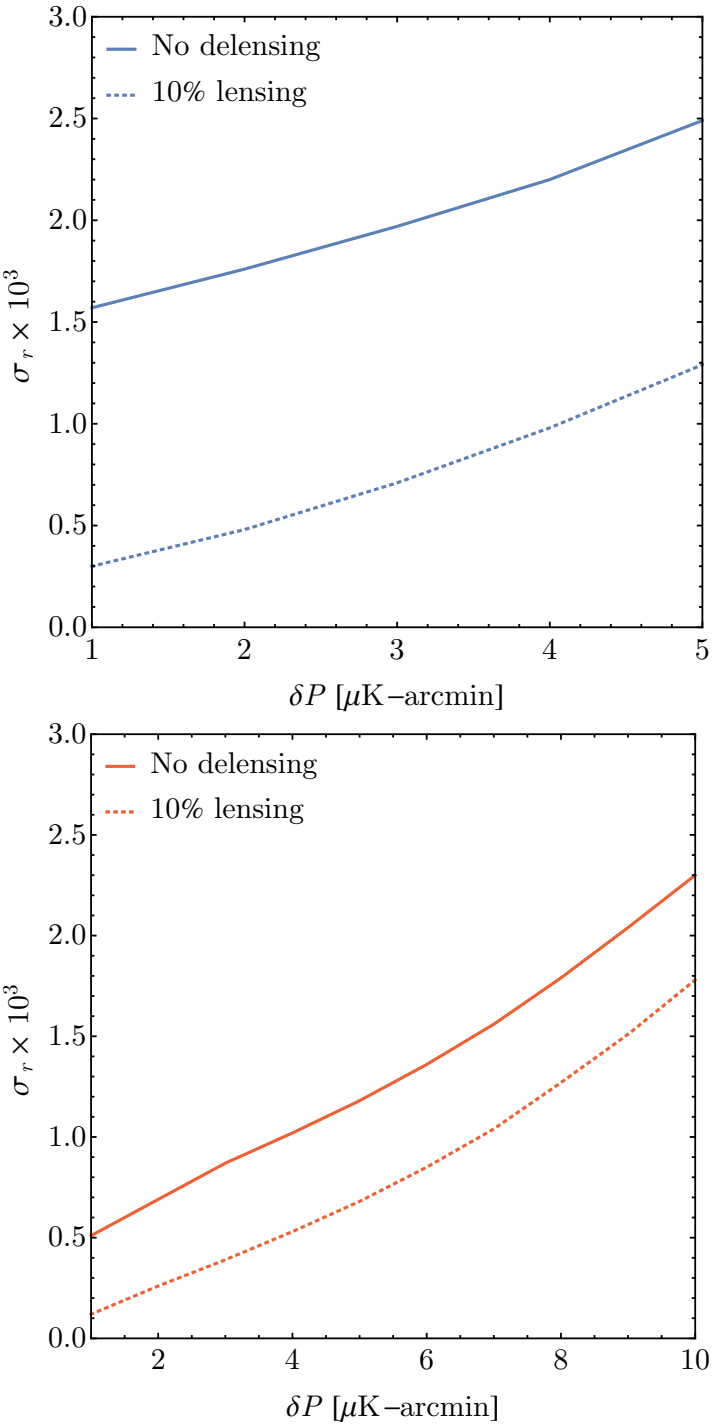

Figure 11: *1σ error on r as a function of the instrumental sensitivity for two hypothetical balloon experiments (BAL and ULDB in Tab. 11). These estimates use a patch of 5% of the sky for BAL and 60% of the sky for the ULDB. The solid line assumes lensing is not subtracted, the dotted line assumes lensing has been reduced to 10% in power. Since also delensing is applied, we considered the multipoles [30, 300].*

detect $r \sim 2 \times 10^{-3}$ with high statistical significance. Notice however that obtaining a noise level close to $1\,\mu$K-arcmin on 60% of the sky with an ULDB seems out of reach with a single 100-days flight (which is the target of this kind of experiments). We will discuss about a futuristic ground-based experiment (GRD) in Sec. 6.4.

6.3.3 *Satellite Experiments*

Finally, let us present our forecasts for various proposed satellite experiments (see Tab. 12 for the specifications). We assume that an effective area of 70% is observed with foregrounds parameters given in Tab. 1, and limit the multipole range to $[2, 300]$ for COrE and CMBPol (EPIC-2m) and $[2, 150]$ for LiteBIRD[5]. The summary of our estimates can be found in Tab. 5, and it shows that with respect to previous forecasts [96] there is only a minor degradation (no more than a factor of 2) of the ability to detect primordial tensor modes. In particular a detection of $r \sim 2 \times 10^{-3}$ is still achievable for the proposed missions. Notice however that the upper limit for $r = 0$ below 10^{-4} are very optimistic and degrade significantly when the reionization bump is excluded (we are going to comment on this in the next section).

6.4 MORE CONSERVATIVE ANALYSES

It is obvious, especially after the case of BICEP2, that a detection of primordial tensor modes must convincingly show that the signal is not contaminated by astrophysical foregrounds. If the description of foregrounds in terms of few parameters is accurate, we saw that future experiments will be able to remove them with very good accuracy. On the other hand, our knowledge of astrophysical foregrounds is rather qualitative and it is not clear at what level the model works. For example, for $r = 2 \times 10^{-3}$ foregrounds at 150 GHz are larger than the primordial signal by a factor of 10 in amplitude at the recombination bump on the cleanest 1% of the sky, and a factor of 50 in the 70% of the sky.

5 The angular resolution of LiteBIRD is not good enough for delensing and there is no advantage in considering higher multipoles when lensing is not subtracted.

	r	CMBPol	COrE	LiteBIRD
CS	0.1	1.6×10^{-3}	1.7×10^{-3}	2.3×10^{-3}
	0.01	3.0×10^{-4}	3.5×10^{-4}	6.7×10^{-4}
	0.001	1.1×10^{-4}	1.7×10^{-4}	3.1×10^{-4}
	0	2.1×10^{-5}	3.3×10^{-5}	8.9×10^{-5}
FG 1%	0.1	2.6×10^{-3}	2.6×10^{-3}	3.8×10^{-3}
	0.01	5.7×10^{-4}	7.1×10^{-4}	1.3×10^{-3}
	0.001	3.6×10^{-4}	5.1×10^{-4}	1.0×10^{-3}
	0	3.4×10^{-4}	4.9×10^{-4}	9.9×10^{-4}

Table 5: *1σ errors on r for various proposed satellite experiments. For CMBPol and COrE a delensing of 10% has been taken into account.*

There are of course various ways to check that we are observing primordial gravitational waves. The primordial signal is homogeneous over the sky and it has Gaussian statistics, contrary to what we expect for foregrounds [112]. Other features that are well known about the signal are its dependence both in frequency and in ℓ. To study the ability of future experiments to check these features, we add to the parameters discussed in the previous section also the possibility of a power-law frequency dependence of the CMB signal $(\nu/\nu_{CMB})^{\beta_{CMB}}$ with $\nu_{CMB} = 150$ GHz. Moreover, we multiply the tensor mode power spectrum by a power-law ℓ-dependence $(\ell/\ell_{CMB})^{\alpha_{CMB}}$ with $\ell_{CMB} = 80$. This roughly corresponds to the tensor tilt, although we are here interested in checking the expected approximate scale-invariance and not to assess the possibility to detect the tensor tilt. A convincing detection of primordial tensors should constrain both α_{CMB} and β_{CMB} to be close to zero. This will also give a sense of how close an unmodelled foreground component must be to the CMB signal to be undistinguishable from it. Since we want to be more conservative we also add as new parameters the ℓ-dependence of dust and synchrotron (α_D and α_S) so that the likelihood is a function of 10 parameters.

The results for ground-based and balloon-borne experiments are reported in Tab. 6 and include only values of r for which a significant detection is possible, since only in this case the additional parameters α_{CMB} and β_{CMB}

	r	σ_r	$\sigma_{\alpha_{CMB}}$	$\sigma_{\beta_{CMB}}$
AdvACT	0.1	9.3×10^{-3}	9.9×10^{-2}	1.3×10^{-1}
	0.01	7.0×10^{-3}	3.3×10^{-1}	1.1
	0.001	—	—	—
CLASS	0.1	2.3×10^{-2}	1.9×10^{-1}	2.2×10^{-1}
	0.01	—	—	—
Keck/BICEP3	0.1	3.1×10^{-2}	5.6×10^{-1}	4.1×10^{-1}
	0.01	—	—	—
Simons Array	0.1	1.9×10^{-2}	1.3×10^{-1}	2.2×10^{-1}
	0.01	—	—	—
SPT-3G	0.1	1.2×10^{-2}	1.3×10^{-2}	2.2×10^{-1}
	0.01	7.2×10^{-3}	9.8×10^{-1}	1.1
	0.001	—	—	—
EBEX 10k	0.1	1.6×10^{-2}	4.7×10^{-1}	3.9×10^{-1}
	0.01	—	—	—
Spider	0.1	3.3×10^{-2}	4.7×10^{-1}	5.4×10^{-1}
	0.01	—	—	—

Table 6: *$1\,\sigma$ errors on r, α_{CMB} and β_{CMB} for future ground-based and balloon-borne experiments.*

	r	σ_r	$\sigma_{\alpha_{CMB}}$	$\sigma_{\beta_{CMB}}$
CMBPol	0.1	1.6×10^{-3}	2.2×10^{-2}	6.8×10^{-3}
	0.01	3.9×10^{-4}	5.1×10^{-2}	2.6×10^{-2}
	0.001	2.1×10^{-4}	1.4×10^{-1}	1.3×10^{-1}
COrE	0.1	1.7×10^{-3}	2.5×10^{-2}	1.0×10^{-2}
	0.01	4.9×10^{-4}	6.1×10^{-2}	4.3×10^{-2}
	0.001	2.7×10^{-4}	1.7×10^{-1}	2.1×10^{-1}
LiteBIRD	0.1	2.7×10^{-3}	3.9×10^{-2}	1.5×10^{-2}
	0.01	1.2×10^{-3}	1.2×10^{-1}	7.3×10^{-2}
	0.001	8.0×10^{-4}	3.4×10^{-1}	3.7×10^{-1}

Table 7: *$1\,\sigma$ errors on r, α_{CMB} and β_{CMB} for future satellite experiments.*

are relevant. We see that the next generation of experiments will not be able to constrain α_{CMB} and β_{CMB}, unless $r \sim 0.1$.

	r	Simons Array	AdvACT	CLASS	CMBPol	COrE	LiteBIRD
CS	0.1	1.0×10^{-2}	7.5×10^{-3}	8.3×10^{-3}	2.7×10^{-3}	2.8×10^{-3}	3.7×10^{-3}
	0.01	8.3×10^{-3}	5.3×10^{-3}	6.1×10^{-3}	3.9×10^{-4}	4.6×10^{-4}	1.0×10^{-3}
	0.001	—	—	—	1.6×10^{-4}	2.4×10^{-4}	7.5×10^{-4}
	0	8.1×10^{-3}	5.0×10^{-3}	5.9×10^{-3}	1.4×10^{-4}	2.1×10^{-4}	7.2×10^{-4}

Table 8: *1σ errors on r for big-patch experiments, assuming $\ell > 30$.*

Our results for satellite experiments are given in Tab. 7: we find that the inclusion of additional parameters does not significantly degrade the errors on r (at most by a factor of 2) . Even for $r = 0.1$ the check of the tensor consistency relation, which would give $\alpha_{CMB} \simeq 10^{-2}$, looks impossible.

Another point of concern about foregrounds is the possibility of detecting the reionization bump. This of course is only relevant for experiments looking at a large portion of the sky. At this stage our knowledge of polarized foregrounds on large scales is very limited and it is not clear whether the reionization bump will be accessible once foregrounds are included. Moreover, ground-based experiments will also be limited by atmospheric

contaminants. While in the previous sections we extended the analysis to low multipoles for experiments with large f_{sky}, in Tab. 8 we consider a more conservative analysis where only the multipoles $\ell > 30$ are considered. To do so we consider the likelihood a function of six parameters, as in the previous section. While the change is moderate for large values of r, since the low multipoles do not help much with the statistics, the effect is relevant for small values of r and becomes dramatic for $r = 0$: the upper limit is degraded by a factor of 10 (this is compatible with the results of [108]). Notice that the amplitude of the reionization bump depends strongly on τ, so that when the measurement of tensor modes relies on the large scales, the error on r is significantly affected by the uncertainty on τ.

Let us now comment on our fiducial threshold $r = 2 \times 10^{-3}$. Ground-based experiments of the so-called stage IV are expected to achieve a sensitivity of the order $1\,\mu$K-arcmin with $\mathcal{O}(10^5)$ detectors over 5 years. For this value of r, in Fig. 12 we show the error on r, α_{CMB} and β_{CMB} for a hypothetical ground-based experiment (GRD) as a function of f_{sky} for two different sensitivities. The detection of $r = 2 \times 10^{-3}$ can be achieved at more than 3σ if the maps are delensed to 10% and roughly 20% of the sky is observed. In this case the constraints on α_{CMB} and β_{CMB} are small enough to allow a clear distinction from our modeled foregrounds. For satellite experiments, from our results shown in Tab. 7 and 8, we see that $r = 2 \times 10^{-3}$ is still detectable with large significance, even when it is not possible to detect the reionization bump. From Tab. 7 we also see that the error on β_{CMB} is small enough to allow for a clear distinction of β_{CMB} from β_D (or β_S).

The skeptical reader may be worried about the possibility of detecting gravitational waves buried under a foreground signal: we can model foregrounds, but how can we be sure that what is left in map is due to tensor modes and not some additional "evil dust" component we are unaware of? It is fair to say that a robust detection of primordial tensor modes requires a detection of the recombination bump. This feature, like a resonance in particle physics, should be robust against foregrounds which are not expected to peak al $\ell \sim 80$. To assess the ability of future experiments to measure the bump and distinguish it from a featureless power-law dependence, we compare the analysis in Sec. 6.3 (extended to include α_{CMB}), with a model which does not include the tensor transfer function, so that the spectrum is just a power law in ℓ. By treating the amplitude of the bump as a continuos

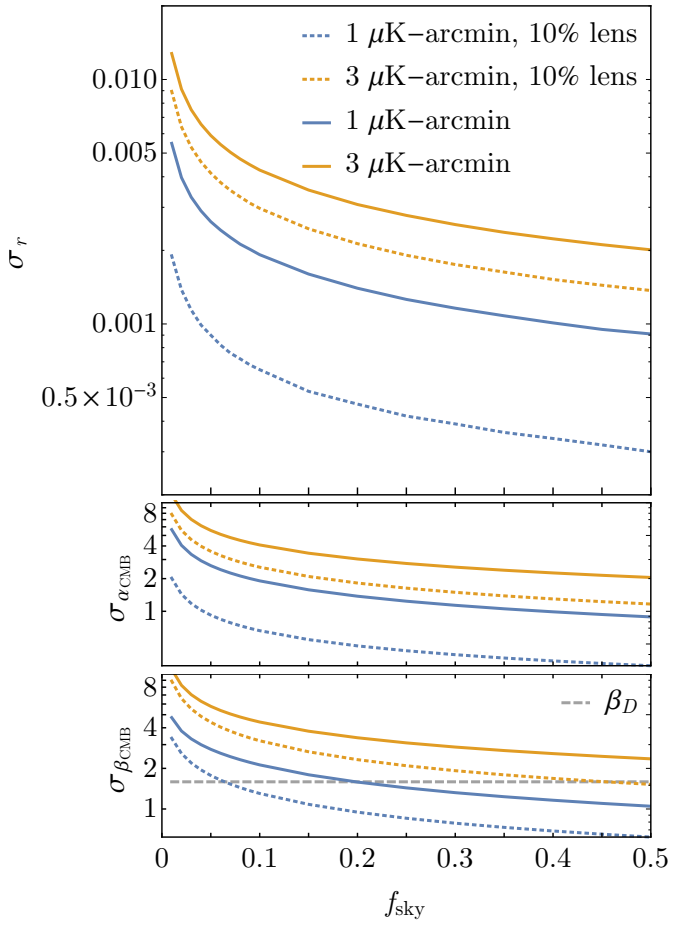

Figure 12: ***Top panel:*** *Error on* $r = 2 \times 10^{-3}$ *as a function of* f_{sky} *for a hypothetical ground experiment (GRD in Tab. 10). Solid lines assumes lensing is not subtracted, dotted lines assumes lensing has been reduced to 10%. Since also delensing is applied, we considered the multipoles [30, 300].*
Middle panel: *Error on* α_{CMB}.
Bottom panel: *Error on* β_{CMB}. *Notice that only for* $f_{sky} \gtrsim 30\%$ *the constraints on the spectral dependence allows to reject dust at* 2σ.

parameter, one can use Wilks's theorem.[6] In Tab. 9 we report for some of the experiments the minimum value of r for which a 3σ evidence of the bump (compared to a featureless power law ℓ-dependence) is possible. The rule of thumb is that a 10σ measurement of r gives a 3σ evidence of the recombination bump. For $r = 2 \times 10^{-3}$ it will be challenging to obtain evidence of the recombination bump even with satellite experiments. Indeed, for such a small value of r the primordial power spectrum at the recombination peak is comparable to the lensing B-modes reduced to 10% in power or 1.4 μK-arcmin.

	Simons Array	**AdvACT**	**CLASS**	**GRD**	**CMBPol**
r_{min}	0.08	0.045	0.095	0.005	0.003

Table 9: *Minimum value of r for which a 3σ detection of the recombination bump is possible. For GRD we choose a noise of $1\,\mu$K-arcmin, 10% delensing and 20% of the sky. Since we are interested in the recombination bump, the analysis is restricted to $\ell > 30$.*

6.5 CONCLUSIONS

We updated the forecasts for various future B-mode experiments taking into account Planck data on foregrounds. For experiments with at least three frequencies, the forecasts on r do not change significantly with respect to previous estimates, provided a simple modeling of foregrounds in terms of few parameters works at the required accuracy.

In particular we focussed on the theoretically motivated target of $r = 2 \times 10^{-3}$. This is achievable both with balloon-borne and ground based experiments if the noise can be reduced to $\sim 1\,\mu$K-arcmin and lensing B-modes are reduced to 10%. The ground-based experiments covering $\gtrsim 30\%$ of the sky should also have the statistical significance to check that the gravitational wave signal has a frequency dependence compatible with the one of the CMB and very different from the known foregrounds. Even for

6 We compute the minimum value of r for which $\frac{1}{2}\left(1 - \mathrm{CDF}\left(2\langle \log \mathcal{L}_{\mathrm{bump}}\rangle - 2\langle \log \mathcal{L}_{\mathrm{no\,bump}}\rangle\right)\right) < 0.003$, which corresponds to a 3σ confidence level, where CDF is the cumulative distribution function for the χ^2 distribution with one degree of freedom.

satellite experiments observing the recombination bump, which would likely be a convincing evidence that the signal is indeed due to primordial tensor modes, will be challenging for $r = 2 \times 10^{-3}$.

Part III

SCALAR BISPECTRUM

7

ISO(4,1) IN THE EFT OF INFLATION

7.1 MOTIVATIONS

The study of non-linearly realized symmetries in the context of inflation has proven to be a powerful tool to make model-independent predictions. A spontaneously broken symmetry is manifested in relations among operators with different number of fields: for example, in the framework of the EFT of inflation [33] one finds a relation between the kinetic term and the cubic operators, as a consequence of the non-linear realization of time diffeomorphisms. This implies that in any model with small speed of sound $c_s \ll 1$, one has parametrically large non-Gaussianities $\propto c_s^{-2}$. This regime is still allowed by observations, although severely constrained by the beautiful Planck data [32].

In this section we study the consequences of the non-linear realization of ISO(4,1), the 5D Poincaré symmetry, in the EFT of inflation. The motivation is twofold. On one hand this symmetry is typical of inflationary models based on brane constructions, where the position of a brane moving in an extra dimension plays the role of the inflaton. Although the inflationary solution spontaneously breaks ISO(4,1), the dynamics of perturbations is constrained by the non-linearly realized symmetries. On the other hand, observations are only sensitive to small perturbations around the inflating solution and their dynamics is encoded in the EFT of inflation. It is then of interest to study the possible symmetries that can be imposed in this theory. In this respect ISO(4,1) naturally stands out, since it contains both the 4D Poincaré group and the shift symmetry of the inflaton, which is usually imposed to justify slow-roll and the consequent approximate scale-invariance of the power spectrum. We will show, for example, that the relation between the cubic operators $\dot{\pi}^3$ and $\dot{\pi}(\partial_i\pi)^2$ which occurs in DBI inflation [19] does not require any UV input, but it is just a consequence of the ISO(4,1) symmetry at the level of the EFT of inflation.

7.2 NONLINEAR REALIZATION OF ISO(4,1).

In general, the homogeneous inflaton background $\phi_0(t)$ breaks the 4D Poincaré symmetry to translations and rotations: ISO(3,1) $\to$ ISO(3). Lets concentrate on scales much shorter than the Hubble scale H, where spacetime can be considered flat; we will consider gravity later on. At leading order in slow-roll, the inflaton ϕ is also endowed with an approximate shift symmetry $\phi \to \phi + c$ and a solution $\phi_0(t) = vt$ preserves a combination of this shift symmetry and time translations.

Perturbations around this background can be parametrized by the Goldstone mode π

$$\phi(\vec{x}, t) = \phi_0(t + \pi(\vec{x}, t)) = v \cdot (t + \pi(\vec{x}, t)), \tag{7.1}$$

and the most general action compatible with the symmetries reads

$$S = \int \mathrm{d}^4x \left(a_0\pi + a_1\dot{\pi}^2 + a_2(\partial_i\pi)^2 + f_1\dot{\pi}^3 + f_2\dot{\pi}(\partial_i\pi)^2 \right.$$
$$\left. + g_1\dot{\pi}^4 + g_2\dot{\pi}^2(\partial_i\pi)^2 + g_3(\partial_i\pi)^4 + \cdots \right). \tag{7.2}$$

All the constants are time independent as a consequence of the residual shift symmetry[1].

Let us now impose the extra symmetry. We want to enlarge ISO(3,1) $\times$ shift (11 generators) to a 15-dimensional group, ISO(4,1). The additional four transformations act as[2]

$$\delta\phi = \omega_\mu x^\mu + \phi\, \omega^\mu \partial_\mu \phi. \tag{7.3}$$

If we interpret ϕ as a coordinate in the extra dimension, for example describing the position of a brane, these transformations are rotations and boosts in the 5th dimension. The shift symmetry of ϕ is interpreted as translation in the 5th dimension to complete the isometry group of 5D flat space. However, the geometric interpretation is not mandatory and we may remain agnostic about the origin of this symmetry.

These transformations act on the Goldstone π as[3]

$$\delta\pi = \frac{1}{v}\delta\phi = \omega_\mu x^\mu + v^2 \cdot (t + \pi)(\omega^\mu \partial_\mu \pi + \omega^0), \tag{7.4}$$

1 The observed deviation from exact scale-invariance [113] implies that the shift symmetry (and therefore the whole ISO(4,1)) is not exact, but slightly broken by corrections of order slow-roll. Here we neglect these corrections.

2 Notice that we are using a parametrization where the 4D coordinates do not transform and the symmetry only acts on fields.

3 In general $\phi_0(t) = c + vt$, but because of the shift symmetry the constant can be set to zero without loss of generality.

where in the last equality we have reabsorbed a factor $1/v$ into the definition of ω_μ. Demanding that the action (7.2) is invariant under these additional transformations imposes some conditions on the coefficients $a_0,\ a_1,\ a_2, \ldots$[4]. Focusing on the variation of the action quadratic in π, we get the following relations

$$a_2 = -a_1(1-v^2), \quad f_1 = a_1 \frac{v^2}{1-v^2}, \quad f_2 = -a_1 v^2. \tag{7.5}$$

The first equation says that the speed of propagation of π excitations, the "speed of sound" c_s is related to v as

$$c_s^2 = 1 - v^2. \tag{7.6}$$

From the 5D geometrical point of view, this is a consequence of the relativistic sum of velocities. Here it is simply a consequence of the ISO(4,1) symmetry in the EFT of inflation. The cubic action is fixed by the second and third relation, so that up to cubic order the action (up to an overall coefficient) reads

$$S = \int \mathrm{d}^4x \left(\dot\pi^2 - c_s^2 (\partial_i \pi)^2 + \frac{1-c_s^2}{c_s^2} \left(\dot\pi^3 - c_s^2 \dot\pi (\partial_i \pi)^2 \right) \right). \tag{7.7}$$

This is exactly the same result one gets in DBI inflation [19], but here we see that one does not need any UV input: this action follows from the ISO(4,1) symmetry in the EFT of inflation.

As we are going to discuss later, these results will not change when gravity is taken into account. In the notation of [114]

$$S_3 = \int \mathrm{d}^4x \sqrt{-g}\ \dot H M_{\rm P}^2 (1-c_s^{-2}) \left[-\frac{1}{a^2} \dot\pi (\partial_i \pi)^2 + \left(1 + \frac{2}{3} \frac{\tilde c_3}{c_s^2} \right) \dot\pi^3 \right], \tag{7.8}$$

the coefficient $\tilde c_3$ (that is in general free), is fixed by ISO(4,1): $\tilde c_3 = \frac{3}{2}(1-c_s^2)$. In terms of the relative coefficient between the two operators $A \equiv -(c_s^2 + \frac{2}{3}\tilde c_3)$, the symmetry fixes $A = -1$. The Planck limits [32] on these parameters are shown in Fig. 13.

4 Notice that the tadpole term a_0 will in general be different from zero, since the background solution will also be affected by terms which are not ISO(4,1) symmetric, as a potential term and the Hubble friction. Anyway a_0 does not enter in the conditions below since its variation, eq. (7.4), is a total derivative.

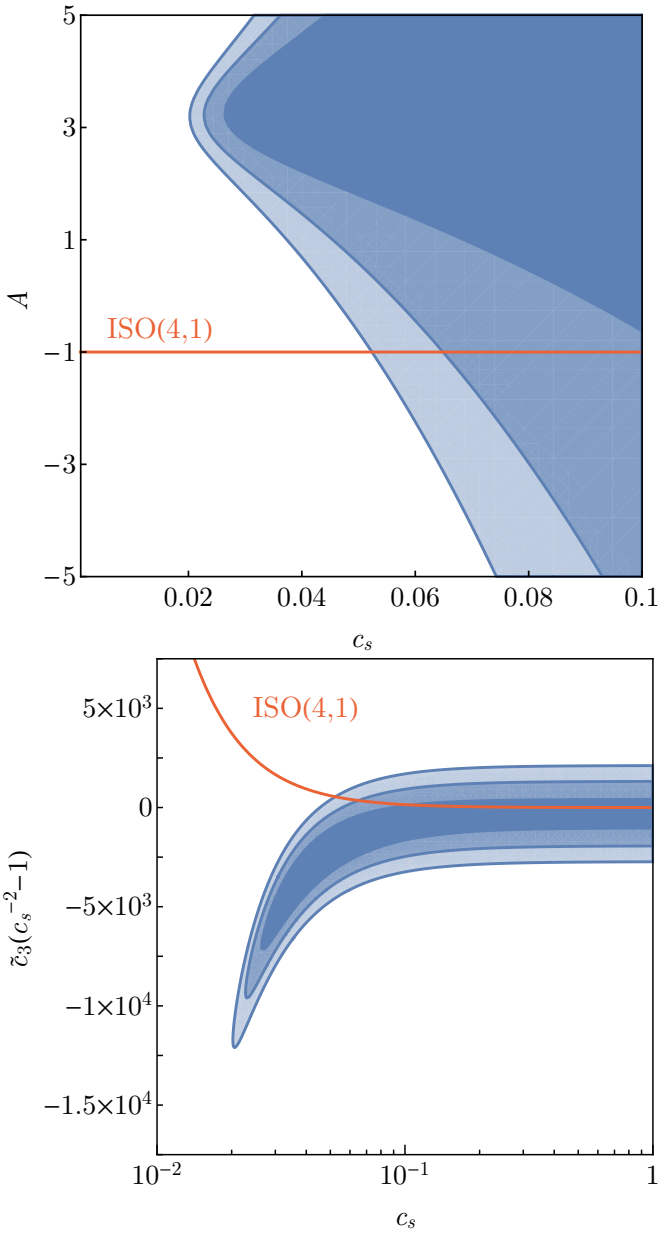

Figure 13: *Planck limits [32]: the 68%, 95% and 99.7% regions in the parameter space $(c_s, \tilde{c}_3)$ (above) and (c_s, A) (below). The orange line shows the prediction imposed by the ISO(4,1) symmetry (the same as in DBI inflation).*

We can go to higher order and set to zero the cubic variation of the action (7.2). We get a simple system of algebraic equations whose solution is

$$\begin{aligned} g_1 &= a_1 \frac{1-c_s^2}{c_s^4}\left(\frac{5}{4}-c_s^2\right), \\ g_2 &= -a_1 \frac{1-c_s^2}{c_s^2}\left(\frac{3}{2}-c_s^2\right), \\ g_3 &= a_1 \frac{1}{4}\left(1-c_s^2\right). \end{aligned} \tag{7.9}$$

Again all the coefficients are completely fixed in terms of a single parameter, the speed of sound c_s. This can be easily explained in terms of symmetries: the only operator with one derivative per field, that *linearly* realizes the 4D Poincaré group and non-linearly realizes ISO(4,1) is the brane tension operator

$$S = M^4 \int \mathrm{d}^4x \left(1 - \sqrt{1 + (\partial\phi)^2}\right), \tag{7.10}$$

so it is not surprising that everything is fixed for operators with one derivative per field. One can check that expanding (7.10) around $\phi_0 = vt$ one gets operators which satisfy (7.5) and (7.9). Still it is nice to see the constraints directly at the level of the EFT of inflation, without assuming to be able to extrapolate far from the inflationary solution.

One can also explore the consequences of ISO(4,1) for operators with more derivatives. If we look at operators with two derivatives on one of the π's then the effective action starts with cubic terms (quadratic terms are total derivatives) and reads

$$\begin{aligned} S = \int \mathrm{d}^4x \Big(&\lambda_1 \dot\pi^2 \partial_i^2 \pi + \lambda_2 (\partial_i \pi)^2 \partial_i^2 \pi \\ &+ \mu_1 \dot\pi^3 \partial_i^2 \pi + \mu_2 \dot\pi (\partial_i \pi)^2 \partial_i^2 \pi + \cdots \Big) \ . \end{aligned} \tag{7.11}$$

Using the transformation (7.4) we can easily find the relations among λ_1, λ_2, μ_1 and μ_2

$$\lambda_2 = \frac{-c_s^2}{2}\lambda_1 \ , \quad \mu_1 = \frac{4}{3}\frac{1-c_s^2}{c_s^2}\lambda_1 \ , \quad \mu_2 = (c_s^2 - 1)\lambda_1 \ . \tag{7.12}$$

As a check, one can start from the brane picture and consider an operator with one extra derivative on π compared to the brane tension: there is only one, the extrinsic curvature of the brane. This gives the following operator which non-linearly realizes ISO(4,1) [115]

$$S = M^3 \int \mathrm{d}^4x \, \frac{1}{1 + (\partial\phi)^2} \partial_\mu \partial_\nu \phi \partial^\mu \phi \partial^\nu \phi \ . \tag{7.13}$$

Indeed, expanding (7.13) around $\phi_0 = vt$ we find that the cubic action for the Goldstone is

$$S_3 = M^3 \int \mathrm{d}^4x \left(\frac{1-c_s^2}{c_s^2} \dot\pi^2 \partial_i^2 \pi + \partial_\mu \partial_\nu \pi \partial^\mu \pi \partial^\nu \pi \right), \tag{7.14}$$

which satisfy the constraints (7.12).

7.3 GALILEAN SYMMETRY AND THE COUPLING WITH GRAVITY.

The ISO(4,1) transformation (7.4) contains a dimensionless parameter v, which can be interpreted in a 5D picture as the brane velocity in the bulk. As we discussed, this parameter fixes the speed of sound of perturbations, Eq. (7.6). One can consistently take the limit $v \to 0$ of the symmetry[5]. This is a group contraction and in this limit the symmetry does not act on coordinates anymore and it thus commutes with the 4D Poincaré group. It reduces to an internal symmetry acting on π only

$$\delta\pi = \omega_\mu x^\mu \ . \tag{7.16}$$

This is the Galilean symmetry studied in [116], whose implications for the EFT of inflation have been discussed in [58] (see also [117]). This symmetry requires $c_s = 1$ and forbids all interactions with a single derivative per field. All interactions come from higher derivative terms. For example in eq. (7.14), for $c_s = 1$ we have only the second operator which can be written as $(\partial\pi)^2\Box\pi$, i.e. the cubic Galileon.

So far we discussed the ISO(4,1) symmetry in Minkowski space, without including gravity. Ultimately we are interested in calculating correlation functions during inflation, so that the coupling with gravity cannot be neglected. Similarly to what happens in the case of the Galilean symmetry discussed above, gravity breaks the ISO(4,1) symmetry[6]. This implies that the symmetry is not a good one for the background evolution, since in general the Hubble friction plays an important role. This is an additional motivation to formulate the symmetry directly in the EFT of inflation as a non-linearly realized symmetry for π on scales much shorter than Hubble, without reference to the background solution.

Another point to address is whether the actions for π derived above can be used, once minimally coupled to gravity, to calculate observables during inflation or gravity will completely change the picture. The breaking

5 Notice that this simply corresponds to the non-relativistic limit, when the brane motion is slow compared to the speed of light. This does *not* imply that the 4D Poincaré symmetry is restored. Indeed the transformation of π under a 4D boost parametrized by β^i is given by

$$\delta\pi = \beta^i x^i + \dot\pi\beta^i x^i + \partial_i\beta^i t \ . \tag{7.15}$$

This does not depend on v and is still non-linearly realized for $v \to 0$.

6 On a curved background, one cannot consistently define the constant vector ω^μ that appears in eq. (7.4): this shows that the symmetry is ill-defined in the presence of gravity.

of the symmetry due to gravity will manifest in two ways. First of all, graviton radiative corrections will induce operators which do not respect the symmetry. This effect is arguably small, as suppressed by powers of $M_{\rm P}$. Second, in calculating π loops on a gravitational background, non-invariant terms will also be generated. These operators will be invariant under a shift of π, as the shift symmetry is compatible with the coupling with gravity, but not fully ISO(4,1) invariant. As these terms arise only on a curved background they will contain powers of the Riemann tensor, schematically

$$(R_{\mu\nu\rho\sigma})^n(\partial\pi)^m \ . \tag{7.17}$$

On a quasi de Sitter background $R \simeq H^2$, so we expect these terms to be suppressed with respect to the ones we considered above by powers of $(H/\Lambda)^2 \ll 1$, where Λ is the UV cut-off of the theory.

These corrections can become relevant if the coefficient of some operator is unnaturally large. For example, the effect of the induced gravity term on a brane is studied in [118, 119] and the conclusion is that the cubic action is in general not uniquely fixed in terms of c_s: a different linear combination of the operators $\dot\pi^3$ and $\dot\pi(\partial_i\pi)^2$ is possible, giving in particular an orthogonal shape of non-Gaussianity. This is at first surprising as the model respect the ISO(4,1) symmetry we are discussing. However, the deviations are indeed due to cubic operators with more than three derivatives in the EFT of inflation [119]: in curved space some of these derivatives can be traded for the curvature scale H and one is left with only three derivatives on π. However a basic tenet of the EFT approach is that operators of higher dimension give small corrections: if they induce $\mathcal{O}(1)$ changes, it is not clear why one can neglect all the other higher dimensional terms.

7.4 ISO(4,1) OR SO(4,2)?

In DBI inflation [19] a probe brane lives in an AdS throat and non-linearly realizes the SO(4,2) group, so that one may wonder why we did not consider this group instead of ISO(4,1). One simple answer is that during inflation the brane does not move much in units of the AdS radius L, so that the difference between flat and curved bulk is immaterial. It is still interesting to understand whether SO(4,2) would give the same predictions.

The answer is no. It is straightforward to check, for example supplementing the DBI action with other SO(4,2)-invariant operators like the AdS

conformal Galileons [115], that the nice predictions of ISO(4,1) are lost. In particular the speed of sound is not fixed in terms of the velocity v in the bulk and the cubic operators $\dot{\pi}^3$ and $\dot{\pi}(\partial_i\pi)^2$ can appear in a general linear combination. The fact that c_s^2 is not fixed in terms of v may come as a surprise: after all it simply comes from the relativistic sum of velocities and this should apply locally also in AdS. This intuition however requires that higher derivative operators are suppressed by a cutoff scale $\Lambda \gg L^{-1}$: in this case only the tension of the brane is important and we get back to the DBI inflation case. When, on the other hand, $\Lambda \sim L^{-1}$ higher derivative operators are unsuppressed, the brane is a thick object in comparison with the AdS radius: it will not follow geodesics and we do not expect the same predictions as for DBI inflation, though the SO(4,2) symmetry is preserved.

All this can also be seen at the level of the EFT. The most general action allowed by the symmetry up to quadratic order is

$$S_{\rm EFT} = \int \mathrm{d}^4x \left(a_0\pi + a_1\dot{\pi}^2 + a_2(\partial_i\pi)^2 + m^2\pi^2\right), \tag{7.18}$$

where all the coefficients are now time dependent. As in the ISO(4,1) case, a background solution with constant velocity is not in general a solution, therefore we have to keep a_0 that will be cancelled by additional terms which are not SO(4,2) symmetric. The non-linear transformation of π that realizes SO(4,2) is

$$\begin{aligned}\delta\pi = \frac{1}{\dot{\phi}_0}\Bigg(&\omega_\mu x^\mu\phi + \omega_\mu x^\mu x^\nu\partial_\nu\phi - \frac{1}{2}x^2\omega^\mu\partial_\mu\phi \\ &+ \frac{1}{2}\omega^\mu\partial_\mu\phi - \frac{1}{2\phi^2}\omega^\mu\partial_\mu\phi\Bigg).\end{aligned} \tag{7.19}$$

Again, requiring the invariance of the action under this transformation leads to a set of three constraints on the coefficients

$$\begin{aligned}&m^2 - \frac{1}{2}\dot{a}_0 + \frac{\ddot{\phi}}{2\dot{\phi}}a_0 = 0, \\ &3a_0 + 4\dot{a}_1 - 2\partial_t\left(a_1\frac{\ddot{\phi}_0\phi_0}{\dot{\phi}_0^2}\right) - 2\frac{\phi_0}{\dot{\phi}_0}m^2 = 0, \\ &6a_2 + 4a_1 + 2\partial_t\left(a_1\frac{\phi_0^4 - \dot{\phi}_0^2}{\phi_0^3\dot{\phi}_0}\right) - 2\frac{\ddot{\phi}_0\phi_0}{\dot{\phi}_0^2}a_1 = 0.\end{aligned} \tag{7.20}$$

It is straightforward to verify that, for a constant $\dot{\phi}_0$, these constraints do not fix the relation among the coefficients of the kinetic term and therefore they do not fix c_s.

A particular case in which these constraints actually fix the form of the speed of sound, is the one in which the background preserves an SO(4,1) subgroup of SO(4,2) [120]. This happens for a background solution $\phi_0(t) = \alpha\, t^{-1}$. In this case the tadpole term is absent and π is massless so that the constraints in (7.20) greatly simplify. The speed of sound is then fixed by the last constraint and the residual dilation symmetry [120]: $c_s^2 = 1 - \alpha^{-2}$.

7.5 CONCLUSIONS

Imposing an ISO(4,1) symmetry in the EFT of inflation leaves (at leading order in derivative) a single free parameter, the speed of sound c_s. It should be straightforward to study the consequences of ISO(4,1) in the EFT of multi-field inflation [34]: this symmetry is indeed at play in multi-field DBI models [121].

8

CONSISTENCY RELATIONS AT SECOND ORDER

8.1 MOTIVATIONS AND MAIN RESULTS

As we saw in Sec. 2.3, at zeroth and first order in gradients, a long mode can be removed by a suitable change of coordinates, so that the correlation function boils down to the effect of this diffeomorphism on the short modes. Single-field consistency relations are therefore completely model-independent and their violation would represent a clear smoking gun of multi-field models. On the other hand these relations are somewhat trivial, as they simply state that the long mode does not affect the short ones in a coordinate-independent way, and so they do not contain any dynamical information. Of course this does not hold at second order in gradients, because at this order the long mode induces curvature [6], which obviously cannot be erased by a change of coordinates.

In this section we study single-field correlation functions in the limit in which one of the momenta, for definiteness we'll use $\vec{q}$, becomes soft, focusing on the leading "physical" effect, i.e. at order q^2. At this order the long mode induces curvature and we expect that, after we take a proper average over directions, its effect is the same as being in a curved Friedmann-Robertson-Walker (FRW) universe. This equivalence will be verifyied in section 8.2. Schematically we will show that for the three-point function

$$\langle \zeta_{\vec{q}} \zeta_{\vec{k}_1} \zeta_{\vec{k}_2} \rangle_{q\to 0,\,\mathrm{avg}} = P_\zeta(q)\, \frac{2}{3} \cdot q^2 \cdot \frac{\partial}{\partial \kappa} \langle \zeta_{\vec{k}_1} \zeta_{-\vec{k}_1} \rangle \,, \tag{8.1}$$

where P_ζ is the power spectrum, κ is the spatial curvature of the FRW and the subscript $_{\mathrm{avg}}$ indicates that an angular average has been taken. Notice that the equation above is rather different from a standard consistency relation, which connects observable correlation functions in our universe, so that one can check whether it is experimentally violated. Here the right-hand side of Eq. (8.1) contains the power spectrum in a *curved* universe, which cannot be measured independently. Therefore one cannot check experimentally whether the relation holds or not. Its interest is mostly conceptual since it allows to understand in simple physical terms the origin

Figure 14: *Parametric dependence of non-Gaussianity on the freezing scale. On the left the freezing scale is the Hubble scale. On the right the freezing scale $k_{ph,f}^{-1}$ is parametrically shorter than Hubble radius H^{-1}: in this case the effect of the curvature induced by the long mode is bigger, since it has to be compared with H^2 in the Friedmann equation.*

of non-Gaussianities in the regime of squeezing, $\mathcal{O}(q^2)$, where they are potentially large. Indeed the equivalence between a long mode and a curved universe allows to deduce some general property of correlation functions.

However from Eq. (8.1) one can draw a general conclusion: *the level of non-Gaussianity is always parametrically enhanced when modes freeze at a wavelength shorter than the Hubble radius.* More precisely

$$f_{\rm NL} \sim \left(\frac{k_{\rm ph,\,f}}{H}\right)^2 , \tag{8.2}$$

where $k_{\rm ph,\,f}$ is the physical freezing scale.

The argument for Eq. (8.2) is very simple and it is illustrated in Figure 14. Let us consider a squeezed triangle with a given ratio between the long and the short modes $\varepsilon \equiv \frac{q}{k} \ll 1$. The power spectrum of short modes is imprinted at freezing and at this moment the long mode has momentum $\varepsilon\, k_{\rm ph,\,f}$. The effect of the long mode is the same as being in a curved FRW, with curvature $\kappa \sim q^2/a^2 \cdot \zeta_q \sim \varepsilon^2 k^2/a^2 \cdot \zeta_q$. Curvature will modify the spectrum of the short modes through its effect in the Friedmann equation and its consequent change of the inflaton speed $\dot\phi$. The relative correction introduced in the Friedmann equation, and thus in the power spectrum for the short modes, is obtained by comparing the spatial curvature with H^2 at freezing time: $(q^2/a_f^2 \cdot \zeta_q)/H^2 \simeq \varepsilon^2 k_{\rm ph,\,f}^2 \zeta_q / H^2$. This implies that the three-point function behaves as $(k_{\rm ph,\,f}/H)^2 (q/k)^2 P(q) P(k)$ in the squeezed limit, i.e. $f_{\rm NL} \sim (k_{\rm ph,\,f}/H)^2$. Although the derivation works only in the squeezed limit, we expect by continuity (since at this order we are capturing

the physical effect of the long mode) that it gives the correct parametric dependence also when modes become comparable[1].

The relation (8.2) obviously works for models with reduced speed of sound [18, 19, 33, 122]:

$$\text{Reduced } c_s: \qquad k_{\rm ph,f} = \frac{H}{c_s} \quad \Rightarrow \quad f_{\rm NL} \sim \left(\frac{k_{\rm ph,f}}{H}\right)^2 \sim \frac{1}{c_s^2}\,. \tag{8.3}$$

Indeed we are going to check Eq. (8.1) both at order $1/c_s^2$, when one can neglect the curved spatial geometry and take only into account its effect on the scale factor and the inflaton speed (see section B.1.2), and at order one, when the check is more complicated since one has to relate the three-point function calculation done in terms of Fourier modes with the spectrum in the curved geometry (see section B.1.3). The same argument works when dissipative effects are present. In this class of models [60] a parameter $\gamma \gg H$ plays the role of an effective friction and the freezing happens when $c_s^2 k^2/a^2 \sim \gamma H$. This means that Eq. (8.2) reads

$$\text{Dissipative}: \qquad k_{\rm ph,f} = \frac{\sqrt{\gamma H}}{c_s} \quad \Rightarrow \quad f_{\rm NL} \sim \left(\frac{k_{\rm ph,f}}{H}\right)^2 \sim \frac{\gamma}{H c_s^2}\,. \tag{8.4}$$

This matches the explicit calculations of [60]. The argument leading to Eq. (8.2) does not rely on a linear dispersion relation for the inflaton perturbations and indeed it gives the correct estimate for Ghost Inflation [123] where the dispersion relation is of the form $\omega = k^2/M$. This gives

$$\text{Ghost Inflation}: \qquad k_{\rm ph,f} = (HM)^{1/2} \quad \Rightarrow \quad f_{\rm NL} \sim \left(\frac{k_{\rm ph,f}}{H}\right)^2 \sim \frac{M}{H}\,. \tag{8.5}$$

The check of Eq. (8.1) for Ghost Inflation is deferred to appendix B.3. A peculiar example is the one of Khronon Inflation [124]: in this case the power

1 Strictly speaking, $f_{\rm NL}$ is defined as proportional to the value of the 3-point function in the equilateral configuration. In this regime, the derivative expansion in q/k clearly does not apply and we therefore have nothing to say for this configuration. Here for $f_{\rm NL}$ we simply mean a typical value of the 3-point function apart from points where it accidentally cancels, or equivalently the observational limit on $f_{\rm NL}$ that would be obtained by a dedicated analysis of the 3-point function in the data. Indeed, since at order q^2 we are capturing a true physical effect, it is hard to imagine that there are cancellations for all configurations so that the size of the non-Gaussianities is parametrically different than the one obtained by extrapolating our expression (8.2) to the equilateral limit. This expectation is indeed confirmed by explicit calculations of the 3-point function in all triangular configurations.

spectrum is not affected by the background curvature at order $1/c_s^2$ since in the quadratic action the scale factor does not appear at this order and the speed of the inflaton background is immaterial due to the field redefinition symmetry. Indeed, we check in appendix B.4 that the $1/c_s^2$ terms of the three-point function at order q^2 vanish, when the proper angular average is taken. The general argument above implies that one has completely non-Gaussian perturbations, i.e. strong coupling, when freezing occurs at a sufficiently short scale

$$\text{Strong coupling :} \qquad \left(\frac{k_{\text{ph, f}}}{H}\right)^2 \sim P_\zeta^{-1/2} \ . \tag{8.6}$$

It is worth noticing that our arguments cannot be extended beyond the q^2 order. At order q^3 one *cannot* interpret the three-point function as a calculation of the two-point function on a long classical background. Indeed, at this order one cannot neglect the time-dependent phase of the long mode and therefore one cannot describe the long mode classically. Moreover, one cannot neglect anymore the probability that two short modes combine to give a long one.

Some of these arguments can be straightforwardly extended to the trispectrum and higher correlation functions. For example one can apply twice the argument leading to Eq. (8.1) to conclude that the amplitude of the four-point function will behave as

$$\tau_{\text{NL}} \sim \left(\frac{k_{\text{ph, f}}}{H}\right)^4 \ . \tag{8.7}$$

This corresponds to $1/c_s^4$ for models with reduced speed of sound and $(M/H)^2$ for Ghost Inflation.

8.2 FROM ζ-GAUGE TO A CURVED FRW UNIVERSE

The consistency relations at zeroth and first order in the Taylor expansion in q of ζ_L, the long wavelength component of ζ, have already been exhaustively considered in [26, 35–41]. Thus in this section we will neglect constant and gradient terms, and consider only the Taylor expansion at second order,

$$\zeta_L(\vec{x}, t) = \zeta_L|_0(t) + \frac{1}{2}\partial_i\partial_j\zeta_L|_0\, x^i x^j \ . \tag{8.8}$$

The time dependence of ζ_L is fixed by the equation of motion of ζ. Focusing on models with reduced speed of sound we have

$$\partial_t \left(\epsilon_H a_0^3 \dot{\zeta}_L\right) - \epsilon_H a_0 c_s^2 \, \partial^2 \zeta_L = 0 \ , \tag{8.9}$$

where a_0 is the scale factor of the flat FRW universe and $\epsilon_H = -\dot{H}/H^2$ is the slow-roll parameter. Notice that we cannot neglect the time dependence of ζ_L since it is of order q^2, if not larger. In this section we will assume that the time dependence of ζ starts at order q^2. Indeed the differential equation above admits, in the limit $q \to 0$, also a time-dependent solution for ζ. This solution is relevant when the background solution has not yet reached the attractor. This leads to a violation of the standard Maldacena consistency condition [125], though we expect that generalized consistency conditions hold even for these cases by considering that the universe in the presence of a long mode can now be locally described as a flat anisotropic one [39, 126]. Here we focus only on the case in which the background has already reached the attractor and the modes are in the Bunch-Davies vacuum, so that the time-dependence of ζ outside the horizon is of order q^2. Substituting in Eq. (8.8) and solving for $\zeta_L(t)$ at first order in the slow-roll parameters, we find that the long mode at quadratic order is ([2])

$$\zeta_L(\vec{x}, t) = -\frac{c_s^2 \partial^2 \zeta_L|_0}{2 a_0^2 H_0^2}(1 - 2\epsilon) + \frac{1}{2}\partial_i \partial_j \zeta_L|_0 \, x^i x^j \ . \tag{8.10}$$

In order to show that at this order the long mode is equivalent to being in a spatially curved FRW, it is enough to consider the perturbed metric in ζ-gauge at linear order (see for example [122])

$$\begin{aligned} g_{00} &= -1 - 2\frac{\dot{\zeta}_L}{H_0} \ , \\ g_{0i} &= -\frac{\partial_i \zeta_L}{H_0} + \frac{a_0^2 \epsilon}{c_s^2}\frac{\partial_i \dot{\zeta}_L}{\partial^2} \ , \\ g_{ij} &= a_0^2 \left(1 + 2\zeta_L\right) \delta_{ij} \ , \end{aligned} \tag{8.11}$$

2 In solving the differential equation (8.9) the lower bounds of the integrals give contributions proportional to q^2 that are either constant in time or decaying as $1/a^3$. The first term can always be reabsorbed in the definition of the asymptotic value of ζ, while we set the other term to zero since it would correspond to a decaying mode proportional to q^2, which is absent for any time-translation invariant state, such as the vacuum state.

and make a gauge transformation to rewrite it in the usual FRW form (i.e. by setting $g_{00} = -1$ and $g_{0i} = 0$). Under the coordinate transformation $x^\mu \to \tilde{x}^\mu = x^\mu + \xi^\mu(\tilde{x})$, the metric transforms as

$$\begin{aligned}\tilde{g}_{00} &= g_{00} + 2\dot{\xi}^0 \ , \\ \tilde{g}_{0i} &= g_{0i} - a_0^2\dot{\xi}^i + \partial_i\xi^0 \ , \\ \tilde{g}_{ij} &= g_{ij} - a_0^2\partial_i\xi^j - a_0^2\partial_j\xi^i - 2a_0^2H_0\xi^0\delta_{ij} \ ,\end{aligned} \tag{8.12}$$

and we can set $\tilde{g}_{00} = -1$ and $\tilde{g}_{0i} = 0$ by choosing the transformation parameters to be

$$\begin{aligned}\xi^0 &= \int^t \mathrm{d}t' \frac{\dot{\zeta}_L}{H_0} = -\frac{c_s^2\partial^2\zeta_L|_0}{2a_0^2H_0^3}\left(1 - \frac{3}{2}\epsilon\right) \ , \\ \xi^i &= -\int^t \mathrm{d}t' \frac{\partial_i\zeta_L}{a_0^2H_0}\left(1-\epsilon\right) = \frac{\partial_i\partial_j\zeta_L|_0\tilde{x}^j}{2a_0^2H_0^2} \ .\end{aligned} \tag{8.13}$$

The effect of the long mode is now entirely encoded in the spatial part of the metric

$$\tilde{g}_{ij} = a_0^2\left(\delta_{ij} - \frac{\partial_i\partial_j\zeta_L|_0}{a_0^2H_0^2} + \epsilon\frac{c_s^2\partial^2\zeta_L|_0}{2a_0^2H_0^2}\delta_{ij}\right)\left(1 + \partial_a\partial_b\zeta_L|_0\tilde{x}^a\tilde{x}^b\right) \ , \tag{8.14}$$

which, once averaged over angles, takes the familiar form

$$\tilde{g}_{ij,\,\mathrm{avg}} = a^2\left(1 - \frac{1}{2}\kappa\tilde{x}^2\right) \ , \tag{8.15}$$

where the spatial curvature κ and the scale factor a in the curved universe are given by

$$\begin{aligned}\kappa &= -\frac{2}{3}\partial^2\zeta_L|_0 \ , \\ a^2 &= a_0^2\left(1 + \frac{\kappa}{2a_0^2H_0^2} - \epsilon\frac{3c_s^2\kappa}{4a_0^2H_0^2}\right) \ .\end{aligned} \tag{8.16}$$

It is important to stress that the change of coordinates (8.13) decays away at late time. This implies that, since we are interested in correlation functions at late times, one can forget about the change of coordinates and just treat the long mode as adding spatial curvature to the FRW solution.

Eventually the consistency condition at this order can be written as

$$\langle\zeta_{\vec{q}}\zeta_{\vec{k}_1}\zeta_{\vec{k}_2}\rangle'_{q\to 0,\,\mathrm{avg}} = P_\zeta(q)\,\frac{2}{3}\cdot q^2\cdot\frac{\partial}{\partial\kappa}\langle\zeta_{\vec{k}_1}\zeta_{-\vec{k}_1}\rangle'_\kappa \ , \tag{8.17}$$

where the subscript κ means that the two-point function is calculated in the curved universe and primes on correlation functions indicate that a

$(2\pi)^3\delta(\sum_i \vec{k}_i)$ of momentum conservation has been removed. As stated above, the assumption used to derive this formula is the fact that the background solution is on the attractor, so that the time-dependence of the long ζ mode starts at order q^2. Additionally, in deriving Eq. (8.16) we used the slow-roll approximation, though we expect the relationship to hold at all orders in the slow-roll expansion. Our consistency condition should indeed hold for all FRW backgrounds that are accelerating so that modes freeze after horizon crossing. This implies that the effect of the long mode on the short ones is captured by a derivative expansion of the long mode at the time when the short modes cross the horizon. This ceases to be the case for decelerating FRW backgrounds, when modes re-enter the Hubble scale, and so the derivative expansion is not applicable.

One can generalize these arguments without taking the angular average and consider a curved anisotropic (but homogeneous) universe. In this case Eq. (8.17) becomes

$$\langle \zeta_{\vec{q}}\zeta_{\vec{k}_1}\zeta_{\vec{k}_2}\rangle'_{q\to 0} = P_\zeta(q)\; q_i q_j \frac{\partial}{\partial(q_i q_j \zeta_{\vec{q}})}\langle \zeta_{\vec{k}}\zeta_{-\vec{k}}\rangle'_{\rm local}\ , \tag{8.18}$$

where $\langle \dots \rangle_{\rm local}$ means that the two-point function is calculated in a locally anisotropic curved universe. We will study the anisotropic case in appendix B.2.

8.3 MODELS WITH REDUCED SPEED OF SOUND

In this section we are going to explicitly check our consistency relation in models with reduced speed of sound. We are going to work in the framework k-inflation [18], while in appendix we derive more general results using the Effective Field Theory of Inflation (EFTI) developed in [33]. Starting from the action for k-inflation in the curved universe of Eq. (1.41),

$$S = \int \mathrm{d}^4x\sqrt{-g}P(X,\phi)\ , \tag{8.19}$$

where $X = -\frac{1}{2}g^{\mu\nu}\partial_\mu\phi\partial_\nu\phi$, and expanding around $\phi(t,x) = \phi(t) + \dot{\phi}(t)\pi(t,x)$, we get the action for the homogeneous background $\phi(t)$

$$S = \frac{1}{2}\int \mathrm{d}^4x \left(a^3 P_X \dot{\phi}^2 - a^3 V(\phi)\right)\ , \tag{8.20}$$

and the equation of motion

$$\partial_t(a^3 P_X \dot{\phi}) - a^3 V' = 0\ . \tag{8.21}$$

Eq. (8.21) implies that the curvature not only changes the scale factor through Friedmann's equation and the spatial part of the metric but it also affects the background velocity $\dot{\phi}(t)$. Solving perturbatively for the background field $\phi(t) = \phi_0(t) + \delta\phi(t)$, one obtains[3]

$$\delta\dot{\phi} = C\, a_0^{-3} + \frac{3}{2} c_s^2 \dot{\phi}_0 \frac{\kappa}{a_0^2 H_0^2} \,. \tag{8.22}$$

Thus in $P(X)$ models one has to consider only the effects induced by the change of the background cosmology, which means the variations of $a(t)$, $H(t)$, and $\dot{\phi}(t)$, and the geometrical effect proportional to x^2. To relate the coefficients of the curved action for perturbations,

$$S = \frac{1}{2}\int d^4x\,\sqrt{-g}\Big((XP_X + 2X^2P_{XX})\dot{\pi}^2 - XP_X g^{ij}\partial_i\pi\partial_j\pi + 3\kappa X P_X \pi^2\Big) \,, \tag{8.23}$$

with those of the flat one, one has to expand Eq. (8.19) around flat quantities using the variations

$$\frac{\delta a(\eta)}{a(\eta)} = \frac{\kappa}{6}\eta^2 \quad \text{and} \quad \frac{\delta X}{X} = 2\frac{\delta\dot{\phi}}{\dot{\phi}} = 3\frac{c_s^2\kappa}{H_0^2 a_0^2} \,. \tag{8.24}$$

so for example

$$P_X \to P_X\left(1 + \frac{XP_{XX}}{P_X}\frac{\delta X}{X}\right) \,, \quad P_{XX} \to P_{XX}\left(1 + \frac{XP_{XXX}}{P_{XX}}\frac{\delta X}{X}\right) \,. \tag{8.25}$$

Using the definition for the parameters c_s^2, λ and Σ of Ref. [122],

$$\frac{XP_{XX}}{P_X} = \frac{1}{2}\left(\frac{1}{c_s^2} - 1\right) \,, \qquad \frac{2X^2P_{XXX}}{P_X} = \frac{3\lambda}{c_s^2\Sigma} - \frac{3}{2}\left(\frac{1}{c_s^2} - 1\right) \,, \tag{8.26}$$

the action in Eq. (8.23) reads

$$S = \int \mathrm{d}^4x\; H_0^2\epsilon a_0^2\left[\frac{1}{c_s^2}\left(1 + \frac{\kappa}{3a_0^2H_0^2} + \frac{9c_s^2\kappa}{a_0^2H_0^2}\frac{\lambda}{\Sigma}\right)\pi'^2 - \left(1 + \frac{11\kappa}{6a_0^2H_0^2}\right)(\partial_i\pi)^2\right] \,. \tag{8.27}$$

Here again we are considering only terms which contribute at order $1/c_s^2$. This greatly simplifies the calculation since the metric can be taken to

3 The homogeneous solution Ca_0^{-3} decays faster than the particular solution and thus can be neglected.

be spatially flat and the field can be decomposed in Fourier modes. The equation of motion derived from this action is

$$\pi_{\vec{k}}'' - \frac{2}{\eta}\pi_{\vec{k}}' + c_s^2 k^2 \pi_{\vec{k}} + \frac{\kappa}{a_0^2 H_0^2}\left(\left(\frac{1}{3} + 9c_s^2\frac{\lambda}{\Sigma}\right)\pi_{\vec{k}}'' + \frac{11}{6}c_s^2 k^2 \pi_{\vec{k}}\right) = 0 \,, \quad (8.28)$$

and can easily be solved perturbatively in κ. Once one has checked that the solution has the correct normalization, the power spectrum for ζ can be calculated using the standard procedure and the result is

$$\langle \zeta_{\vec{k}}\zeta_{-\vec{k}}\rangle_\kappa' = P_\zeta(k)\left(1 - \frac{19 + 18\frac{\lambda}{\Sigma}}{8c_s^2 k^2}\kappa\right) \,. \quad (8.29)$$

The contribution to the squeezed limit of the three-point function is then obtained by averaging over the long mode and substituting $\kappa = \frac{2}{3}q^2\zeta_{\vec{q}}$

$$\langle \zeta_{\vec{q}}\zeta_{\vec{k}_1}\zeta_{\vec{k}_2}\rangle_{q\to 0}' = -P_\zeta(q)P_\zeta(k)\frac{1}{c_s^2}\left(\frac{19}{12} + \frac{3}{2}\frac{\lambda}{\Sigma}\right)\frac{q^2}{k^2} \,. \quad (8.30)$$

Indeed, this agrees with the squeezed limit of the three-point function calculated with the standard *in-in* formalism, Eq. (2.40), once the angular average is taken and terms not enhanced by $1/c_s^2$ are neglected.

8.4 CONCLUSIONS

We have shown and verified in few examples that, in single-field models of inflation, the three-point function in the squeezed limit at order q^2 can be understood as the effect of spatial curvature on the short modes, i.e. calculating the power spectrum in a curved FRW. This gives a nice alternative way to understand the connection between large non-Gaussianity and freezing at a scale shorter than H^{-1}. In some sense this represents the "last" consistency relation for scalars (for relations including also tensor modes see [40]): at order q^3 one cannot think about non-Gaussianity as the effect of a classical background mode modifying the dynamics of the short modes.

ACKNOWLEDGMENTS

During my PhD I had the invaluable chance to work with fantastic people. Surely I have to begin with Paolo. I am truly in debt with him, for his constant presence and help, positive attitude and friendship. Definitely I would not be at this point without him. 1+1 is not 12.

I would like to thank Marko, as friend and collaborator, for countless times discussing and joking in and outside the office.

Acknowledgments also goes to all the collaborators I have had the opportunity to work with, Sergei Dubovsky, Razieh Emami, Diana Lopez Nacir, Ashley Perko, Leonardo Senatore, Marco Serone, Enrico Trincherini, Giovanni Villadoro, and Matias Zaldarriaga.

I would also like to thank many people who I have met in the past years and from whom I have learnt a lot, Nima Arkani-Hamed, Daniel Baumann, Emanuele Castorina, Mehrdad Mirbabayi, Marcello Musso, Alberto Nicolis, Enrico Pajer, Aseem Paranjape, Emiliano Sefusatti, and Ravi Sheth.

Last, I would like to thank SISSA and ICTP for giving me the means to get to this point and the IAS for hospitality during the spring of 2014. It was a very valuable period.

APPENDIX

A

INSTRUMENTAL SPECIFICATIONS

A.1 BALLOONS AND GROUND-BASED EXPERIMENTS

Experiment	f_{sky} [%]	ν [GHz]	θ_{FWHM} [′]	δP [μK′]
AdvACT	50	90	2.2	7.8
		150	1.3	6.9
		230	0.9	25
CLASS	70	38	90	39
		93	40	13
		148	24	15
		217	18	43
Keck/BICEP3	1	95	30	9.0
		150	30	2.3
		220	30	10
Simons Array	65	95	5.2	13.9
		150	3.5	11.4
		220	2.7	30.1
SPT-3G	6	95	1	6.0
		150	1	3.5
		220	1	6.0
GRD	[1,50]	100, 150, 220	5	1, 3

Table 10: *Specifications for ground-based experiments used in our forecasts: [127–134]. The sensitivity $\delta P = \sigma_{pix}\theta_{FWHM}$ is for the Stokes Q and U.*

Experiment	f_{sky} [%]	ν [GHz]	θ_{FWHM} [′]	δP [μK′]
EBEX	1	150	8	5.8
		250	8	17
		410	8	150
Spider	7.5	94	49	17.8
		150	30	13.6
		280	17	52.6
BAL	5	150, 220, 280, 350	5	[1,5]
ULDB	60	150, 220, 280, 350	5	[1,10]

Table 11: *Specifications for balloon-borne experiments used in our forecasts: [127–134]. The sensitivity $\delta P = \sigma_{pix}\theta_{FWHM}$ is for the Stokes Q and U.*

A.2 SATELLITES

Experiment	ν **[GHz]**	θ_{FWHM} [′]	δP [μK′]
CMBPol (EPIC-2m)	30	26	19.2
	45	17	8.3
	70	11	4.2
	100	8	3.2
	150	5	3.1
	220	3.5	4.8
	340	2.3	21.6
COrE	45	23	9.1
	75	14	4.7
	105	10	4.6
	135	7.8	4.6
	165	6.4	4.6
	195	5.4	4.5
	225	4.7	4.6
	255	4.1	10.5
	285	3.7	17.4
	315	3.3	46.6
	375	2.8	119
LiteBIRD	60	32	10.3
	78	58	6.5
	100	45	4.7
	140	32	3.7
	195	24	3.1
	280	16	3.8

Table 12: *Specifications for satellite experiments used in our forecasts: [96, 135, 136]. The sensitivity $\delta P = \sigma_{pix}\theta_{FWHM}$ is for the Stokes Q and U. All experiments target approximately 70% of the sky.*

B

CONSISTENCY RELATION

B.1 CHECKS OF THE CONSISTENCY RELATION

In this appendix we want to show how it is possible to obtain the same result obtained in section 8.3 with the dictionary of the Effective Field Theory of Inflation (EFTI) developed in [33]. The EFTI is built on the fact that during inflation there is a physical clock that breaks spacetime diffeomorphism invariance while preserving time-dependent spatial diffeomorphisms. Thus the dynamics of the inflaton is captured in an effective action derived by writing all terms consistent with the residual symmetries around a given cosmological background. The most general effective action around the flat FRW background at lowest order in derivatives and up to cubic order in perturbations is [33]

$$S = \int \mathrm{d}^4x\sqrt{-g}M_{\mathrm{P}}^2\left[-\left(3H_0^2+\dot{H}_0\right)+\dot{H}_0 g^{00}\right.$$
$$\left.+\frac{1}{2}\left(\frac{c_s^2-1}{2c_s^2}\right)\dot{H}_0\left(g^{00}+1\right)^2+\frac{1}{6}\left(\frac{1-c_s^2}{2c_s^4}c_3\right)\dot{H}_0\left(g^{00}+1\right)^3+\ldots\right], \tag{B.1}$$

where a_0 is the unperturbed history for the spatially flat FRW, c_s is the speed of sound of the perturbations, and c_3 is a dimensionless parameter not fixed by symmetries. For simplicity we take c_s and c_3 to be time independent. To describe the fluctuations around a flat FRW background it is useful to introduce the Goldstone boson π that nonlinearly realizes time diffeomorphisms. Following [33], at leading order in slow-roll, we can neglect metric fluctuations and go to the decoupling limit. The cubic action for π becomes

$$S^{(3)} = \int \mathrm{d}^4x\, a_0^3\left(-\frac{\dot{H}_0M_{\mathrm{P}}^2}{c_s^2}\right)\left[-(1-c_s^2)\dot{\pi}\frac{(\partial_i\pi)^2}{a_0^2}+(1-c_s^2)\left(1+\frac{2}{3}\frac{c_3}{c_s^2}\right)\dot{\pi}^3\right]. \tag{B.2}$$

Now it is straightforward to calculate the three-point function. Using $\zeta = -H_0\pi$, we get the following expression

$$\langle\zeta_{\vec{k}_1}\zeta_{\vec{k}_2}\zeta_{\vec{k}_3}\rangle' = \left(\frac{H_0^2}{4\epsilon c_s M_{pl}^2}\right)^2 \frac{1}{\prod_i 2k_i^3}\left[\left(1-\frac{1}{c_s^2}\right)\left(c_3+\frac{3}{2}c_s^2\right)\frac{32k_1^2k_2^2k_3^2}{k_t^2}\right.$$
$$\left.-4\left(1-\frac{1}{c_s^2}\right)\left(12\frac{k_1^2k_2^2k_3^2}{k_t^3}-\frac{8}{k_t}\sum_{i>j}k_i^2k_j^2+\frac{4}{k_t^2}\sum_{i\neq j}k_i^2k_j^3+\sum_i k_i^3\right)\right], \tag{B.3}$$

with $k_t \equiv k_1+k_2+k_3$. In order to find the squeezed limit we can expand the expression above using

$$\vec{k}_1 = \vec{k}-\frac{1}{2}\vec{q}\,, \quad \vec{k}_2 = -\vec{k}-\frac{1}{2}\vec{q}\,, \quad \vec{k}_3 = \vec{q}\,, \quad q \ll k\,, \tag{B.4}$$

because in this way it is evident that the three-point function does not have corrections that are linear in q. Expanding up to second order in q we find

$$\langle\zeta_{\vec{q}}\zeta_{\vec{k}_1}\zeta_{\vec{k}_2}\rangle'_{q\to 0} = P_\zeta(q)P_\zeta(k)\left(1-\frac{1}{c_s^2}\right)\left[\left(2+\frac{1}{2}c_3+\frac{3}{4}c_s^2\right)\frac{q^2}{k^2}-\frac{5}{4}\frac{(\vec{k}\cdot\vec{q})^2}{k^4}\right]. \tag{B.5}$$

What is left to do in order to verify the consistency condition (8.17) is to calculate the two-point function in the spatially curved FRW. What makes this calculation nontrivial is that the two-point function in the curved universe must be expressed in terms of flat universe parameters (the speed of sound c_s and c_3) because we want to compare it to the three-point function. In the rest of this section we are going to show how this can be done. First, we will derive the quadratic action for short modes in a curved FRW and match the parameters with the flat ones. Then, we will calculate the two-point function and show that the consistency relation is satisfied.

B.1.1 *Quadratic action for short modes in a curved FRW universe*

In order to calculate the two-point function in a curved FRW we need the action for the short modes. The most straightforward thing to do is to write the EFTI for a curved FRW [33],

$$\tilde{S} = \int \mathrm{d}^4\tilde{x}\sqrt{-\tilde{g}}\; M_{\mathrm{P}}^2\left[-\left(3H^2+\dot{H}+2\frac{\kappa}{a^2}\right)+\left(\dot{H}-\frac{\kappa}{a^2}\right)\tilde{g}^{00}\right.$$
$$\left.+\frac{1}{2}\left(\frac{\tilde{c}_s^2-1}{2\tilde{c}_s^2}\right)\left(\dot{H}-\frac{\kappa}{a^2}\right)\left(\tilde{g}^{00}+1\right)^2\right], \tag{B.6}$$

where tildes indicate curved quantities, and introduce the Goldstone $\tilde{\pi}_S$ via the Stueckelberg trick $\tilde{t} \to \tilde{t} + \tilde{\pi}_S$. This procedure leads to the following action

$$\tilde{S}_{\rm avg} = -\int \mathrm{d}^4\tilde{x}\, \sqrt{-\tilde{g}} \left(\dot{H} - \frac{\kappa}{a^2}\right) M_{\rm P}^2 \left[\frac{1}{\tilde{c}_s^2}\dot{\tilde{\pi}}_S^2 - \partial^i\tilde{\pi}_S\partial_i\tilde{\pi}_S + 3\dot{H}\tilde{\pi}_S^2\right]. \quad \text{(B.7)}$$

Note however that $\tilde{c}_s$, which represents the speed of propagation of the $\tilde{\pi}_S$ waves, is a free parameter which is not determined by the background cosmology and has to be related to c_s and c_3, the parameters of the effective action in the flat universe. The relation can be found by noticing that the speed of propagation is a physical quantity that can be measured on short scales, where the universe is locally flat. Thus the speed of propagation must be the same in the curved and in the flat EFTI, provided that in the latter we take into account the background of the long wave π_L. The speed of π_S waves over the background of the long mode can be read directly from the action in the flat universe Eq. (B.1) once in the interaction Lagrangian in Eq. (B.2) we replace $\pi = \pi_L + \pi_S$. We can go on short scales and neglect the space dependence of π_L. The relevant action reads

$$\begin{aligned} S = \int \mathrm{d}^4x\, \epsilon M_{\rm P}^2 H_0^2 a_0^3 \frac{1}{c_s^2}\Bigg[&\left(1 + (1-c_s^2)\left(1 + \frac{2}{3}\frac{c_3}{c_s^2}\right)3\dot{\pi}_L\right)\dot{\pi}_S^2 \\ &- c_s^2\left(1 + \frac{1}{c_s^2}(1-c_s^2)\dot{\pi}_L\right)\frac{(\partial_i\pi_S)^2}{a_0^2}\Bigg]. \end{aligned} \quad \text{(B.8)}$$

If we consider the long mode of π: $\pi_L = -\zeta_L/H_0$, where ζ_L is given in Eq. (8.10), we obtain the following quadratic action for π_S

$$\begin{aligned} S^{(2)} = \int \mathrm{d}^4x\, \epsilon M_{\rm P}^2 H_0^2 a_0^3 \frac{1}{c_s^2}\Bigg[&\left(1 + (1-c_s^2)\left(3c_s^2 + 2c_3\right)\frac{3\kappa}{2a_0^2H_0^2}\right)\dot{\pi}_S^2 \\ &- c_s^2\left(1 + (1-c_s^2)\frac{3\kappa}{2a_0^2H_0^2}\right)\frac{(\partial_i\pi_S)^2}{a_0^2}\Bigg]. \end{aligned} \quad \text{(B.9)}$$

From this we can read the speed of sound in the flat EFTI and this must be the same as $\tilde{c}_s^2$:

$$\tilde{c}_s^2 = c_s^2\frac{\left(1 + (1-c_s^2)\frac{3\kappa}{2a_0^2H_0^2}\right)}{\left(1 + (1-c_s^2)\left(3c_s^2+2c_3\right)\frac{3\kappa}{2a_0^2H_0^2}\right)} \simeq c_s^2\left(1 + \frac{3\kappa}{2a_0^2H_0^2}\left(c_s^2-1\right)\left(3c_s^2+2c_3-1\right)\right), \quad \text{(B.10)}$$

where in the second passage we have expanded up to linear order in κ, as we always do in this thesis. This fixes the speed of sound in the curved EFTI.

We can now plug this value for $\tilde{c}_s$ and use the scale factor of Eq. (8.16) in the action of Eq. (B.7) to obtain the action for the short modes. At first order in κ and ϵ it reads

$$S_{\rm avg}= \int \mathrm{d}^4x\ \epsilon M_{\rm P}^2 H_0^2 a_0^2 \left(1-\frac{3}{4}\kappa x^2\right)\left[\frac{1}{c_s^2}\left(1+\frac{3\kappa}{4a_0^2H_0^2}\left(1+4c_3+10c_s^2-4c_3c_s^2-6c_s^4\right)\right)\pi_S'^2 - \left(1+\frac{1}{2}\kappa x^2\right)\left(1+\frac{\kappa}{4a_0^2H_0^2}\left(7+6c_s^2\right)\right)(\partial_i\pi_S)^2+3\kappa\pi_S^2\right], \tag{B.11}$$

where we have used conformal time and suppressed tildes for simplicity. Starting from this action, in the next sections, we will calculate the two-point function of the short modes and check the consistency relation.

However, before doing so, it is important to notice that the two Goldstone modes – $\tilde{\pi}_S$ in the curved universe and π_S in the flat universe – are different given that we are expanding around different backgrounds. To relate the two it is sufficient to consider the change of coordinates in Eq. (8.13). Since $\tilde{\pi}_S$ is the perturbation around $\tilde{t}$ and π_S is the perturbation around t, the relation between the two is

$$\tilde{\pi}_S = (1+\dot{\xi}^0)\pi_S\ , \tag{B.12}$$

where the time dependence of ξ^0 is a_0^{-2}. Eventually the effect of curvature and anisotropy goes to zero at late times and thus $\tilde{\pi}_S = \pi_S$ when we evaluate correlation functions. This also means that we can directly relate correlation functions of $\tilde{\pi}_S$ in the local curved universe to correlation functions of global quantities. The nonlinear relationship between ζ_S and π_S in the flat FRW universe is

$$\zeta_S = -H_0\pi_S + \frac{1}{2}\dot{H}_0\pi_S^2\ , \tag{B.13}$$

at second order, plus terms with derivatives of π_S that vanish after horizon crossing [36]. The π_S^2 term in Eq. (B.13) is slow-roll suppressed so we can neglect its contribution to the three-point function. We then find that at late times the local $\tilde{\pi}_S$ is related to the global ζ_S as

$$\zeta_S = -H_0\tilde{\pi}_S\ , \tag{B.14}$$

to leading order in the slow-roll parameter ϵ.

B.1.2 *The two-point function at leading order in* $1/c_s^2$

Now that we have the action for the short modes in the curved universe (B.11), we can proceed with the calculation of the two-point function and check the consistency relation. In this subsection we will focus on the case of leading order in $1/c_s^2$ for an isotropic long mode. When the speed of sound is parametrically smaller than 1 the relevant effects of the long mode are the modifications of the scale factor, the Hubble constant and the speed of sound. As we discussed in the introduction, these affect the 2-point function of the short k-modes proportionally to $\kappa/H^2 \sim (q^2/a_f^2 \cdot \zeta_q)/H^2 \sim \varepsilon^2 k_{\mathrm{ph,f}}^2 \zeta_q/H^2 \sim \varepsilon^2 \zeta_q/c_s^2$, where q is the long mode and $\varepsilon = q/k \ll 1$ is the squeezing parameter. On the contrary, geometrical effects scale as $\kappa\, x^2 \sim q^2/k^2 \cdot \zeta_q \sim \varepsilon^2 \zeta_q$, and are therefore not enhanced for $c_s \ll 1$.

Given that at order $1/c_s^2$ geometrical effects and the mass term do not contribute, the leading part of the action (B.11) is given by

$$S_{\mathrm{avg}} = \int \mathrm{d}^4x\ \epsilon M_{\mathrm{P}}^2 H_0^2 a_0^2 \left[\frac{1}{c_s^2}\left(1+\frac{3\kappa}{4a_0^2H_0^2}(4c_3+1)\right)\pi'^2 - \left(1+\frac{7\kappa}{4a_0^2H_0^2}\right)(\partial_i\pi)^2\right] . \tag{B.15}$$

In this approximation space can be considered to be flat and one can get the power spectrum for the short modes using the standard quantization of the scalar field. After going to Fourier space the equation of motion for the short modes is

$$\pi_{\vec{k}}'' - \frac{2}{\eta}\pi_{\vec{k}}' + c_s^2 k^2 \pi_{\vec{k}} + \frac{\kappa}{4a_0^2H_0^2}\left(3(4c_3+1)\pi_{\vec{k}}'' + 7c_s^2k^2\pi_{\vec{k}}\right) = 0 , \tag{B.16}$$

and it can be easily solved perturbatively in κ. The zeroth order solution is proportional to the standard de Sitter modes, but the normalization can be in principle different. In order to fix it we have to demand that the commutator of the field π and the generalized momentum Π is given by

$$[\pi_{\vec{k}}(\eta), \Pi_{\vec{k}'}(\eta)] = i\delta(\vec{k}+\vec{k}') . \tag{B.17}$$

After fixing the normalization it is easy to find the two-point function in the late time limit. The result is

$$\langle \zeta_{\vec{k}}\zeta_{-\vec{k}}\rangle'_\kappa = P_\zeta(k)\left(1 - \frac{19+6c_3}{8c_s^2k^2}\kappa\right) . \tag{B.18}$$

We can use this result to get the contribution to the squeezed limit of the three-point function. We only have to average over the long mode and recall that $\kappa = \frac{2}{3}q^2\zeta_{\vec{q}}$

$$\langle \zeta_{\vec{q}}\zeta_{\vec{k}_1}\zeta_{\vec{k}_2}\rangle'_{q\to 0} = -P_\zeta(q)P_\zeta(k)\frac{1}{c_s^2}\frac{19+6c_3}{12}\frac{q^2}{k^2}\,. \tag{B.19}$$

Comparing this result with (B.5), we can see that two expressions are the same at the leading order in $1/c_s^2$ expansion if the proper angular average is taken into account.

B.1.3 *The two-point function at all orders in c_s*

Similar arguments can be used to recover the squeezed limit of the three-point function at all orders in c_s. In this case we have to use the full action (B.11). The effects that induce the change of the two-point function are coming from the mass term, the curvature of the spatial slices (geometrical effects) and the change of the scale factor, the Hubble constant and the speed of sound induced by the long mode. Given that everything is perturbative in ζ_L we will treat these two effects separately.

Let us for the moment focus on the mass term, the change of a, H and c_s and neglect geometrical effects. This simplifies the calculation since we can still use Fourier transform and standard quantization procedure as before to obtain the power spectrum. The equation of motion obtained from (B.11) neglecting the geometrical effects can be solved perturbatively in κ and the normalization can be fixed in the same way as in the previous subsection. Looking at the late time limit of the solution, the two-point function we get is

$$\langle \zeta_{\vec{k}}\zeta_{-\vec{k}}\rangle'_\kappa = P_\zeta(k)\left[1+\frac{3}{2}\left(\frac{1}{2}+\frac{c_3}{2}-\frac{19}{12c_s^2}-\frac{c_3}{2c_s^2}+\frac{3}{4}c_s^2\right)\frac{\kappa}{k^2}\right]\,. \tag{B.20}$$

The squeezed limit of the three-point function can be obtained straightforwardly by correlating with the long mode, which gives

$$\langle \zeta_{\vec{q}}\zeta_{\vec{k}_1}\zeta_{\vec{k}_2}\rangle'_{q\to 0} = P_\zeta(q)P_\zeta(k)\left(\frac{1}{2}+\frac{c_3}{2}-\frac{19}{12c_s^2}-\frac{c_3}{2c_s^2}+\frac{3}{4}c_s^2\right)\frac{q^2}{k^2}\,. \tag{B.21}$$

Finally, we can focus on the contribution to the two-point function coming from the geometrical effects. We can read from (B.11) that the relevant part of the action is

$$S = \int \mathrm{d}^4x\ \epsilon M_{\rm P}^2 H_0^2 a_0^2 \left(1 - \frac{3}{4}\kappa x^2\right)\left[\frac{1}{c_s^2}\pi'^2 - \left(1 + \frac{1}{2}\kappa x^2\right)(\partial_i\pi)^2\right] \ . \quad \text{(B.22)}$$

In principle, we can proceed as before solving the equation of motion. However, given that we are not in flat space anymore, we cannot expand π in Fourier modes. The easiest way to calculate the two-point function is to treat the terms proportional to the curvature as an interaction. Then we can use the standard in-in calculation which guarantees the correct choice of the normalization and the choice of the vacuum for the modes. The interacting Hamiltonian is given by

$$H_{int} = \int \mathrm{d}^4x\ \epsilon M_{\rm P}^2 H_0^2 a_0^2 \left[\frac{3}{4c_s^2}\kappa x^2 \pi'^2 - \frac{1}{4}\kappa x^2 (\partial_i\pi)^2\right] \ , \quad \text{(B.23)}$$

and the contribution to the two-point function is

$$\delta\langle\pi(x_1)\pi(x_2)\rangle_\kappa = -2\mathrm{Re}\left[i\int^\eta \mathrm{d}^3\vec{x}\mathrm{d}\eta'\ \pi(x_1)\pi(x_2)H_{int}(\vec{x},\eta')\right] \ , \quad \text{(B.24)}$$

where the contour of integration has been implicitly rotated to pick up the interacting vacuum in the past. At the end we want to write the result in momentum space. Using $x^2 = \int \frac{\mathrm{d}^3\vec{p}}{(2\pi)^3}(-\nabla_p^2\delta(\vec{p}))e^{i\vec{p}\cdot\vec{x}}$, we get the following equality

$$\int \mathrm{d}^3\vec{k}_1\mathrm{d}^3\vec{k}_2\langle\pi_{\vec{k}_1}\pi_{\vec{k}_2}\rangle e^{i\vec{k}_1\cdot\vec{x}_1+i\vec{k}_2\cdot\vec{x}_2} = \int \mathrm{d}^3\vec{k}_1\mathrm{d}^3\vec{k}_2\ F(\vec{k}_1,\vec{k}_2)\nabla^2_{\vec{k}_1}\delta(\vec{k}_1+\vec{k}_2)e^{i\vec{k}_1\cdot\vec{x}_1+i\vec{k}_2\cdot\vec{x}_2} \ , \quad \text{(B.25)}$$

where the function $F(\vec{k}_1,\vec{k}_2)$ is

$$F(\vec{k}_1,\vec{k}_2) = (2\pi)^3\ \mathrm{Re}\left[i\epsilon\kappa M_{\rm P}^2\ \pi^*_{\vec{k}_1}\pi^*_{\vec{k}_2}\int^\eta \frac{\mathrm{d}\eta'}{\eta'^2}\left(\frac{3}{c_s^2}\pi'_{\vec{k}_1}\pi'_{\vec{k}_2} + \vec{k}_1\cdot\vec{k}_2\,\pi_{\vec{k}_1}\pi_{\vec{k}_2}\right)\right] . \quad \text{(B.26)}$$

In the late time limit $\eta \to 0$, we find

$$F(\vec{k}_1,\vec{k}_2) = (2\pi)^3\frac{\kappa}{4\epsilon c_s M_{\rm P}^2}\frac{3k_1^2k_2^2 + \vec{k}_1\cdot\vec{k}_2(k_1^2+k_1k_2+k_2^2)}{4k_1^3k_2^3(k_1+k_2)} \ . \quad \text{(B.27)}$$

Plugging back this result in Eq. (B.38) and integrating by parts we are left with three kind of terms: with two derivatives on F, with one derivative on

F and one on the exponent, and with two derivatives on the exponent. All of them are multiplied by the delta function and have to be evaluated for $\vec{k}_2 = -\vec{k}_1$. It can be easily shown that

$$F(\vec{k}_1, -\vec{k}_1) = 0 \,, \quad \text{and} \quad \nabla_{k_1} F(\vec{k}_1, \vec{k}_2)\Big|_{\vec{k}_2=-\vec{k}_1} = 0 \,. \tag{B.28}$$

This means that the only term that survives is the one where two derivatives act on the function $F(\vec{k}_1, \vec{k}_2)$. The perturbation of the two-point function is therefore

$$\delta\langle \pi_{\vec{k}_1} \pi_{\vec{k}_2} \rangle = \delta(\vec{k}_1 + \vec{k}_2) \nabla^2_{k_1} F\Big|_{\vec{k}_2=-\vec{k}_1} = (2\pi)^3 \delta(\vec{k}_1 + \vec{k}_2) P_\pi(k_1) \frac{\kappa}{2k^2} \,, \tag{B.29}$$

so that the contribution to the squeezed limit of the three-point function becomes

$$\langle \zeta_{\vec{q}} \zeta_{\vec{k}_1} \zeta_{\vec{k}_2} \rangle'_{q\to 0} = P_\zeta(q) P_\zeta(k) \frac{q^2}{3k^2} \,. \tag{B.30}$$

If we sum up this result with the contributions (B.21), we get

$$\langle \zeta_{\vec{q}} \zeta_{\vec{k}_1} \zeta_{\vec{k}_2} \rangle'_{q\to 0} = P_\zeta(q) P_\zeta(k) \left(\frac{5}{6} + \frac{c_3}{2} - \frac{19}{12 c_s^2} - \frac{c_3}{2c_s^2} + \frac{3}{4} c_s^2 \right) \frac{q^2}{k^2} \,. \tag{B.31}$$

which agrees with of Eq. (B.5) once the angular average is taken into account.

B.2 FULL DIFFEOMORPHISM FROM FLAT TO CURVED EFTI

In section B.1.1 we used a simple physical argument to find the curved speed of sound by giving a VEV to π. Alternatively it is possible to derive the curved action directly by doing the full diffeomorphism from the flat action (B.1). Using this method the speed of sound can be read off directly from the action in curved coordinates in terms of c_s and c_3. We will check that this procedure gives the same result for $\tilde{c}_s$ as Eq. (B.10).

To find the action for $\tilde{\pi}$ we have to transform (B.1) to $\tilde{x}$ coordinates and then introduce the Goldstone boson $\tilde{\pi}$. It is important to note that the two Goldstone modes – $\tilde{\pi}$ in the curved universe and π in the flat universe – are different given that we are expanding around different backgrounds. As a consequence, in order to go from the action (B.1) to the action for the short modes in curved coordinates $\tilde{\pi}$ we have to do two steps. One is the change of coordinates that brings us to the locally curved universe and the other

is a field redefinition that corresponds to the redefinition of π due to the change of the background. In order to combine these two steps we have to take $\tilde{t} \to \tilde{t} + \tilde{\pi}(\tilde{t})$, where the curved FRW coordinates are related to the flat FRW coordinates by $\tilde{t} = t + \xi^0(\tilde{t})$, with ξ^0 given by Eq. (8.13). Then we can introduce the curved Goldstone boson $\tilde{\pi}$ in the action (B.1) using the transformation

$$\begin{aligned} t &= \tilde{t} + T(\tilde{x}) \ , \\ x &= \tilde{x} + \xi^i(\tilde{t}) \ , \end{aligned} \tag{B.32}$$

where $T(\tilde{x}) = \tilde{\pi}(\tilde{x})(1 - \dot{\xi}^0(\tilde{t})) - \xi^0(\tilde{t})$. Under this change of coordinates the parameters in the action transform as

$$g^{00}(x) = \tilde{g}^{\mu\nu}(\tilde{x}) \frac{\partial(\tilde{t} + T(\tilde{x}))}{\partial \tilde{x}^\mu} \frac{\partial(\tilde{t} + T(\tilde{x}))}{\partial \tilde{x}^\nu} \ , \ H_0(t) = H_0(\tilde{t} + T(\tilde{x})) \ , \ \dots \ . \tag{B.33}$$

Implementing the transformation (B.32) on the action (B.1), we find that at quadratic order in $\tilde{\pi}$ the action for the short modes in curved coordinates is

$$\begin{aligned} \tilde{S} = \int \mathrm{d}^4\tilde{x} \ \epsilon M_{\rm P}^2 H_0^2 a_0^3 \left(1 + \frac{3}{2}\partial_i\partial_j\zeta_L|_0 \tilde{x}^i\tilde{x}^j\right) \times \\ \left[\frac{1}{c_s^2}\left(1 + \frac{\partial^2\zeta_L|_0}{2a_0^2H_0^2}\left(-1 - 4c_3 + 2\left(-5 + 2c_3\right)c_s^2 + 6c_s^4\right)\right)\dot{\tilde{\pi}}^2 \right. \\ \left. - \left(1 - \partial_i\partial_j\zeta_L|_0\tilde{x}^i\tilde{x}^j\right)\left(1 - \frac{\partial^2\zeta_L|_0}{2a_0^2H_0^2}\left(3 + 2c_s^2\right)\right)\frac{\left(\partial_i\tilde{\pi}\right)^2}{a_0^2} - \frac{\partial_i\partial_j\zeta_L|_0}{a_0^2H_0^2}\frac{\partial_i\tilde{\pi}\partial_j\tilde{\pi}}{a_0^2} - 2\frac{\partial^2\zeta_L|_0}{a_0^2}\tilde{\pi}^2\right] \ . \end{aligned}$$

After angular averaging we find

$$\begin{aligned} \tilde{S}_{\rm avg} = \int \mathrm{d}^4\tilde{x} \ \epsilon M_{\rm P}^2 H_0^2 a_0^3 \left(1 - \frac{3}{4}\kappa\tilde{x}^2\right)\left[\frac{1}{c_s^2}\left(1 + \frac{3\kappa}{4a_0^2H_0^2}\left(1 + 4c_3 + 2\left(5 - 2c_3\right)c_s^2 - 6c_s^4\right)\right)\dot{\tilde{\pi}}^2 \right. \\ \left. - \left(1 + \frac{1}{2}\kappa\tilde{x}^2\right)\left(1 + \frac{\kappa}{4a_0^2H_0^2}\left(7 + 6c_s^2\right)\right)\frac{\left(\partial_i\tilde{\pi}\right)^2}{a_0^2} + 3\frac{\kappa}{a_0^2}\tilde{\pi}^2\right] \ . \end{aligned} \tag{B.34}$$

We can match this to the angular average of the action (B.7), the most general effective action that has the metric (B.6), to find $\tilde{c}_s$. We find that the actions (B.34) and (B.7) match if the speed of sound in the curved background is given by Eq. (B.10). Thus we confirm that this is the correct speed of sound in the curved background.

We can use the action (B.34) to compute the fully anisotropic squeezed limit of the three-point function in the same way that we calculated the isotropic limit in Section B.1.3.

The non-geometric two-point function that we find from the equation of motion of Eq. (B.34) can be solved straightforwardly. We find that the late time limit is

$$\langle\zeta_{\vec{k}}\zeta_{-\vec{k}}\rangle'_{\kappa} = P_\zeta(k)\left[1+\left(-\frac{1}{2}-\frac{c_3}{2}+\frac{2}{c_s^2}+\frac{c_3}{2c_s^2}-\frac{3}{4}c_s^2\right)\frac{\partial^2\zeta_L|_0}{k^2}-\frac{5}{4c_s^2}\frac{\partial_i\partial_j\zeta_L|_0 k_i k_j}{k^4}\right] . \tag{B.35}$$

Correlating Eq. (B.35) with the long mode gives the non-geometric part of the squeezed limit of the three-point function,

$$\langle\zeta_{\vec{q}}\zeta_{\vec{k}_1}\zeta_{\vec{k}_2}\rangle'_{q\to 0} = P_\zeta(q)P_\zeta(k)\left[\left(-\frac{2}{c_s^2}-\frac{c_3}{2c_s^2}+\frac{1}{2}+\frac{c_3}{2}+\frac{3c_s^2}{4}\right)\frac{q^2}{k^2}+\frac{5}{4c_s^2}\frac{(\vec{q}\cdot\vec{k})^2}{k^4}\right] . \tag{B.36}$$

Now we need to include geometric effects. The geometric interaction Hamiltonian is given by

$$H_{int} = \int \mathrm{d}^4x\ \epsilon M_{\rm P}^2 H_0^2 a_0^2\left[-\frac{3}{2}\partial_i\partial_j\zeta_L|_0 x^i x^j\frac{1}{c_s^2}\pi'^2+\frac{1}{2}\partial_i\partial_j\zeta_L|_0 x^i x^j(\partial_a\pi)^2\right] . \tag{B.37}$$

The two-point function can be written as

$$\int \mathrm{d}^3\vec{k}_1\mathrm{d}^3\vec{k}_2\langle\pi_{\vec{k}_1}\pi_{\vec{k}_2}\rangle e^{i\vec{k}_1\cdot\vec{x}_1+i\vec{k}_2\cdot\vec{x}_2} = \int \mathrm{d}^3\vec{k}_1\mathrm{d}^3\vec{k}_2\ F_{ij}(\vec{k}_1,\vec{k}_2)\partial_{k_{1i}}\partial_{k_{1j}}\delta(\vec{k}_1+\vec{k}_2)e^{i\vec{k}_1\cdot\vec{x}_1+i\vec{k}_2\cdot\vec{x}_2} , \tag{B.38}$$

where the function $F_{ij}(\vec{k}_1,\vec{k}_2)$ is

$$F_{ij}(\vec{k}_1,\vec{k}_2) = -2(2\pi)^3\ \mathrm{Re}\left[i\epsilon M_{\rm P}^2\partial_i\partial_j\zeta_L|_0\ \pi^*_{\vec{k}_1}\pi^*_{\vec{k}_2}\int^\eta\frac{\mathrm{d}\eta'}{\eta'^2}\left(\frac{3}{c_s^2}\pi'_{\vec{k}_1}\pi'_{\vec{k}_2}+\vec{k}_1\cdot\vec{k}_2\pi_{\vec{k}_1}\pi_{\vec{k}_2}\right)\right] . \tag{B.39}$$

In the late time limit we find

$$F_{ij}(\vec{k}_1,\vec{k}_2) = -2(2\pi)^3\frac{\partial_i\partial_j\zeta_L|_0}{4\epsilon c_s M_{\rm P}^2}\frac{3k_1^2k_2^2+\vec{k}_1\cdot\vec{k}_2(k_1^2+k_1k_2+k_2^2)}{4k_1^3k_2^3(k_1+k_2)} . \tag{B.40}$$

After integrating Eq. (B.38) by parts we find that the perturbation of the two-point function is

$$\begin{aligned}\delta\langle\pi_{\vec{k}_1}\pi_{\vec{k}_2}\rangle &= \delta(\vec{k}_1+\vec{k}_2)\partial_{k_{1i}}\partial_{k_{1j}}F_{ij}\Big|_{\vec{k}_2=-\vec{k}_1}\\ &= (2\pi)^3\delta(\vec{k}_1+\vec{k}_2)P_\pi(k_1)\frac{5\partial_i\partial_j\zeta_L|_0 k_{1i}k_{1j}-3\partial^2\zeta_L|_0 k_1^2}{4k_1^4} ,\end{aligned} \tag{B.41}$$

because F_{ij} satisfies

$$F_{ij}(\vec{k}_1,-\vec{k}_1) = 0 , \quad \text{and} \quad \partial_{\vec{k}_1}F_{ij}(\vec{k}_1,\vec{k}_2)\Big|_{\vec{k}_2=-\vec{k}_1} = 0 , \tag{B.42}$$

just as we found in the isotropic case. The geometric part of the squeezed limit of the three-point function is then

$$\langle \zeta_{\vec{q}} \zeta_{\vec{k}_1} \zeta_{\vec{k}_2} \rangle'_{q\to 0} = P_\zeta(q) P_\zeta(k) \frac{-5(\vec{q}\cdot\vec{k})^2 + 3q^2k^2}{4k^4} \,. \tag{B.43}$$

Combining this result with the non-geometric contribution (B.36), we find that the squeezed limit of the three-point function is

$$\langle \zeta_{\vec{q}} \zeta_{\vec{k}_1} \zeta_{\vec{k}_2} \rangle'_{q\to 0} = P_\zeta(q) P_\zeta(k) \left[\left(-\frac{2}{c_s^2} - \frac{c_3}{2c_s^2} + \frac{5}{4} + \frac{c_3}{2} + \frac{3c_s^2}{4} \right) \frac{q^2}{k^2} - \frac{5}{4} \frac{(\vec{q}\cdot\vec{k})^2}{k^4} \left(1 - \frac{1}{c_s^2} \right) \right] \,. \tag{B.44}$$

which agrees with Eq. (B.5).

B.3 GHOST INFLATION

In this appendix we show that the argument presented in the main part of the thesis can be applied also in the case of ghost inflation [123]. The ghost condensate can be thought as a model in which the background field is brought dynamically in a minimum of $P(X)$. This means that the equation of motion for the background

$$\partial_t (a^3 P_X \dot{\phi}) = 0 \tag{B.45}$$

is trivially satisfied for a constant velocity $\dot{\phi}$ equal to the unperturbed one, so that the curvature does not change the background solution. The curvature thus will enter only through the change of the scale factor[1]. The quadratic action for perturbations in conformal time reads

$$S = \int \mathrm{d}^4x \left(2M_2^4 a^2 \pi'^2 - \frac{\bar{M}^2}{2} (\partial^2 \pi)^2 \right) \,. \tag{B.46}$$

From this, the variation of the two point function in the presence of curvature is easily obtained by solving perturbatively the equation of motion

$$4M_2^4 \partial_\eta \left(a_0^2 \left(1 + 2\frac{\delta a}{a} \right) \pi' \right) + \bar{M}^2 k^4 \pi = 0 \,, \tag{B.47}$$

by defining $\pi = \pi_0 + \kappa H_0^{-2} \pi_1$. The solution of the unperturbed equation

$$4M_2^4 \pi_0'' + 8M_2^4 \mathcal{H}_0 \pi_0' + \bar{M}^2 \frac{k^4}{a_0^2} \pi_0 = 0 \,, \tag{B.48}$$

1 We are neglecting here the geometrical effects coming from the x-dependent part of the metric.

is given by [123]

$$\pi_0(k,\eta) = 2^{-1/4} H_0^{1/4} M_2^{-1/2} \bar{M}^{-3/4} k^{-3/2} F\left(\frac{H_0^{1/2}\bar{M}^{1/2}}{\sqrt{2}M_2} k\eta\right) , \quad \text{(B.49)}$$

where we defined $F(x) = \sqrt{\pi/8}(-x)^{3/2} H^{(1)}_{3/4}(x^2/2)$, and $H^{(1)}_\alpha$ is the Hankel function of first kind. After expanding Eq. (B.47) at first order in κ, we have to solve

$$4M_2^4 \pi_1'' + 8M_2^4 \mathcal{H}_0 \pi_1' + \bar{M}^2 \frac{k^4}{a_0^2} \pi_1 = -\frac{4M_2^4}{3a_0^2} \pi_0'' \, . \quad \text{(B.50)}$$

This can be done using the Green function of the unperturbed equation of motion, which is given by the commutator of the free fields

$$G(x_1, x_2) = i\, a^{-2}(\eta_2)\, \theta(\eta_1 - \eta_2)\, [\pi_0(x_1), \pi_0(x_2)] \, . \quad \text{(B.51)}$$

The first order solution is then given by

$$\begin{aligned} \pi_1(k_1,\eta) &= -\frac{4H_0^4 M_2^4}{3} \int_{-\infty}^{\eta} \mathrm{d}\tau\, a_0^4(\tau)\, G(k_1,\eta;k_2,\tau)\, \tau^2 \pi_0''(k_2,\tau) \\ &= -\frac{4H_0^2 M_2^4}{3} \int_{-\infty}^{\eta} \mathrm{d}\tau\, i\theta(\eta-\tau)\, [\pi_0(k_1,\eta), \pi_0(k_2,\tau)]\, \pi_0''(k_2,\tau) \, . \end{aligned} \quad \text{(B.52)}$$

The field π_0, being the solution of the unperturbed equation of motion, is normalized in such a way that

$$[\pi_0(\eta), \Pi_{\pi_0}(\eta)]_{\kappa=0} = 4M_2^4 a_0^2 [\pi_0(\eta), \pi_0'(\eta)] = i \, , \quad \text{(B.53)}$$

where Π_{π_0} is the conjugated momentum. We can check that the same condition is satisfied by π at first order in κ without changing the normalization of the homogeneous part, by direct evaluation of the commutator

$$\begin{aligned} [\pi(\eta), \Pi_\pi(\eta)] &= 4M_2^4 a^2 [\pi_0(\eta), \pi_0'(\eta)] + 4M_2^4 a_0^2 \kappa H_0^{-2} \Big([\pi_0(\eta), \pi_1'(\eta)] + [\pi_1(\eta), \pi_0'(\eta)] \Big) \\ &= i + i\frac{\kappa\eta^2}{3} + 4M_2^4 a_0^2 \frac{\kappa}{H_0^2} \Big([\pi_0(\eta), \pi_1'(\eta)] + [\pi_1(\eta), \pi_0'(\eta)] \Big) \, , \end{aligned} \quad \text{(B.54)}$$

where the commutators involving π_0 and π_1 are

$$\begin{aligned} [\pi_0(\eta), \pi_1'(\eta)] &= -\frac{4H_0^2 M_2^4}{3} \int_{-\infty}^{\eta} \mathrm{d}\tau\, i\theta(\eta-\tau)\, [\pi_0'(\eta), \pi_0(\tau)]\, [\pi_0(\eta), \pi_0''(\tau)] \, , \\ [\pi_1(\eta), \pi_0'(\eta)] &= -\frac{4H_0^2 M_2^4}{3} \int_{-\infty}^{\eta} \mathrm{d}\tau\, i\theta(\eta-\tau)\, [\pi_0(\eta), \pi_0(\tau)]\, [\pi_0''(\tau), \pi_0'(\eta)] \, . \end{aligned} \quad \text{(B.55)}$$

After many integrations by parts the commutators appearing in the RHS can be written as commutators at equal time. Furthermore, when the two are summed we obtain

$$\begin{aligned}[\pi_0(\eta),\pi_1'(\eta)]+[\pi_1(\eta),\pi_0'(\eta)] &= -i\frac{4M_2^4}{3}[\pi_0(\eta),\pi_0'(\eta)][\pi_0'(\eta),\pi_0(\eta)]\\ &= -i\frac{1}{12M_2^4a_0^4}\,.\end{aligned} \tag{B.56}$$

Plugging this result back in Eq. (B.54) gives $[\pi(\eta),\Pi_\pi(\eta)]=i$, thus the solution is correctly normalized.

The two point function in the presence of the long mode is then given by the following expression

$$\langle\pi\pi\rangle'_{\pi_L}=\pi^*(0)\pi(0)=P_\pi+\frac{2\kappa}{H_0^2}\,\mathrm{Re}[\pi_0^*(0)\pi_1(0)]\,, \tag{B.57}$$

where $P_\pi(k)=\langle\pi_0\pi_0\rangle'=2^{-1/2}H_0^{1/2}M_2^{-1}\bar{M}^{-3/2}|F(0)|^2k^{-3}$, and its perturbation is

$$\begin{aligned}\delta\langle\pi\pi\rangle'_{\pi_L} &= \frac{2\kappa}{H_0^2}\,\mathrm{Re}[\pi_0^*(0)\pi_1(0)]\\ &= -\frac{4M_2^2\kappa}{3H_0\bar{M}^3k^5}\frac{H_0^{1/2}\bar{M}^{1/2}}{\sqrt{2}M_2}\,\mathrm{Re}\left[iF^*(0)\int_{-\infty}^0\mathrm{d}x\Big(F(0)F^*(x)-F^*(0)F(x)\Big)F''(x)\right]\\ &= -\frac{8M_2^2\kappa}{3H_0\bar{M}^3k^5}\frac{H_0^{1/2}\bar{M}^{1/2}}{\sqrt{2}M_2}|F(0)|^2\,\mathrm{Re}\left[i\int_{-\infty}^0\mathrm{d}x\,\mathrm{Re}[F(x)]F''(x)\right]\\ &= \frac{8M_2^2\kappa}{3H_0\bar{M}k^2}P_\pi(k)\,\mathrm{Im}\left[\int_{-\infty}^0\mathrm{d}x\,\mathrm{Re}[F(x)]F''(x)\right]\,.\end{aligned} \tag{B.58}$$

Now we can use the following property of the function $F(x)$

$$\int_{-\infty}^0\mathrm{d}x\,\mathrm{Re}[F(x)]F''(x)=\frac{1}{2}\int_{-\infty}^0\mathrm{d}x\,F(x)F''(x)\,, \tag{B.59}$$

to rewrite the variation of the power spectrum as

$$\delta\langle\pi_{\vec{k}}\pi_{-\vec{k}}\rangle'_{\pi_L}=\frac{4M_2^2\kappa}{3H_0\bar{M}k^2}P_\pi(k)\,\mathrm{Im}\left[\int_{-\infty}^0\mathrm{d}x\,F(x)F''(x)\right]\,. \tag{B.60}$$

Taking the average over the long mode and using $\zeta=-H_0\pi$ and $\kappa=\frac{2}{3}q^2\zeta_{\vec{q}}$, we find the three-point function in the squeezed limit

$$\langle\pi_{\vec{q}}\pi_{\vec{k}_1}\pi_{\vec{k}_2}\rangle'_{q\to0}=-\frac{8M_2^2}{9\bar{M}}P_\pi(q)P_\pi(k)\frac{q^2}{k^2}\mathrm{Im}\left[\int_{-\infty}^0\mathrm{d}x\,F(x)F''(x)\right]\,. \tag{B.61}$$

This result has to be compared with the squeezed limit of the three-point function in [123],

$$\langle \pi_{\vec{k}_1}\pi_{\vec{k}_2}\pi_{\vec{k}_3}\rangle' = N\frac{1}{\prod k_a^3}2\mathrm{Re}\left[\int_{-\infty}^{0}\frac{\mathrm{d}\eta}{\eta}\left(F^*(k_1\eta)F^*(k_2\eta)F'^*(k_3\eta)k_3(\vec{k}_1\cdot\vec{k}_2)+\text{symm.}\right)\right] , \tag{B.62}$$

where the constant N is given by

$$N = -\frac{(2\pi)^{3/2}}{\Gamma(1/4)^3}\frac{H_0^5}{2M_2^2}\left(\frac{2M_2^2}{\bar{M}H_0}\right)^4\left(\frac{1}{2M_2^2}\right)^3 . \tag{B.63}$$

The terms in the parentheses are proportional at least to q, so if we use the symmetric expansion (B.4) the product in front of the integral gives only the leading contribution $1/q^3k^6$ (corrections are of order q^2). Keeping only the terms contributing at order q^2, we get

$$\langle \pi_{\vec{q}}\pi_{\vec{k}_1}\pi_{\vec{k}_2}\rangle'_{q\to 0} = -\frac{8}{3}\frac{M_2^2}{\bar{M}}P_\pi(q)P_\pi(k)\frac{q^2}{k^2}\mathrm{Im}\left[\int_{-\infty}^{0}\mathrm{d}x\left(-\frac{1}{x}F^*(x)F'^*(x)+F^*(x)F''^*(x)\right)\right] . \tag{B.64}$$

We can then numerically show that the following relation holds

$$\mathrm{Im}\int_{-\infty}^{0}\mathrm{d}x\left(-\frac{1}{x}F^*(x)F'^*(x)\right) = -\frac{4}{3}\,\mathrm{Im}\int_{-\infty}^{0}\mathrm{d}xF^*(x)F''^*(x) , \tag{B.65}$$

such that

$$\mathrm{Im}\left[\int_{-\infty}^{0}\mathrm{d}x\left(-\frac{1}{x}F^*(x)F'^*(x)+F^*(x)F''^*(x)\right)\right] = \frac{1}{3}\,\mathrm{Im}\int_{-\infty}^{0}\mathrm{d}xF(x)F''(x) . \tag{B.66}$$

Finally, we get for the squeezed limit of the three-point function

$$\langle \pi_{\vec{q}}\pi_{\vec{k}_1}\pi_{\vec{k}_2}\rangle'_{q\to 0} = -\frac{8}{9}\frac{M_2^2}{\bar{M}}P_\pi(q)P_\pi(k)\frac{q^2}{k^2}\mathrm{Im}\int_{-\infty}^{0}\mathrm{d}xF(x)F''(x) , \tag{B.67}$$

which indeed agrees with Eq. (B.61).

B.4 KHRONON INFLATION

In this appendix we want to check that our consistency relation (8.17) works also for Khronon Inflation [124]. We concentrate only on terms enhanced by c_s^{-2} and on the isotropic case. The action for Khronon Inflation at leading order in derivatives and in the decoupling limit is

$$S = \frac{1}{2}\int \mathrm{d}^4x\sqrt{-g}\left(M_\lambda^2(\nabla_\mu u^\mu + 3H_0)^2 + M_\alpha^2 u^\mu u^\nu\nabla_\mu u_\rho\nabla_\nu u^\rho\right) , \tag{B.68}$$

where $u_\mu = \frac{\partial_\mu \phi}{\sqrt{g^{\alpha\beta}\partial_\alpha\phi\partial_\beta\phi}}$. Since in this model time reparametrization is promoted to an exact symmetry, the curvature will not affect the background solution and perturbations can be expanded around $\phi(t) = t + \pi$. Moreover the term proportional to M_α^2, when expanded at quadratic order, does not depend on the scale factor a: since this is the only term enhanced by $c_s^{-2} = (M_\lambda/M_\alpha)^{-2}$, we expect no variation of the two-point function at this order. Indeed the action for perturbations, at first order in curvature, reads

$$S = \frac{1}{2}\int \mathrm{d}^4x \left(M_\alpha^2(\partial\pi')^2 - M_\lambda^2\left((\partial^2\pi)^2 - 6a^2(H_0 - H)H(\partial\pi)^2\right)\right) . \tag{B.69}$$

Expanding the equation of motion at first order in κ, we see that the curvature does not source any variation of the action enhanced by c_s^{-2}, so there is no variation of the two-point function $\propto c_s^{-2}$. This means that the three-point function in the squeezed limit at order q^2, after we take the angular average, should not be enhanced by c_s^{-2}. Indeed the three-point function $\propto c_s^{-2}$ reads [124]

$$\langle\zeta_{\vec{k}_1}\zeta_{\vec{k}_2}\zeta_{\vec{k}_3}\rangle' = \frac{1}{\prod k_i^3}P_\zeta^2\left[-\frac{1}{c_s^2}\frac{k_1^3}{k_t^2}\vec{k}_2\cdot\vec{k}_3\right] + \text{cyclic perms.}\,, \tag{B.70}$$

and the angular average of the $\mathcal{O}(q^2)$ term is zero. The consistency relations holds.

BIBLIOGRAPHY

[1] Paolo Creminelli et al. "Detecting Primordial B-Modes after Planck." In: (2015). arXiv: 1502.01983 [astro-ph.CO].

[2] Paolo Creminelli et al. "Implications of the scalar tilt for the tensor-to-scalar ratio." In: (2014). arXiv: 1412.0678 [astro-ph.CO].

[3] Paolo Creminelli et al. "ϕ^2 Inflation at its Endpoint." In: *Phys.Rev.* D90.8 (2014), p. 083513. DOI: 10.1103/PhysRevD.90.083513. arXiv: 1405.6264 [astro-ph.CO].

[4] Paolo Creminelli et al. "ϕ^2 or Not ϕ^2: Testing the Simplest Inflationary Potential." In: *Phys.Rev.Lett.* 112.24 (2014), p. 241303. DOI: 10.1103/PhysRevLett.112.241303. arXiv: 1404.1065 [astro-ph.CO].

[5] Paolo Creminelli et al. "Inequivalence of Coset Constructions for Spacetime Symmetries." In: *JHEP* 1502 (2015), p. 037. DOI: 10.1007/JHEP02(2015)037. arXiv: 1403.3095 [hep-th].

[6] Paolo Creminelli et al. "The Physical Squeezed Limit: Consistency Relations at Order q^2." In: *JCAP* 1311 (2013), p. 015. DOI: 10.1088/1475-7516/2013/11/015. arXiv: 1307.0503 [astro-ph.CO].

[7] Paolo Creminelli et al. "ISO(4,1) Symmetry in the EFT of Inflation." In: *JCAP* 1307 (2013), p. 037. DOI: 10.1088/1475-7516/2013/07/037. arXiv: 1304.4238 [hep-th].

[8] Jaswant Yadav et al. "Testing homogeneity on large scales in the Sloan Digital Sky Survey Data Release One." In: *Mon.Not.Roy.Astron.Soc.* 364 (2005), pp. 601–606. DOI: 10.1111/j.1365-2966.2005.09578.x. arXiv: astro-ph/0504315 [astro-ph].

[9] Steven Weinberg. "Cosmology." In: (2008).

[10] Scott Dodelson. "Modern cosmology." In: (2003).

[11] P.A.R. Ade et al. "Planck 2015 results. XIII. Cosmological parameters." In: (2015). arXiv: 1502.01589 [astro-ph.CO].

[12] Alexei A. Starobinsky. "A New Type of Isotropic Cosmological Models Without Singularity." In: *Phys.Lett.* B91 (1980), pp. 99–102. DOI: 10.1016/0370-2693(80)90670-X.

[13] Alan H. Guth. "The Inflationary Universe: A Possible Solution to the Horizon and Flatness Problems." In: *Phys.Rev.* D23 (1981), pp. 347–356. DOI: 10.1103/PhysRevD.23.347.

[14] Andrei D. Linde. "A New Inflationary Universe Scenario: A Possible Solution of the Horizon, Flatness, Homogeneity, Isotropy and Primordial Monopole Problems." In: *Phys.Lett.* B108 (1982), pp. 389–393. DOI: 10.1016/0370-2693(82)91219-9.

[15] Andrei D. Linde. "Chaotic Inflation." In: *Phys.Lett.* B129 (1983), pp. 177–181. DOI: 10.1016/0370-2693(83)90837-7.

[16] Andreas Albrecht and Paul J. Steinhardt. "Cosmology for Grand Unified Theories with Radiatively Induced Symmetry Breaking." In: *Phys.Rev.Lett.* 48 (1982), pp. 1220–1223. DOI: 10.1103/PhysRevLett.48.1220.

[17] Daniel Baumann. "TASI Lectures on Inflation." In: (2009). arXiv: 0907.5424 [hep-th].

[18] Jaume Garriga and Viatcheslav F. Mukhanov. "Perturbations in k-inflation." In: *Phys.Lett.* B458 (1999), pp. 219–225. DOI: 10.1016/S0370-2693(99)00602-4. arXiv: hep-th/9904176 [hep-th].

[19] Mohsen Alishahiha, Eva Silverstein, and David Tong. "DBI in the sky." In: *Phys.Rev.* D70 (2004), p. 123505. DOI: 10.1103/PhysRevD.70.123505. arXiv: hep-th/0404084 [hep-th].

[20] Viatcheslav F. Mukhanov and G. V. Chibisov. "Quantum Fluctuation and Nonsingular Universe. (In Russian)." In: *JETP Lett.* 33 (1981), pp. 532–535.

[21] S.W. Hawking. "The Development of Irregularities in a Single Bubble Inflationary Universe." In: *Phys.Lett.* B115 (1982), p. 295. DOI: 10.1016/0370-2693(82)90373-2.

[22] Alan H. Guth and S.Y. Pi. "Fluctuations in the New Inflationary Universe." In: *Phys.Rev.Lett.* 49 (1982), pp. 1110–1113. DOI: 10.1103/PhysRevLett.49.1110.

[23] Alexei A. Starobinsky. "Dynamics of Phase Transition in the New Inflationary Universe Scenario and Generation of Perturbations." In: *Phys.Lett.* B117 (1982), pp. 175–178. DOI: 10.1016/0370-2693(82)90541-X.

[24] James M. Bardeen, Paul J. Steinhardt, and Michael S. Turner. "Spontaneous Creation of Almost Scale - Free Density Perturbations in an Inflationary Universe." In: *Phys.Rev.* D28 (1983), p. 679. DOI: 10.1103/PhysRevD.28.679.

[25] Viatcheslav F. Mukhanov. "Gravitational Instability of the Universe Filled with a Scalar Field." In: *JETP Lett.* 41 (1985), pp. 493–496.

[26] Juan Martin Maldacena. "Non-Gaussian features of primordial fluctuations in single field inflationary models." In: *JHEP* 0305 (2003), p. 013. DOI: 10.1088/1126-6708/2003/05/013. arXiv: astro-ph/0210603 [astro-ph].

[27] Steven Weinberg. "Quantum contributions to cosmological correlations." In: *Phys.Rev.* D72 (2005), p. 043514. DOI: 10.1103/PhysRevD.72.043514. arXiv: hep-th/0506236 [hep-th].

[28] Xingang Chen et al. "Large Primordial Trispectra in General Single Field Inflation." In: *JCAP* 0908 (2009), p. 008. DOI: 10.1088/1475-7516/2009/08/008. arXiv: 0905.3494 [astro-ph.CO].

[29] Frederico Arroja et al. "On the full trispectrum in single field DBI-inflation." In: *Phys.Rev.* D80 (2009), p. 043527. DOI: 10.1103/PhysRevD.80.043527. arXiv: 0905.3641 [hep-th].

[30] Daniel Babich, Paolo Creminelli, and Matias Zaldarriaga. "The Shape of non-Gaussianities." In: *JCAP* 0408 (2004), p. 009. DOI: 10.1088/1475-7516/2004/08/009. arXiv: astro-ph/0405356 [astro-ph].

[31] Paolo Creminelli. "On non-Gaussianities in single-field inflation." In: *JCAP* 0310 (2003), p. 003. DOI: 10.1088/1475-7516/2003/10/003. arXiv: astro-ph/0306122 [astro-ph].

[32] P.A.R. Ade et al. "Planck 2015 results. XVII. Constraints on primordial non-Gaussianity." In: (2015). arXiv: 1502.01592 [astro-ph.CO].

[33] Clifford Cheung et al. "The Effective Field Theory of Inflation." In: *JHEP* 0803 (2008), p. 014. DOI: 10.1088/1126-6708/2008/03/014. arXiv: 0709.0293 [hep-th].

[34] Leonardo Senatore and Matias Zaldarriaga. "The Effective Field Theory of Multifield Inflation." In: *JHEP* 1204 (2012), p. 024. DOI: 10.1007/JHEP04(2012)024. arXiv: 1009.2093 [hep-th].

[35] Paolo Creminelli and Matias Zaldarriaga. "Single field consistency relation for the 3-point function." In: *JCAP* 0410 (2004), p. 006. DOI: 10.1088/1475-7516/2004/10/006. arXiv: astro-ph/0407059 [astro-ph].

[36] Clifford Cheung et al. "On the consistency relation of the 3-point function in single field inflation." In: *JCAP* 0802 (2008), p. 021. DOI: 10.1088/1475-7516/2008/02/021. arXiv: 0709.0295 [hep-th].

[37] Paolo Creminelli, Jorge Norena, and Marko Simonovic. "Conformal consistency relations for single-field inflation." In: *JCAP* 1207 (2012), p. 052. DOI: 10.1088/1475-7516/2012/07/052. arXiv: 1203.4595 [hep-th].

[38] Kurt Hinterbichler, Lam Hui, and Justin Khoury. "Conformal Symmetries of Adiabatic Modes in Cosmology." In: *JCAP* 1208 (2012), p. 017. DOI: 10.1088/1475-7516/2012/08/017. arXiv: 1203.6351 [hep-th].

[39] Leonardo Senatore and Matias Zaldarriaga. "A Note on the Consistency Condition of Primordial Fluctuations." In: *JCAP* 1208 (2012), p. 001. DOI: 10.1088/1475-7516/2012/08/001. arXiv: 1203.6884 [astro-ph.CO].

[40] Kurt Hinterbichler, Lam Hui, and Justin Khoury. "An Infinite Set of Ward Identities for Adiabatic Modes in Cosmology." In: *JCAP* 1401 (2014), p. 039. DOI: 10.1088/1475-7516/2014/01/039. arXiv: 1304.5527 [hep-th].

[41] Walter D. Goldberger, Lam Hui, and Alberto Nicolis. "One-particle-irreducible consistency relations for cosmological perturbations." In: *Phys.Rev.* D87.10 (2013), p. 103520. DOI: 10.1103/PhysRevD.87.103520. arXiv: 1303.1193 [hep-th].

[42] Xingang Chen et al. "A Single Field Inflation Model with Large Local Non-Gaussianity." In: *Europhys.Lett.* 102 (2013), p. 59001. DOI: 10.1209/0295-5075/102/59001. arXiv: 1301.5699 [hep-th].

[43] P.A.R. Ade et al. "Detection of B-Mode Polarization at Degree Angular Scales by BICEP2." In: *Phys.Rev.Lett.* 112.24 (2014), p. 241101. DOI: 10.1103/PhysRevLett.112.241101. arXiv: 1403.3985 [astro-ph.CO].

[44] David H. Lyth. "What would we learn by detecting a gravitational wave signal in the cosmic microwave background anisotropy?" In: *Phys.Rev.Lett.* 78 (1997), pp. 1861–1863. DOI: 10.1103/PhysRevLett.78.1861. arXiv: hep-ph/9606387 [hep-ph].

[45] Eva Silverstein and Alexander Westphal. "Monodromy in the CMB: Gravity Waves and String Inflation." In: *Phys.Rev.* D78 (2008), p. 106003. DOI: 10.1103/PhysRevD.78.106003. arXiv: 0803.3085 [hep-th].

[46] Katherine Freese, Joshua A. Frieman, and Angela V. Olinto. "Natural inflation with pseudo - Nambu-Goldstone bosons." In: *Phys.Rev.Lett.* 65 (1990), pp. 3233–3236. DOI: 10.1103/PhysRevLett.65.3233.

[47] Katherine Freese and William H. Kinney. "Natural Inflation: Consistency with Cosmic Microwave Background Observations of Planck and BICEP2." In: *JCAP* 1503 (2015), p. 044. DOI: 10.1088/1475-7516/2015/03/044. arXiv: 1403.5277 [astro-ph.CO].

[48] Nima Arkani-Hamed et al. "Extra natural inflation." In: *Phys.Rev.Lett.* 90 (2003), p. 221302. DOI: 10.1103/PhysRevLett.90.221302. arXiv: hep-th/0301218 [hep-th].

[49] Nemanja Kaloper, Albion Lawrence, and Lorenzo Sorbo. "An Ignoble Approach to Large Field Inflation." In: *JCAP* 1103 (2011), p. 023. DOI: 10.1088/1475-7516/2011/03/023. arXiv: 1101.0026 [hep-th].

[50] Ewan D. Stewart and David H. Lyth. "A More accurate analytic calculation of the spectrum of cosmological perturbations produced during inflation." In: *Phys.Lett.* B302 (1993), pp. 171–175. DOI: 10.1016/0370-2693(93)90379-V. arXiv: gr-qc/9302019 [gr-qc].

[51] Scott Dodelson. "How much can we learn about the physics of inflation?" In: *Phys.Rev.Lett.* 112 (2014), p. 191301. DOI: 10.1103/PhysRevLett.112.191301. arXiv: 1403.6310 [astro-ph.CO].

[52] Luca Amendola et al. "Cosmology and fundamental physics with the Euclid satellite." In: *Living Rev.Rel.* 16 (2013), p. 6. DOI: 10.12942/lrr-2013-6. arXiv: 1206.1225 [astro-ph.CO].

[53] Philippe Andre et al. "PRISM (Polarized Radiation Imaging and Spectroscopy Mission): A White Paper on the Ultimate Polarimetric Spectro-Imaging of the Microwave and Far-Infrared Sky." In: (2013). arXiv: 1306.2259 [astro-ph.CO].

[54] Renata Kallosh, Andrei Linde, and Alexander Westphal. "Chaotic Inflation in Supergravity after Planck and BICEP2." In: *Phys.Rev.* D90.2 (2014), p. 023534. DOI: 10.1103/PhysRevD.90.023534. arXiv: 1405.0270 [hep-th].

[55] Keisuke Harigaya and Tsutomu T. Yanagida. "Discovery of Large Scale Tensor Mode and Chaotic Inflation in Supergravity." In: *Phys.Lett.* B734 (2014), pp. 13–16. DOI: 10.1016/j.physletb.2014.05.012. arXiv: 1403.4729 [hep-ph].

[56] Jerod Caligiuri and Arthur Kosowsky. "Inflationary Tensor Perturbations After BICEP2." In: *Phys.Rev.Lett.* 112 (2014), p. 191302. DOI: 10.1103/PhysRevLett.112.191302. arXiv: 1403.5324 [astro-ph.CO].

[57] Daniel Baumann and Daniel Green. "Signatures of Supersymmetry from the Early Universe." In: *Phys.Rev.* D85 (2012), p. 103520. DOI: 10.1103/PhysRevD.85.103520. arXiv: 1109.0292 [hep-th].

[58] Paolo Creminelli et al. "Galilean symmetry in the effective theory of inflation: new shapes of non-Gaussianity." In: *JCAP* 1102 (2011), p. 006. DOI: 10.1088/1475-7516/2011/02/006. arXiv: 1011.3004 [hep-th].

[59] Leonardo Senatore and Matias Zaldarriaga. "A Naturally Large Four-Point Function in Single Field Inflation." In: *JCAP* 1101 (2011), p. 003. DOI: 10.1088/1475-7516/2011/01/003. arXiv: 1004.1201 [hep-th].

[60] Diana Lopez Nacir et al. "Dissipative effects in the Effective Field Theory of Inflation." In: *JHEP* 1201 (2012), p. 075. DOI: 10.1007/JHEP01(2012)075. arXiv: 1109.4192 [hep-th].

[61] Leonardo Senatore, Eva Silverstein, and Matias Zaldarriaga. "New Sources of Gravitational Waves during Inflation." In: *JCAP* 1408 (2014), p. 016. DOI: 10.1088/1475-7516/2014/08/016. arXiv: 1109.0542 [hep-th].

[62] Xingang Chen and Yi Wang. "Large non-Gaussianities with Intermediate Shapes from Quasi-Single Field Inflation." In: *Phys.Rev.* D81 (2010), p. 063511. DOI: 10.1103/PhysRevD.81.063511. arXiv: 0909.0496 [astro-ph.CO].

[63] Nathaniel Craig and Daniel Green. "Testing Split Supersymmetry with Inflation." In: *JHEP* 1407 (2014), p. 102. DOI: 10.1007/JHEP07(2014)102. arXiv: 1403.7193 [hep-ph].

[64] Liang Dai, Marc Kamionkowski, and Junpu Wang. "Reheating constraints to inflationary models." In: *Phys.Rev.Lett.* 113 (2014), p. 041302. DOI: 10.1103/PhysRevLett.113.041302. arXiv: 1404.6704 [astro-ph.CO].

[65] P.A.R. Ade et al. "Planck 2013 results. XVI. Cosmological parameters." In: *Astron.Astrophys.* 571 (2014), A16. DOI: 10.1051/0004-6361/201321591. arXiv: 1303.5076 [astro-ph.CO].

[66] Dmitry I. Podolsky et al. "Equation of state and beginning of thermalization after preheating." In: *Phys.Rev.* D73 (2006), p. 023501. DOI: 10.1103/PhysRevD.73.023501. arXiv: hep-ph/0507096 [hep-ph].

[67] Jean Francois Dufaux et al. "Preheating with trilinear interactions: Tachyonic resonance." In: *JCAP* 0607 (2006), p. 006. DOI: 10.1088/1475-7516/2006/07/006. arXiv: hep-ph/0602144 [hep-ph].

[68] Liam McAllister, Eva Silverstein, and Alexander Westphal. "Gravity Waves and Linear Inflation from Axion Monodromy." In: *Phys.Rev.* D82 (2010), p. 046003. DOI: 10.1103/PhysRevD.82.046003. arXiv: 0808.0706 [hep-th].

[69] Liam McAllister et al. "The Powers of Monodromy." In: *JHEP* 1409 (2014), p. 123. DOI: 10.1007/JHEP09(2014)123. arXiv: 1405.3652 [hep-th].

[70] Diederik Roest. "Universality classes of inflation." In: *JCAP* 1401.01 (2014), p. 007. DOI: 10.1088/1475-7516/2014/01/007. arXiv: 1309.1285 [hep-th].

[71] Viatcheslav Mukhanov. "Quantum Cosmological Perturbations: Predictions and Observations." In: *Eur.Phys.J.* C73 (2013), p. 2486. DOI: 10.1140/epjc/s10052-013-2486-7. arXiv: 1303.3925 [astro-ph.CO].

[72] D. Boyanovsky, Hector J. de Vega, and Norma G. Sanchez. "Clarifying Inflation Models: Slow-roll as an expansion in $1/N_{efolds}$." In: *Phys.Rev.* D73 (2006), p. 023008. DOI: 10.1103/PhysRevD.73.023008. arXiv: astro-ph/0507595 [astro-ph].

[73] Lotfi Boubekeur et al. "Phenomenological approaches of inflation and their equivalence." In: *Phys.Rev.* D91.8 (2015), p. 083006. DOI: 10.1103/PhysRevD.91.083006. arXiv: 1411.7237 [astro-ph.CO].

[74] Hayden Lee, S. C. Su, and Daniel Baumann. "The Superhorizon Test of Future B-mode Experiments." In: (2014). arXiv: 1408.6709 [astro-ph.CO].

[75] Juan Garcia-Bellido and Diederik Roest. "Large-N running of the spectral index of inflation." In: *Phys.Rev.* D89.10 (2014), p. 103527. DOI: 10.1103/PhysRevD.89.103527. arXiv: 1402.2059 [astro-ph.CO].

[76] Daniel Baumann and Liam McAllister. "Inflation and String Theory." In: (2014). arXiv: 1404.2601 [hep-th].

[77] C.P. Burgess, M. Cicoli, and F. Quevedo. "String Inflation After Planck 2013." In: *JCAP* 1311 (2013), p. 003. DOI: 10.1088/1475-7516/2013/11/003. arXiv: 1306.3512 [hep-th].

[78] Juan Garcia-Bellido et al. "Lyth bound of inflation with a tilt." In: *Phys.Rev.* D90.12 (2014), p. 123539. DOI: 10.1103/PhysRevD.90.123539. arXiv: 1408.6839 [hep-th].

[79] Philippe André et al. "PRISM (Polarized Radiation Imaging and Spectroscopy Mission): An Extended White Paper." In: *JCAP* 1402 (2014), p. 006. DOI: 10.1088/1475-7516/2014/02/006. arXiv: 1310.1554 [astro-ph.CO].

[80] Patrick Fox, Aaron Pierce, and Scott D. Thomas. "Probing a QCD string axion with precision cosmological measurements." In: (2004). arXiv: hep-th/0409059 [hep-th].

[81] D. Seckel and Michael S. Turner. "Isothermal Density Perturbations in an Axion Dominated Inflationary Universe." In: *Phys.Rev.* D32 (1985), p. 3178. DOI: 10.1103/PhysRevD.32.3178.

[82] Nima Arkani-Hamed et al. "The String landscape, black holes and gravity as the weakest force." In: *JHEP* 0706 (2007), p. 060. DOI: 10.1088/1126-6708/2007/06/060. arXiv: hep-th/0601001 [hep-th].

[83] Renata Kallosh, Andrei Linde, and Diederik Roest. "Large field inflation and double α-attractors." In: *JHEP* 1408 (2014), p. 052. DOI: 10.1007/JHEP08(2014)052. arXiv: 1405.3646 [hep-th].

[84] P.A.R. Ade et al. "A Measurement of the Cosmic Microwave Background B-Mode Polarization Power Spectrum at Sub-Degree Scales with POLARBEAR." In: *Astrophys.J.* 794.2 (2014), p. 171. DOI: 10.1088/0004-637X/794/2/171. arXiv: 1403.2369 [astro-ph.CO].

[85] R. Adam et al. "Planck intermediate results. XXX. The angular power spectrum of polarized dust emission at intermediate and high Galactic latitudes." In: (2014). arXiv: 1409.5738 [astro-ph.CO].

[86] A. Benoit et al. "First detection of polarization of the submillimetre diffuse galactic dust emission by archeops." In: *Astron. Astrophys.* 424 (2004), pp. 571–582. DOI: 10.1051/0004-6361:20040042. arXiv: astro-ph/0306222 [astro-ph].

[87] A. Kogut et al. "Three-Year Wilkinson Microwave Anisotropy Probe (WMAP) Observations: Foreground Polarization." In: *Astrophys. J.* 665 (2007), pp. 355–362. DOI: 10.1086/519754. arXiv: 0704.3991 [astro-ph].

[88] P. A. R. Ade et al. "Planck 2015 results. XX. Constraints on inflation." In: (2015). arXiv: 1502.02114 [astro-ph.CO].

[89] J. Aumont. *ESLAB 2013: Component separation for CMB polarization*. Apr. 2013. URL: http://www.rssd.esa.int/SA/PLANCK/docs/eslab47/Session09_Data_Processing/47ESLAB_April_04_10_30_Aumont.pdf.

[90] Antony Lewis, Anthony Challinor, and Anthony Lasenby. "Efficient Computation of CMB anisotropies in closed FRW models." In: *Astrophys. J.* 538 (2000), pp. 473–476. eprint: astro-ph/9911177.

[91] LLoyd Knox. "Determination of inflationary observables by cosmic microwave background anisotropy experiments." In: *Phys. Rev.* D52 (1995), pp. 4307–4318. DOI: 10.1103/PhysRevD.52.4307. arXiv: astro-ph/9504054 [astro-ph].

[92] L. Page et al. "Three year Wilkinson Microwave Anisotropy Probe (WMAP) observations: polarization analysis." In: *Astrophys.J.Suppl.* 170 (2007), p. 335. DOI: 10.1086/513699. arXiv: astro-ph/0603450 [astro-ph].

[93] Planck Collaboration et al. "Planck intermediate results. XXIX. All-sky dust modelling with Planck, IRAS, and WISE observations." In: *ArXiv e-prints* (Sept. 2014). arXiv: 1409.2495.

[94] Raphael Flauger, J. Colin Hill, and David N. Spergel. "Toward an Understanding of Foreground Emission in the BICEP2 Region." In: *JCAP* 1408 (2014), p. 039. DOI: 10.1088/1475-7516/2014/08/039. arXiv: 1405.7351 [astro-ph.CO].

[95] Giuseppe Di Bernardo et al. "Diffuse Synchrotron Emission from Galactic Cosmic Ray Electrons." In: (Apr. 2015). eprint: 1504.05735. URL: http://arxiv.org/abs/1504.05735.

[96] Daniel Baumann et al. "CMBPol Mission Concept Study: Probing Inflation with CMB Polarization." In: *AIP Conf.Proc.* 1141 (2009), pp. 10–120. DOI: 10.1063/1.3160885. arXiv: 0811.3919 [astro-ph].

[97] A. Abergel et al. "Planck 2013 results. XI. All-sky model of thermal dust emission." In: *ArXiv e-prints* (Dec. 2013). arXiv: 1312.1300.

[98] Kendrick M. Smith and Matias Zaldarriaga. "A general solution to the E-B mixing problem." In: *Phys.Rev.* D76 (2007), p. 043001. DOI: 10.1103/PhysRevD.76.043001. arXiv: astro-ph/0610059 [astro-ph].

[99] Planck Collaboration et al. "Planck intermediate results. XXII. Frequency dependence of thermal emission from Galactic dust in intensity and polarization." In: *ArXiv e-prints* (May 2014). arXiv: 1405.0874.

[100] Licia Verde, Hiranya Peiris, and Raul Jimenez. "Optimizing CMB polarization experiments to constrain inflationary physics." In: *JCAP* 0601 (2006), p. 019. DOI: 10.1088/1475-7516/2006/01/019. arXiv: astro-ph/0506036 [astro-ph].

[101] M.P. Hobson et al. "Foreground separation methods for satellite observations of the cosmic microwave background." In: *Mon.Not.Roy.Astron.Soc.* (1998). arXiv: astro-ph/9806387 [astro-ph].

[102] Carlo Baccigalupi et al. "Extracting cosmic microwave background polarisation from satellite astrophysical maps." In: *Mon.Not.Roy.Astron.Soc.* 354 (2004), pp. 55–70. DOI: 10.1111/j.1365-2966.2004.08168.x. arXiv: astro-ph/0209591 [astro-ph].

[103] F. Stivoli et al. "Maximum likelihood, parametric component separation and CMB B-mode detection in suborbital experiments." In: *Mon.Not.Roy.Astron.Soc.* 408 (2010), pp. 2319–2335. DOI: 10.1111/j.1365-2966.2010.17281.x. arXiv: 1004.4756 [astro-ph.CO].

[104] J. Errard, F. Stivoli, and R. Stompor. "Framework for performance forecasting and optimization of CMB B-mode observations in the presence of astrophysical foregrounds." In: *Physical Review D* 84.6, 063005 (Sept. 2011), p. 063005. DOI: 10.1103/PhysRevD.84.063005.

[105] Lloyd Knox and Yong-Seon Song. "A Limit on the detectability of the energy scale of inflation." In: *Phys.Rev.Lett.* 89 (2002), p. 011303. DOI: 10.1103/PhysRevLett.89.011303. arXiv: astro-ph/0202286 [astro-ph].

[106] M. Kesden, A. Cooray, and M. Kamionkowski. "Separation of Gravitational-Wave and Cosmic-Shear Contributions to Cosmic Microwave Background Polarization." In: *Physical Review Letters* 89.1 (July 2002), p. 011304. DOI: 10.1103/PhysRevLett.89.011304. eprint: astro-ph/0202434.

[107] Uros Seljak and Christopher M. Hirata. "Gravitational lensing as a contaminant of the gravity wave signal in CMB." In: *Phys.Rev.* D69 (2004), p. 043005. DOI: 10.1103/PhysRevD.69.043005. arXiv: astro-ph/0310163 [astro-ph].

[108] Kendrick M. Smith et al. "Delensing CMB Polarization with External Datasets." In: *JCAP* 1206 (2012), p. 014. DOI: 10.1088/1475-7516/2012/06/014. arXiv: 1010.0048 [astro-ph.CO].

[109] J. Errard and R. Stompor. "Astrophysical foregrounds and primordial tensor-to-scalar ratio constraints from cosmic microwave background B-mode polarization observations." In: *Physical Review D* 85.8, 083006 (Apr. 2012), p. 083006. DOI: 10.1103/PhysRevD.85.083006. arXiv: 1203.5285 [astro-ph.CO].

[110] P.A.R. Ade et al. "A Joint Analysis of BICEP2/Keck Array and Planck Data." In: (2015). arXiv: 1502.00612 [astro-ph.CO].

[111] Antony Lewis. *Detecting CMB tensor modes*. 2002. URL: http://cosmologist.info/notes/tensors.ps.

[112] Marc Kamionkowski and Ely D. Kovetz. "Statistical diagnostics to identify Galactic foregrounds in B-mode maps." In: *Phys.Rev.Lett.* 113.19 (2014), p. 191303. DOI: 10.1103/PhysRevLett.113.191303. arXiv: 1408.4125 [astro-ph.CO].

[113] P.A.R. Ade et al. "Planck 2013 results. XXII. Constraints on inflation." In: (2013). arXiv: 1303.5082 [astro-ph.CO].

[114] Leonardo Senatore, Kendrick M. Smith, and Matias Zaldarriaga. "Non-Gaussianities in Single Field Inflation and their Optimal Limits from the WMAP 5-year Data." In: *JCAP* 1001 (2010), p. 028. DOI: 10.1088/1475-7516/2010/01/028. arXiv: 0905.3746 [astro-ph.CO].

[115] Claudia de Rham and Andrew J. Tolley. "DBI and the Galileon reunited." In: *JCAP* 1005 (2010), p. 015. DOI: 10.1088/1475-7516/2010/05/015. arXiv: 1003.5917 [hep-th].

[116] Alberto Nicolis, Riccardo Rattazzi, and Enrico Trincherini. "The Galileon as a local modification of gravity." In: *Phys.Rev.* D79 (2009), p. 064036. DOI: 10.1103/PhysRevD.79.064036. arXiv: 0811.2197 [hep-th].

[117] Clare Burrage et al. "Galileon inflation." In: *JCAP* 1101 (2011), p. 014. DOI: 10.1088/1475-7516/2011/01/014. arXiv: 1009.2497 [hep-th].

[118] Sebastien Renaux-Petel, Shuntaro Mizuno, and Kazuya Koyama. "Primordial fluctuations and non-Gaussianities from multifield DBI Galileon inflation." In: *JCAP* 1111 (2011), p. 042. DOI: 10.1088/1475-7516/2011/11/042. arXiv: 1108.0305 [astro-ph.CO].

[119] Sébastien Renaux-Petel. "DBI Galileon in the Effective Field Theory of Inflation: Orthogonal non-Gaussianities and constraints from the Trispectrum." In: *JCAP* 1308 (2013), p. 017. DOI: 10.1088/1475-7516/2013/08/017. arXiv: 1303.2618 [astro-ph.CO].

[120] Kurt Hinterbichler et al. "DBI Realizations of the Pseudo-Conformal Universe and Galilean Genesis Scenarios." In: *JCAP* 1212 (2012), p. 030. DOI: 10.1088/1475-7516/2012/12/030. arXiv: 1209.5742 [hep-th].

[121] David Langlois et al. "Primordial fluctuations and non-Gaussianities in multi-field DBI inflation." In: *Phys.Rev.Lett.* 101 (2008), p. 061301. DOI: 10.1103/PhysRevLett.101.061301. arXiv: 0804.3139 [hep-th].

[122] Xingang Chen et al. "Observational signatures and non-Gaussianities of general single field inflation." In: *JCAP* 0701 (2007), p. 002. DOI: 10.1088/1475-7516/2007/01/002. arXiv: hep-th/0605045 [hep-th].

[123] Nima Arkani-Hamed et al. "Ghost inflation." In: *JCAP* 0404 (2004), p. 001. DOI: 10.1088/1475-7516/2004/04/001. arXiv: hep-th/0312100 [hep-th].

[124] Paolo Creminelli et al. "Khronon inflation." In: *JCAP* 1211 (2012), p. 032. DOI: 10.1088/1475-7516/2012/11/032. arXiv: 1206.1083 [hep-th].

[125] Mohammad Hossein Namjoo, Hassan Firouzjahi, and Misao Sasaki. "Violation of non-Gaussianity consistency relation in a single field inflationary model." In: *Europhys.Lett.* 101 (2013), p. 39001. DOI: 10.1209/0295-5075/101/39001. arXiv: 1210.3692 [astro-ph.CO].

[126] Guilherme L. Pimentel, Leonardo Senatore, and Matias Zaldarriaga. "On Loops in Inflation III: Time Independence of zeta in Single Clock Inflation." In: *JHEP* 1207 (2012), p. 166. DOI: 10.1007/JHEP07(2012)166. arXiv: 1203.6651 [hep-th].

[127] "Precision Epoch of Reionization studies with next-generation CMB experiments." In: *JCAP* 1408 (2014), p. 010. DOI: 10.1088/1475-7516/2014/08/010. arXiv: 1406.4794 [astro-ph.CO].

[128] Amber Miller. 2015. URL: http://physics.princeton.edu/cmb50/talks/amber_miller.ppt.

[129] R. W. Ogburn et al. "BICEP2 and Keck array operational overview and status of observations." In: *Society of Photo-Optical Instrumentation Engineers (SPIE) Conference Series*. Vol. 8452. Society of Photo-Optical Instrumentation Engineers (SPIE) Conference Series. Sept. 2012. DOI: 10.1117/12.925731. arXiv: 1208.0638 [astro-ph.IM].

[130] Adrian Lee. *The POLARBEAR-1, POLARBEAR-2, and Simons Array Experiments*. 2013. URL: http://max.ifca.unican.es/EPI2013/epi2013_talks/Thursday/EPI_27062013_01_Lee.pdf.

[131] K. Arnold et al. *The Simons Array: expanding POLARBEAR to three multichroic telescopes*. 2014. DOI: 10.1117/12.2057332. URL: http://dx.doi.org/10.1117/12.2057332.

[132] A.A. Fraisse et al. "SPIDER: Probing the Early Universe with a Suborbital Polarimeter." In: *JCAP* 1304 (2013), p. 047. DOI: 10.1088/1475-7516/2013/04/047. arXiv: 1106.3087 [astro-ph.CO].

[133] A.S. Rahlin et al. "Pre-flight integration and characterization of the SPIDER balloon-borne telescope." In: (2014). arXiv: 1407.2906 [astro-ph.IM].

[134] B. A. Benson et al. "SPT-3G: a next-generation cosmic microwave background polarization experiment on the South Pole telescope." In: *Society of Photo-Optical Instrumentation Engineers (SPIE) Conference Series*. Vol. 9153. Society of Photo-Optical Instrumentation Engineers (SPIE) Conference Series. July 2014, p. 1. DOI: 10.1117/12.2057305. arXiv: 1407.2973 [astro-ph.IM].

[135] F.R. Bouchet et al. "COrE (Cosmic Origins Explorer) A White Paper." In: (2011). arXiv: 1102.2181 [astro-ph.CO].

[136] T. Matsumura et al. "Mission Design of LiteBIRD." In: *Journal of Low Temperature Physics* 176 (Sept. 2014), pp. 733–740. DOI: 10.1007/s10909-013-0996-1. arXiv: 1311.2847 [astro-ph.IM].